CANADIAN THESES

THÈSES CANADIENNES

NOTICE

The quality of this microfiche is heavily dependent upon the quality of the original thesis submitted for microfilming. Every effort has been made to ensure the highest quality of reproduction possible.

If pages are missing, contact the university which granted the degree.

Some pages may have indistinct print especially if the original pages were typed with a poor typewriter ribbon or if the university sent us an inferior photocopy.

Previously copyrighted materials (journal articles, published tests, etc.) are not filmed.

Reproduction in full or in part of this film is governed by the Canadian Copyright Act, R.S.C. 1970, c. C-30.

AVIS

La qualité de cette microfiche dépend grandement de la qualité de la thèse soumise au microfilmage. Nous avons tout fait pour assurer une qualité supérieure de reproduction.

S'il manque des pages, veuillez communiquer avec l'université qui a conféré le grade.

La qualité d'impression de certaines pages peut laisser à désirer, surtout si les pages originales ont été dactylographiées à l'aide d'un ruban usé ou si l'université nous a fait parvenir une photocopie de qualité inférieure.

Les documents qui font déjà l'objet d'un droit d'auteur (articles de revue, examens publiés, etc.) ne sont pas microfilmés.

La reproduction, même partielle, de ce microfilm est soumise à la Loi canadienne sur le droit d'auteur, SRC 1970, c. C-30.

THIS DISSERTATION HAS BEEN MICROFILMED EXACTLY AS RECEIVED

LA THÈSE A ÉTÉ MICROFILMÉE TELLE QUE NOUS L'AVONS REÇUE

Canada

Quantitative Fractographic Examination
of
Aircraft Components Subjected To
Fatigue and Damage Tolerance Testing

Eugen Abramovici

A Thesis

in

The Department

of

Mechanical Engineering

ABSTRACT

Quantitative Fractographic Examination Of Aircraft Components Subjected To Fatigue And Damage Tolerance Testing.

Eugen Abramovici

The Canadair Challenger CL 600/601 business airplane certification program required fractographic examination of various components which had failed during the fatigue and damage tolerance test, to assist in the construction of fatigue cracking propagation (F.C.P.) curves.

A literature survey was carried-out to understand the processes of fatigue crack initiation, propagation and associated phenomena such as: striation formation, crack closure, the overloading effect, and the influence of other parameters on striation appearance and on the F.C.P. rate. Various procedures and techniques of quantitative fractography are described and the reliability of this method is discussed.

The experimental section consists of two programs. The first, carried-out on specimens cracked using a constant amplitude loading spectrum, had as an objective, (to prove the reliabilty of quantitative fractography by comparing F.C.P. curves determined by this method with those determined by macroscopic observation. The results showed that

fractographic analysis provides more accurate data than visual monitoring of the crack growth.

The second program was carried-out on standard aircraft components from a flap/vane fatigue and damage tolerance test. Due to the impossibility of monitoring crack growth in these components during test, the objective was to provide sufficient data to construct the F.C.P. curves. Detailed explanations about the fractographic analysis are given, as well as the numerical estimation of the fatigue initiation moment and the first N.D.T. inspection interval. The data obtained from this program were submitted, as part of the final certification of the aircraft, to flight safety authorities in Canada (MOT) and United States (FAA .

Dedicated to My Son

and

to the memory of My Father

and My Mother.

27 March 1986.

ACKNOWLEDGEMENTS

canadair

Fractographic examination of fatigue and damage
tolerance test articles for the Canadair Challenger
certification program is considered an acceptable
subject for your M.E. thesis at Concordia.

You may use "Canadair" and "Challenger" in the text.

Rafe Sherwin
Manager
Materials and Processes
Engineering

RS/b

cc: E. Aubrey
    K.C. Overbury

TABLE OF CONTENTS

1. INTRODUCTION

Fatigue is defined as "the phenomenon leading to fracture under repeated or fluctuating stresses having a maximum value less than the tensile strength of the material". [1] Despite all the energy and care invested in designing, testing and fabricating of an airframe, fatigue failures are by far the most common mode of fracture found in the materials laboratories of aircraft manufactures.

Two basic philosophies have been developed over the years for the design of aircraft components:

- safe-life

- fail-safe

Safe-life design implies an evaluation of a component's life based on traditional design methods, then carrying-out of a full-scale test using an appropriate spectrum loading. A safety margin, called scatter factor, is then selected to allow for the difference between the calculated lifetime and the actual test lifetime.

The new generation of airplanes manufactured in the last two decades are engineered in accordance with fail-safe (damage tolerance) design philosophy. Basically, damage tolerance is "the ability of structure to sustain anticipated loads in the presence of fatigue, corrosion, or accidental damage, while such damage is detected through inspections or malfunctions and repaired." [2]

1

"The basic assumption of damage tolerance concept is that flaws do exist even in new structures and that they may go undetected". [3] Occasionally during the service life of the component, cracks may develop and propagate, originating from these initial flaws.

"The key element of the damage tolerance approach is the ability to detect damage." [2] The establishing of an accurate inspection program must consider the loading on each structural component, the regions with the highest probability of developing a crack, the crack growth rate, the inspectable crack length, the proper non-destructive technique to be employed and many other parameters. This information can be obtained from both analytical data and experimental tests.

The Canadair Challenger Cl-600/601 business-jet airplanes were among the first aircrafts to be qualified to the stringent damage tolerance requirements of FAR (Federal Airworthiness Regulations) Part 25.271 Amendment 45. This amendment requires "a detailed study of crack growth rates and critical crack lengths" [4] to establish appropriate inspection intervals. A schematic view of the sequential procedure applied in damage tolerance evaluation of the Canadair CL-600 is shown in Figure 1.
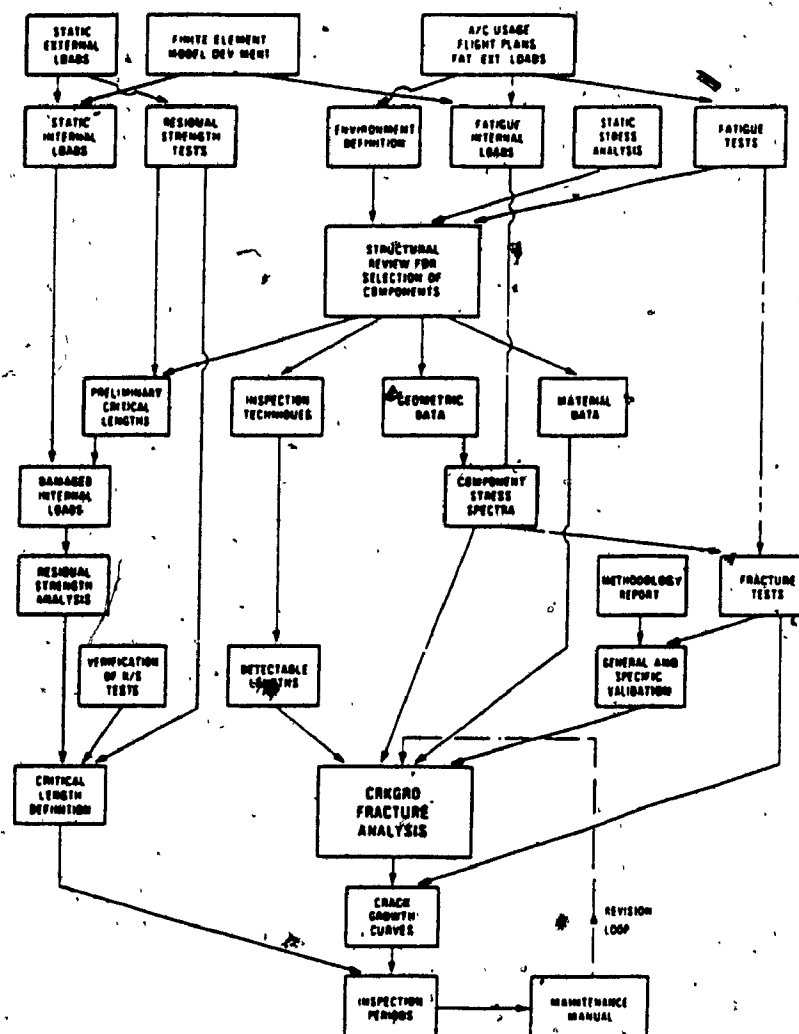
Figure 1.

Damage tolerance evaluation procedure [4]

It is obvious that one of the most crucial pieces of information needed to develop an accurate inspection schedule is the growth rate of cracks developed in structural components. The scheme from Figure 1 shows how the crack growth curve was constructed on the base of the information synthesized from both, the CRKGRO analytical program and the

results of the fracture tests.

The fatigue tests conducted at Canadair "comprises a structurally complete Challenger airframe including fuselage, wings, empennage, vertical and horizontal stabilizer." [4] The test must prove the design objective of "30,000 hours substantially crack-free period," which will ensure a "20-30 year crack-free life." [4] The load spectra selected for the test are described in [4]. Basically, they were established by consideration of typical missions covering the range of anticipated use of the Challenger Cl-600/601.

During the fatigue tests, cracks may appear or be artifically introduced in the component. Generally, "cracks were introduced into the fatigue test airframe after it had completed 20,000 hours of testing without significant natural cracking having occurred. Growth of these cracks has been monitored during the period from 20,000 hours to 43,000 hours currently on the specimen and continues to be monitored as the test proceeds" [4]. The observations of the cracks growth collected during the testing were used to plot the crack growth curves, which were compared to the crack growth rate curves as determined by the analytical method.

The determination of the crack growth rates by fractographic examination is required to supplement the data obtained by either analytical or experimental methods. In more specific cases where the crack growth cannot be

monitored during the test, the quantitative fractographic examination is the only source of information to assess the real crack growth rate. In any case, quantitative fractographic examination is a desirable test to be carried out after teardown of the fatigue tested components. As has been stated in [5] "the desirability of this type of FCP (Fatigue crack propagation) data is reflected in the United States Air Force (USAF) Military specification that states: At the end of the full-scale durability test... This inspection shall include disassembly and laboratory-type inspection of critical structural areas. Fractographic examinations shall be conducted to obtain crack growth data and to assist in the assessment of the quality of the airframe." [5]

This thesis consists basically of two parts:

The first part consists of a literature survey which provides an explanation of theoretical models of fatigue cracking, striation formation and their relationship with other fracture mechanics parameters.

The second part of the thesis explains the detailed quantitative fractographic techniques developed at Canadair Ltd, Materials and Process Engineering Laboratory, during the Challenger Cl 600/601 certification program, with emphasis on the fractographic examination of the flap/vane assembly.

2. FATIGUE DAMAGE

2.1. GENERALITIES

Fatigue as a mode of failure could be classified as either:

- low cycle fatigue
- high cycle fatigue

As stated the literature [4], the distinction between these two modes of fatigue failure depends on the magnitude of the overstress which is defined as "the amount by which the nominal stress exceeds the fatigue limit or the long-life fatigue strength of the material used in a component." If the overstress is low, the number of cycles applied before the final fracture is high, hence a high cycle fatigue mode of failure. Obviously if the overstress is high the component will fail after a low number of cycles, hence low cycle fatigue. There is an arbitrary, but commonly accepted border between these two modes of fatigue failure: that is 100,000 cycles. Usually it is difficult to distinguish between those two modes; however, fractographic examination which reveals the number of origins, the microscopic fatigue striation spacing, the size of the final fast fracture and other characteristics can provide the necessary data to

establish the mode of fatigue failure.

Fatigue failures can have their loading source either in mechanical stresses or in thermal stresses. In addition the fatigue failures are in many situations assisted by corrosion, creep, hydrogen embrittlement and many other unfavourable conditions.

The fatigue cracking process is a progressive mode of failure which usually involves two distinct stages:

- fatigue crack initiation stage

- fatigue crack propagation stage

Some authors consider that the last stage can also be divided in two or three more stages. McMillan and Hertzberg consider that in stage two "the crack will shift into a position leading to plain strain and in stage three to plane stress" [6]. Stage four represents the final fracture. Other authors consider the fatigue cracking process as a double stage process only [7]: initiation and propagation.

The author of the present thesis considers that a three stage classification will give a better description of the overall picture of the fatigue process:

Stage 1: Fatigue Initiation

Stage 2: Fatigue Propagation

Stage 3: Final Fast Fracture

This classification takes into account that shifting from plane strain to plane stress is a condition depending on the

component thickness and in many situations does not occur at all. The final fast fracture is considered a separate stage because the loading conditions are different than those described in the fatigue process definition. In this stage, which usually occurs in one last cycle the fluctuating stress becomes equal or higher in magnitude than the component residual strength, which has been substantially reduced by the fatigue cracking propagation stage.

The predominance in time (or in number of cycles) of either one of two the first stages can be affected by several factors such as: stress concentration factor, presence of initiation site, microstructure, level of stress. Laird [8] showed that the stage I (initiation) is predominant in the cases of fatigue failures at low stress (unnotched specimens) whereas the stage II (propagation) is predominant in the cases of fatigue failures at high stress. As Rich and Impellizzeri [9] showed "a significant percentage of the total fatigue life is spent in both crack initiation and crack growth; neither stage can be neglected", Figures 2 & 3.

The term crack initiation is an arbitrary term as well; Rich and Impellizzeri defined it as a development of a 0.25 mm (0.01") crack. However, in industrial applications for the purpose of non destructive testing a detectable crack size is considered a length of approximately 1.25 mm (0.05").

8
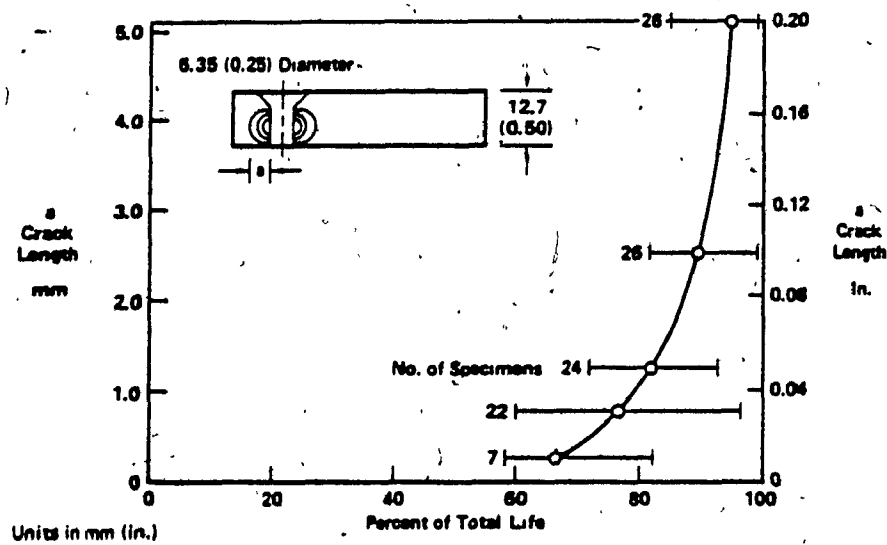
Figure 2

Growth rate (average trends) of a fatigue crack initiated at
a rivet hole. Material: Ti-6AL-4V. Approximate initiation
stage: 65% of total life. [10]
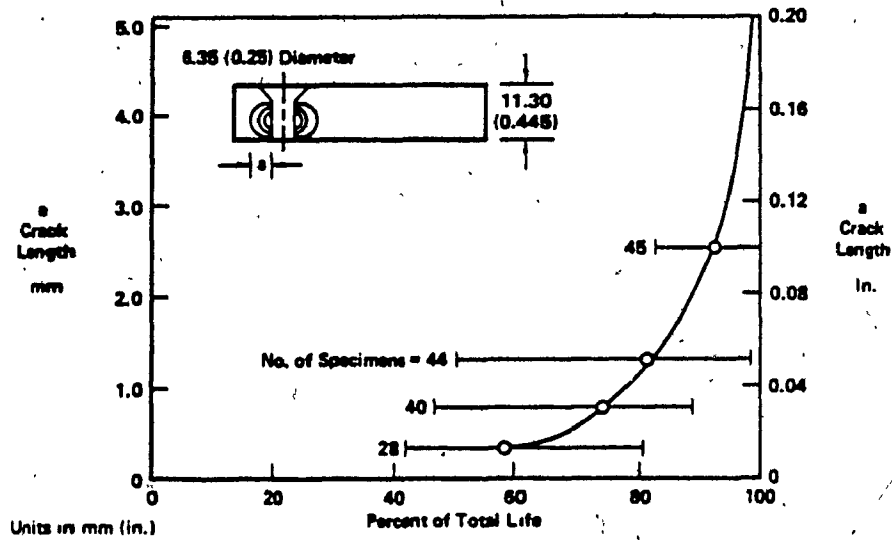
Figure 3

Growth rate (average trends) of a fatigue crack initiated at
a rivet hole. Material: 7075-T651 aluminum alloy.
Approximate initiation stage: 55% of total life. [10]

2.2. FATIGUE CRACKING INITIATION

In most cases the fatigue initiation stage may represent a significant portion of the total fatigue life of the component; however, in the total percentage of the fracture surface this stage is very small. Usually the initiation stage is not considered to affect more than the first two to five grains from the surface, Figure 4.
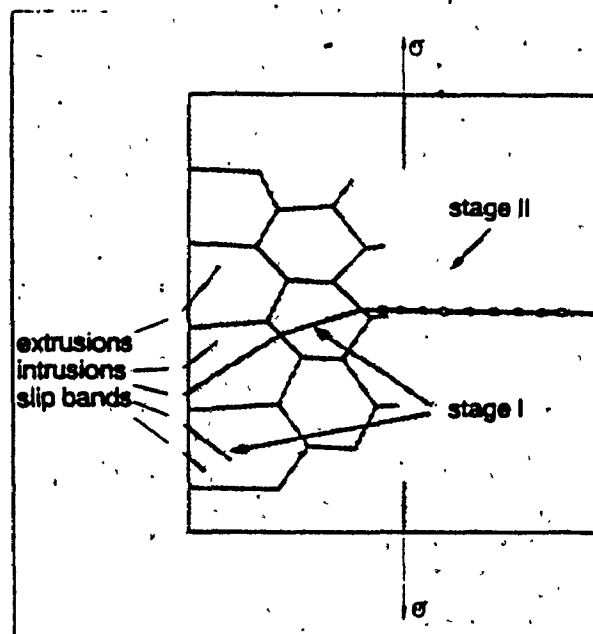
Figure 4

Schematic representation of the initiation and the propagation stages.[11]

On the micro and macroscopic scales the process of the fatigue initiation is strongly related to the inherent surface or subsurface defects such as machining marks, notches, pores, holes or inclusions. Eylon and Kerr [2] classified the initiation sites into:

1) initiation related to the surface conditions

2) initiation related to subsurface conditions

    2a) defects such as: pores, inclusions

    2b) microstructural features.

Other authors [7] classified the discontinuities as: structural (inclusions or second phase particles) or geometrical (such as scratches). These discontinuities may be present from the beginning or they "may develop during cyclic deformation as for example, at the persistent slip bands (PSB)." [7], Figure 5.

In the opinion of the author of the present thesis a general classification of the initiation sites could be synthesized as in Table 1.

Since the pre-existent macroscropic discontinuities and to some extent the microscopic ones are detectable, the scientific and industrial effort has been oriented towards limiting the number and the size of these discontinuities in the normal commercial applications. In the case of non-pre-existent discontinuities the major approach has been concentrated in understanding of the mechanism which produces

11
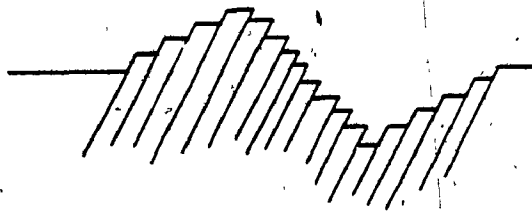
a)

b)

Figure 5

a) Schematic representation of the extrusions and intrusions
[13]
b) Scanning electron micrograph showing extrusions
and intrusions on prepolished surface. [13]
Magnification: 7000x

12

Table 1

Crack initiation sites classification

Initiation Site at:	Scale	Location	Description
Pre-existent discontinuities	Macroscopic	Surface	Machining marks, scratches, etc
		Subsurface	Holes, pores, etc
	Microscopic	Subsurface	Inclusions, second phase particles, grain boundaries,etc
Non-pre-existent discontinuities	Submicroscopic	Surface	Intrusions, extrusions at PSB.

the surface discontinuities. This mechanism has become strongly associated with dislocation movements. The proposed dislocation models attempt to explain the generation of extrusions and intrusions by non-reversible (persistent) slip.

The term persistent slip arose from the persistance of the slip bands near the specimen surface after the removal of the geometrically affected surface layer. In other words, a test specimen is subjected to cyclic deformation until it exhibits slip bands which are removed by electropolishing to a smooth surface. When the specimen is retested, the slip bands appear again in the same places. These persistent slip bands are indicative that significant fatigue damage has

already been produced, even though no crack yet has been observed.

As explained by McLean [14], "dislocation theory gives three ways in which slip could shift from plane to plane to produce a notch (or an extrusion)." The most acceptable of these three ways is the one depicted in Figure 6. "The source S_1 operates before S_2 on each cycle because the resolved shear stress on its slip plane is supposed to be greater. If successive cycles exactly repeated the movements depicted, the notch and the ridge would get deeper but not wider" [14]. A confirmation of this model can be found in some works
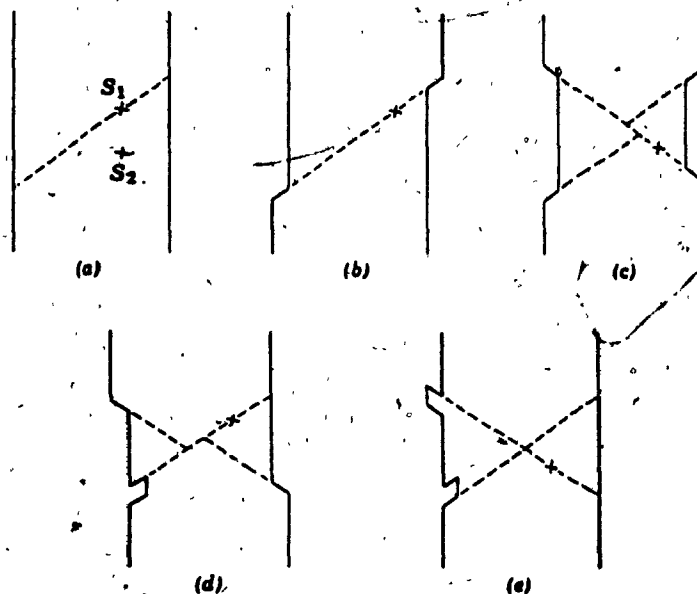
Figure 6.

Laird's mechanism of slip movements to produce an intrusion and an extrusion. [14]

[15,16] which revealed that, in an early stage of fatigue initiation, "not persistant slip bands, but only rows of dots (in 67/33 brass, aluminum, copper and mild steel) which appear to extend and join up on further fatiguing. A detailed investigation [17] of these dots led to the conclusion that they were holes some microns deep and they were particulary prominent at points where one slip band intersected another" [7].

The dislocation structure of the PSB has been investigated extensively, as well. Lucas and Klesnil [18] showed the relationship between the stacking fault energy and cross-slip, respectively in the development of dislocation structure within the PSB's. Kuhlman-Wilsdorf and Laird gave another interpretation of preferential nucleation of fatigue cracks at surfaces. Kramer [19] suggested an alternate mechanism which during cycling, involves the formation on the component surface of a high dislocation density layer. This layer becomes strong enough to sustain a dislocation pile-up. Therefore "the stress concentration associated with this pile-up would eventually trigger the development of a crack within the hardened layer."[13] This model can very well explain the improvement of fatigue life by periodic surface polishing. However this model contradicts the experiment which found that softening of the matrix takes place during

the cyclic straining [20].

It must be mentioned that the dislocation motion plays
an important role in the fatigue initiation stage, even in
the case of pre-existent discontinuities. Figure 7 shows a
schematic representation of the interaction between the
dislocations and a pre-existant microstructural
discontinuity.

Figure 7.

Mechanism of crack initiation produced by:
a) interaction between dislocations and an inclusion [7]
b) interaction between dislocations and a grain boundry [7]

2.3. FATIGUE CRACKING PROPAGATION (F.C.P.)

The second stage of the phenomena of fatigue damage is
the fatigue crack propagation (F.C.P.) Basically this stage
involves propagation of the crack at right angles to the
direction of tensile stress (Figure 4).

The understanding of this stage is especially important
for the applications where the damage tolerance design
philosophy is used, because the non-destructive inspection
intervals are established based on the crack growth-rate
curves.

The F.C.P. is a complex phenomenon and several important factors affect it. These factors will be summarized in the following sections.

2.3.1 F.C.P. Models

Most of the theoretical effort has been concentrated in proposing a mathematical model capable of predicting with accuracy the crack growth rate under certain loading conditions. Over the last two decades, in which this theoretical effort has been concentrated, a number of theories and models were proposed, none of them with total success.

Kaninen and coworkers [21] synthesized three basic conditions to be met in the development process of an accurate F.C.P. model:

a) The model must be capable of handling load cycles that vary arbitrarly from cycle to cycle while taking the load interaction effects properly into account.

b) The material properties required by the model must be based upon well established material properties that are independent of the particular load spectrum under consideration.

c) The computational procedure evolved must be efficient enough to enable calculations to be carried out over load histories comparable to actual service conditions.

17

As it has been demonstrated during the last two decades when the "battle" for an accurate F.C.P. model took place, a number of phenomena such as: crack tip plasticity, crack closure and load interaction play an important role in the fatigue process. Consequently these phenomena must be understood and explained before proceedings to elaborate a F.C.P. model.

2.3.1.1. Crack tip plasticity

The concepts of elasticity theory allows the determination of the stress field surrounding a crack tip. The analysis (see reference [13]), shows that the stress distribution around a crack tip depends on the distance between the crack tip and the point where stresses are to be computed, Figure 8. When this parameter approaches zero, the local stresses could reach extremely high levels. However, this circumstance is precluded by the onset of plastic deformation at the crack tip. Broek [22] showed that "in most structural materials the crack tip stress will cause local plastic deformation. As a consequence, the stresses are limited by the flow stress." The elastic theory permits calculation of the distance between the crack tip and the point where the stress is equal to the yield stress. A general equation of the plastic zone size can be written as:

$$r_\theta = \alpha \left(\frac{K}{\sigma_y} \right)^2$$

18
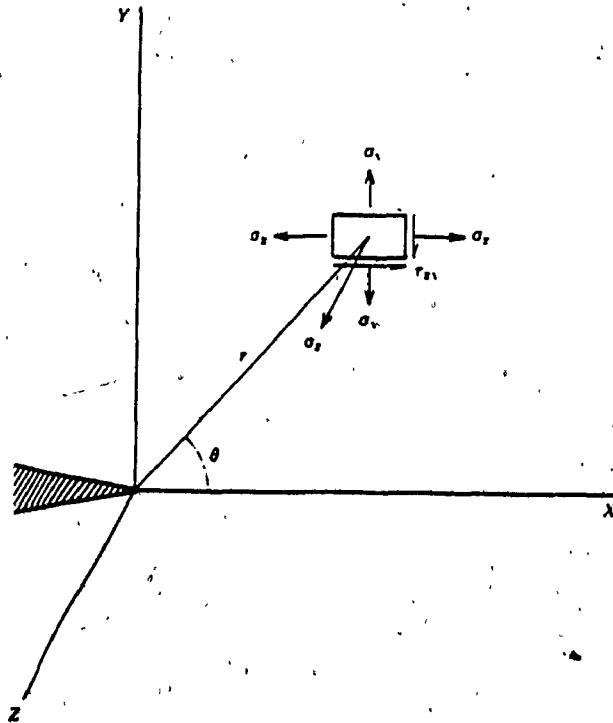
Figure 8

Geometry of analysis of stresses in vicinity of crack tip.
[13]

where r_θ = distance from the crack tip
        α = parameter
        K = stress intensity factor
        σ_y = yield stress

Numerous theories have been proposed to predict the plastic
zone size, that is, to find proper values for parameter α.
Table 2 shows a synthesis of the theoretical values of
parameter α , as given by Lankford and co-workers [23].

19

Table 2

Theoretical values of parameter α. [23]

α, Plane Stress		Reference	α, Plane Strain		Reference
α_n[a]	α_n[b]		α_n[a]	α_n[b]	
0.392	0.318	[2]	. . .	0.053	[4]
0.199	0.159	[3]	. . .	0.106	[3,10]
. . .	0.382	[5]	0.138	. . .	[11]
0.199 to 0.392	0.159 to 0.382	range	~0.150	0.041	[12]
			~0.140	0.035	[14]
			0.138 to 0.150	0.035 to 0.106	range

[a] α_n determined by calculating r_p normal (90 deg) to the plane of the crack.
[b] α_n determined by calculating r_p parallel (0 deg) to the plane of the crack.

[2] Rice
[3] Broek
[5] Dugdale
[4] Irwin
[3,10] Broek, Irwin, McClintock
[11] Levy
[12] Rice
[14] Tracey

Hertzberg [13] stated that for many of the usual applications the plastic zone size could be calculated as follows:

$$r_y \cong \frac{1}{2\pi} \cdot \left(\frac{K}{\sigma y}\right)^2$$

This corresponds to Broek's model for plane stress

$$r_y \cong \frac{1}{6\pi} \cdot \left(\frac{K}{\sigma y}\right)^2$$

This corresponds to Irwin's model for plane strain

In addition to the influence of parameter r, the angle θ (Figure 8), also plays an important role. Further, Hertzberg presents [13] a more general equation of the plastic zone size:

$$r_y \cong \left(\frac{K^2}{2\pi \cdot \sigma_y^2}\right) \cdot \cos^2\frac{\theta}{2} \cdot \left[1 + 3\sin^2\left(\frac{\theta}{2}\right)\right]$$

from which the plastic zone assumes the shape represented in
Figure 9.

(a)

(b)
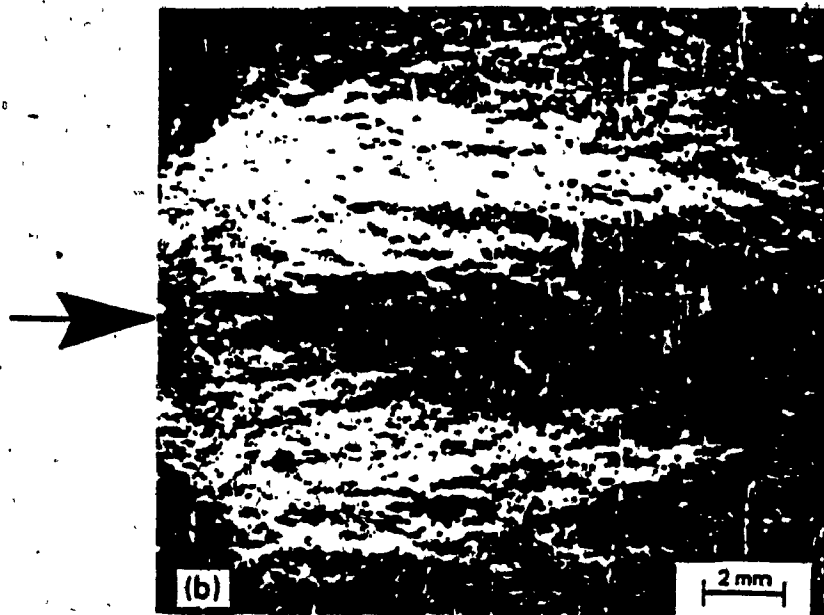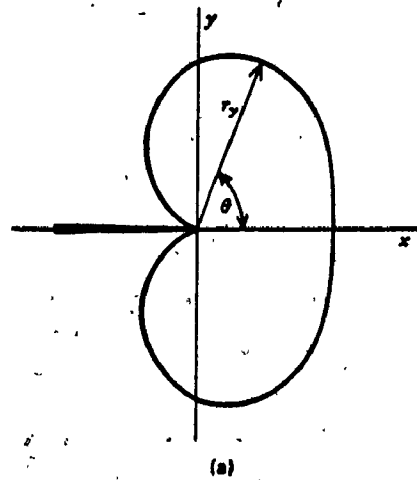
Figure 9

Crack tip plastic zone [13]
a) Variation of the plastic zone shape and size as a function
   of r and θ.
b) Microphotograph showing the plastic zone shape.

21

Different techniques were developed over the years to verify the theoretical predictions of the plastic zone shape and size. One of the most modern and interesting techniques has been developed by Lankford and others [23]. This technique designed to measure the plastic zone parameters involves "rocking the collimated electron beam in the SEM about a point (10 μm in diameter) on the specimen surface", perpendicular to the crack plane. "Deformation causes systematic degradation in the resulting electron channeling patterns (ECP). The crack tip plastic zone is determined by interrogating numerous small volumes of material with the electron beam..."[23].

Two other important phenomena are associated with the plastic zone. The first one is the three-dimensionality of the plastic zone. Figure 10 shows the three-dimensional plastic zone through the thickness of a plate which it is assumed to be sufficiently thick to develop plane strain conditions the center. As was demonstrated by Lankford and others [23] by considering the three-dimensional effect, a large hydrostatic stress is created directly ahead of the crack tip." It was estimated that for a non-hardening material, this results in stresses of three times the uniaxal yield stress; a strain hardening material will have even higher stresses. "The stress elevation ahead of the crack tip is not due to strain hardening in the sense of cyclic

22
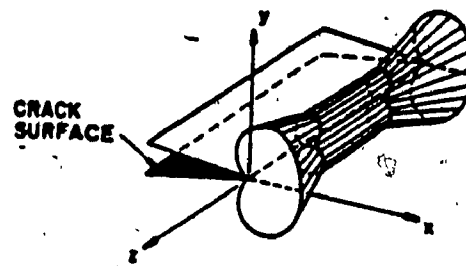
Figure 10

The three-dimensional effect of the plastic zone at the crack tip. [23]

deformation but rather is due to the constraint and the resulting hydrostatic stress, which increases the effective yield stress" [23].

The second phenomena is related to generation of an envelope of plastic zones in the wake of the moving crack tip. The earlier works in the field of crack propagation assumed that a crack behaves like a saw cut of zero width. However as has been demonstrated by Elber, a fatigue crack differs from a saw cut primarily because during fatigue crack propagation, a zone of residual tensile deformation (plastic zone) is left in the wake of the moving crack tip. A graphic representation of the development of a plastic zone envelope is shown in Figure 11, where a fatigue crack produced under constant amplitude loading is shown at three crack lengths.
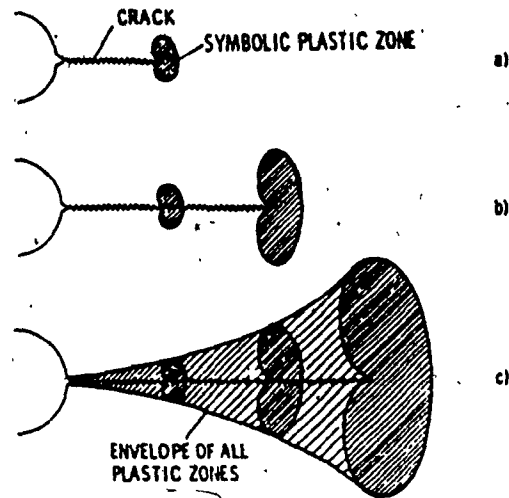
Figure 11

Development of a plastic zone envelope around a fatigue crack as imagined by Elber. [24]

Figure 11a shows the plastic zone generated after the crack reached a certain length. During further crack advances to deeper lengths, larger plastic zones are generated, Figure 11b: however, the previous plastic deformation zone remains behind the crack tip. All these increasingly large plastic zones can be incorporated in an envelope of all plastic zones, Figure 11c. To show the significance of the residual tensile deformation a comparison between a fatigue crack and a saw cut crack is shown in Figure 12. At an arbitrary section y-y behind the crack tip the residual strains ϵ_{oy} existing inside the envelope of all previous plastic zones are shown, whereas the saw cut crack has no residual strains.

The phenomenon of plastic zone envelope is strongly related to the crack closure as will be described in the next section.
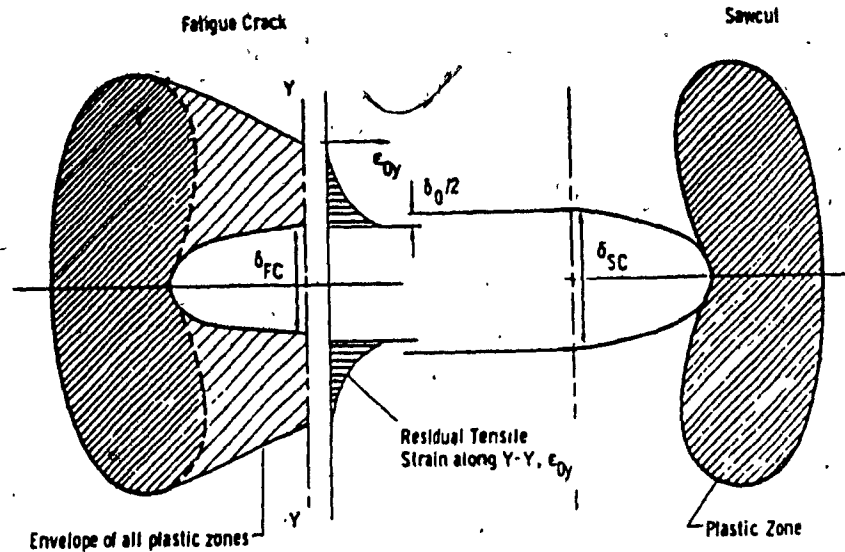
Figure 12

Comparison of plastic deformations near the crack tip for a fatigue crack and a saw cut crack. [24]

2.3.1.2. Fatigue crack closure

The phenomena of crack closure is strongly related to residual tensile deformation. As was mentioned before, the fatigue crack was hypothesized to behave like a saw cut of zero width. A direct consequence of that was the assumption that the crack would be closed under compressive loads and would be open under tensile loads. However, several experimental works and especially work done by Elber [24] showed that a fatigue crack produced under a zero to tension loading spectrum closes during the unloading and therefore

large residual compressive stresses exist normal to the
fracture surfaces at zero load. The phenomena of crack
closure was proved experimentally by using closure gauges. A
new type of closure gauge and a sectioning technique are
described in [25].

Several theories explaining crack closure phenomena were
proposed; Bailon and co-workers [26] discussed the four basic
mechanisms most frequently invoked:

a) Plastically induced crack closure - (Elber)

b) Roughness induced crack closure - (Cooke and Beevers)

c) Oxide induced crack closure - (Ritchie)

d) Hydrogen embrittlement - (Ritchie).

A graphic representation of the first three of these
mechanisms is shown in Figure 13.
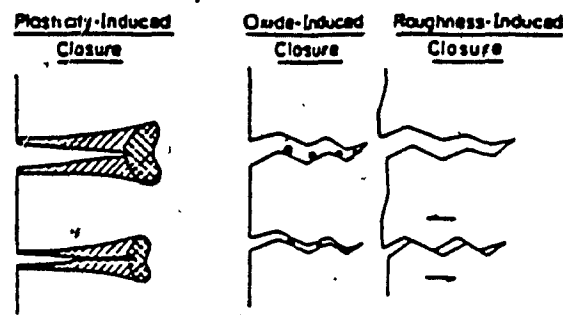
Figure 13

Schematic representation of fatigue closure models. [9]

26

a) Plastically induced crack closure

This model, proposed by Elber, [24] showed that the residual plastic deformation of the fatigue specimen can be obtained from the equation

$$\delta_0 = \int \varepsilon_{0y} \, dy$$

(For identification of terms see Figure 12)

At the same section, the saw cut crack (displacement δ_{SC}) has no residual strains. The crack opening displacement of the fatigue crack δ_{FC} at section y-y is therefore less than δ_{SC} by the amount δ_0 . On unloading the crack opening displacement of both cracks will decrease at the same rate. Because of smaller maximum value of δ_{SC} the fatigue crack will close, δ_{FC} = o , before δ_{SC} will reach zero.

Therefore large residual compressive stresses appear at zero loading on a fatigue specimen. The effect of the plastic zone in front of the crack tip combined with the effect of the envelope of plastic zones in the wake of the growing fatigue crack was studied by de Koning [27]:

"In general it can be concluded that plastic deformations of the crack tip tends to increase the crack opening displacements. A reduction of the crack opening stress occurs."

-"Clearly, the plastic deformations left in the wake of a growing fatigue crack tend to increase the crack opening load."

27

Thus, two conclusions could be synthesized in the general statement that "the plastic deformations in front of the crack tip tend to increase the crack opening displacement (COD) whereas permanent deformations left in the wake of the growing crack tend to reduce them. With respect to the crack opening stress level the opposite tendency is observed."[27] The crack closure level is therefore a result of the competition between the two plasticity effects.

b   Roughness induced crack closure model

This model proposed by Cooke and Beevers takes into account the strong crystallographic aspects of fracture surfaces in the near-threshold regime. The effect of roughness induced crack closure arises from the surface roughness and an irregular fracture morphology in conjunction with a shear displacement.

c   Oxide induced crack closure model

This model proposed by Ritchie, Suresh and Blom [28], takes into account the corrosion products on the newly exposed fracture surfaces. Their works supplies the evidence for the microroughness of the fracture surface enhancing formation of oxide debris on the fracture surface and then generating an oxide-reducing closure.

d) Hydrogen embrittlement

Only recently a relationship between the crack
propagation rate and the embrittlement reaction produced by
hydrogen pick-up was established, especially as the cause of
intergranular cracking at very low crack propagation rates.

It must be pointed out, without any intention to support
anyone of these mechanisms in favour of the others, that some
new theoretical and experimental work [9] revealed that the
plastic zones in the wake of the crack tip have indeed an
influence on the crack closure phenomena. In the case of
short cracks with limited wake, it is expected that there
will be less crack closure than for longer cracks and hence
shorter cracks will grow faster than the longer cracks. The
experimental work shown in [9] did confirm this expectation.

2.3.1.3. Influence_of_loading_history_on_F.C.P.

The behaviour of the fatigue crack growth changes when
the loading fluctuates during the test or during the service
life of the component. Experimental observations showed that
if certain overloads are applied, significant FCP delays
occur. This effect is called "retardation." Paradoxically,
the above observation means that if an airplane would
encounter more severe turbulence during its flight history,
it is expected that the airframe would have a longer life
than an airplane which had a less severe weather history.
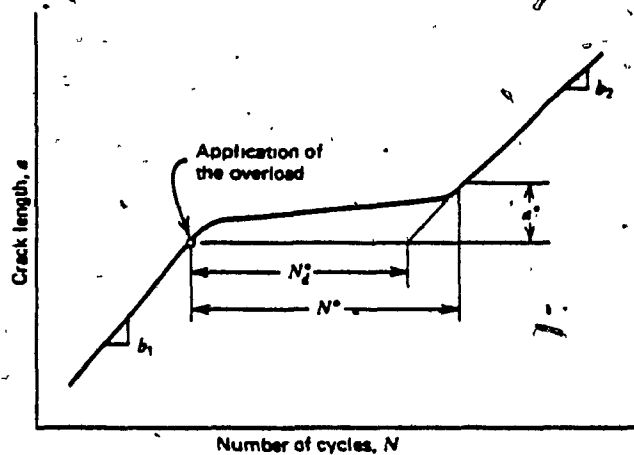
Figure 14

Crack growth rate plot showing the effect of a single overload. Note the crack growth retardation. [13]

The retarding effect of a single peak overload is demonstrated in Figure 14. The FCP rate before the application of the overload is given by the slope b_1. After the application of the overload the FCP rate is obviously depressed over a distance a* from the point of the overload. Hertzberg and others demonstrated [29] that the distance a* corresponds to the plastic zone dimension of the overload. Therefore the FCP rate is retarded as long as the resumption of normal amplitude cycles produces crack advances smaller than the plastic zone generated by the overload peak. As soon as the crack advances beyond this plastic zone the FCP rate returns to the initial value.

The mathematical expression given by Hertzberg to calculate the total number of cycles necessary to traverse the overload plastic zone is:

$$N_d^\star = N^\star - \frac{a^\star}{b_2}$$

where $\frac{a^\star}{b_2}$ is the number of cycles necessary for a crack to traverse a distance $a^\star$ at a fixed rate b_2: Surprisingly the crack velocity reaches a minimum only after the crack has progressed 1/8 to 1/4 the distance into the overload plastic zone; this is known as "delayed retardation."[29] Extensive literature has been published in the field of FCP retardation and the author considers that this particular aspect is beyond the scope of this thesis; some classical models of FCP which account for retardation will be discussed in section 2.3.1.4. One more work, however will be mentioned here. Eastabrooke [30] performed an extensive mathematical demonstration of a model which replaces the plastic zone by a slit subjected to the stresses as indicated in Figure 15 and practically reduces the concept to a numerical fracture mechanics problem. This model apparently is the first mathematical explanation of the phenomena of delayed retardation.

2.3.1.4. Synthesis of F.C.P. models

Extensive theoretical and experimental research was done in order to predict the fatigue crack propagation life by using a mathematical model.

The magnitude and degree of the difficulty of such a

31
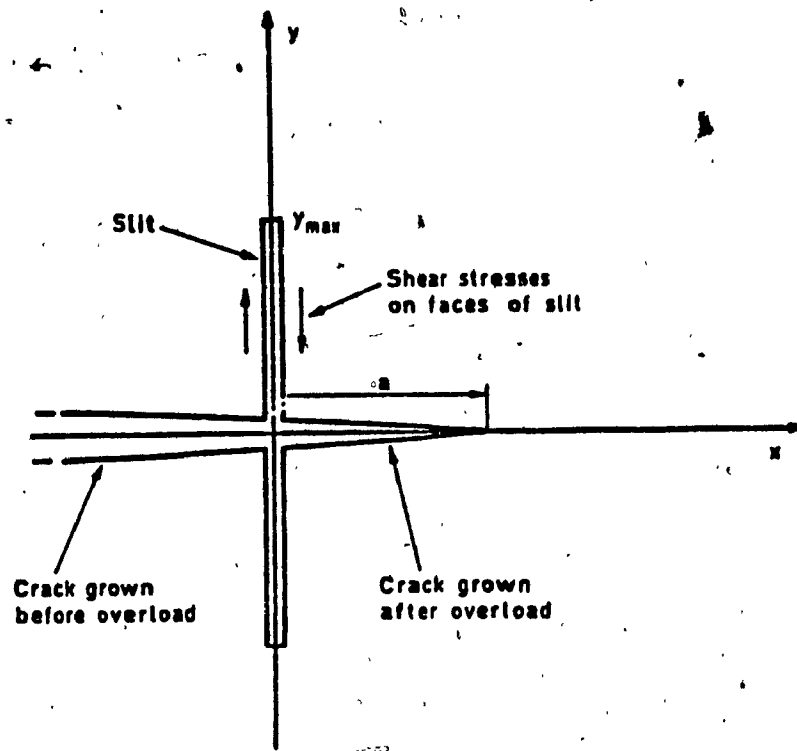
Figure 15

Eastabrooke's model. The plastic zone was simulated as a slit with shear stresses.

task is obvious. The wrought metallic material.is very often anisotropic, the microstructural components are randomly oriented, have different shapes and properties, the influence of the environment (corrosion, temperature etc) are only a few of the countless factors which must be taken into account in creating an accurate F.C.P. model. In addition, the loading history, the type of loading spectrum as well as the size and shape of the part are completely different from component to component. It is beyond the scope of this

thesis to go deeper into elaborate description of these

models. However a short synthesis of the most used models is

given below.

At the beginning of the research into the fracture

mechanics of fatigue cracking a number of empirical and

theoretical laws of the following type were proposed:

$$\frac{da}{dN} \cong f(\sigma, a)$$

where: a = crack length
     σ = stress
     N = number of cycles

As Hertzberg shows in [13] very often these functions assumed

the form of a simple power relationship such as:

$$\frac{da}{dN} \cong \sigma^m a^n$$

where: m is in the range 2-7
              n is in the range 1-2

Some earlier works tried to determine accurate values for m

and n. For example "Liu theorized that m and n to be 2 and 1,

respectively, while Frost found empirically for the materials

he tested that m=3 and n=1" [13]. During the 1960's Paris

postulated that the stress intensity factor--itself a

function of stress and crack length--is the overall

controlling factor of FCP process. These findings and the

subsequent application of linear fracture mechanics to

fatigue studies allowed the description of the crack growth

rate as a function of the stress intensity factor at the

33

crack tip. A general equation of FCP could be written as:

$$\frac{da}{dN} = f(\Delta K, R) \qquad [31]$$

where   R= stress ratio $= \dfrac{P_{min}}{P_{max}}$

If other parameters were taken into account a more general
relationship could be written as:

$$\frac{da}{dN} \cong \frac{\Delta a}{\Delta N} \cong F(\Delta K, R, K_{max}, frequency, temperature, \ldots) \qquad [7]$$

To determine the component life one must integrate the above
formula:

$$N_{failure} = \int \frac{da}{F(\Delta K, R, K_{max}, frequency, \ldots)}$$

If the increase of the crack length is plotted versus the
number of cycles that propagated it, to such a length a curve
similar to the one in Figure 16 is obtained.

The curve of log crack propagation rate versus log ΔK is
shown in Figure 17. This curve can be divided in stages I,
II and III. It must be emphasized that in some extent these
three stages are similar to the general three stage division
of the fatigue phenomena as described in section 2.1. To be
more accurate the inferior limit of the stage I as given in
the curve from Figure 17 is equivalent to the stage I
(initiation), whereas the superior limit of the
stage III as given in the curve corresponds to the stage III

34
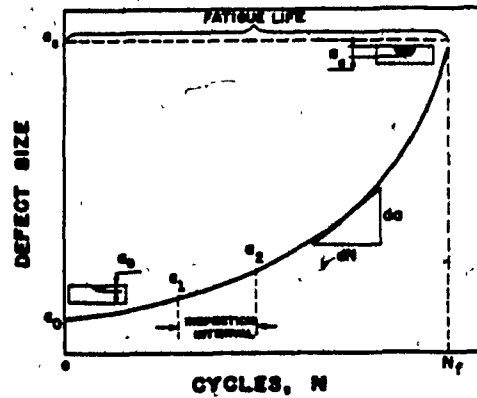
Figure 16

Crack length "a" as a function of number of cycles "N" (schematic) [7]
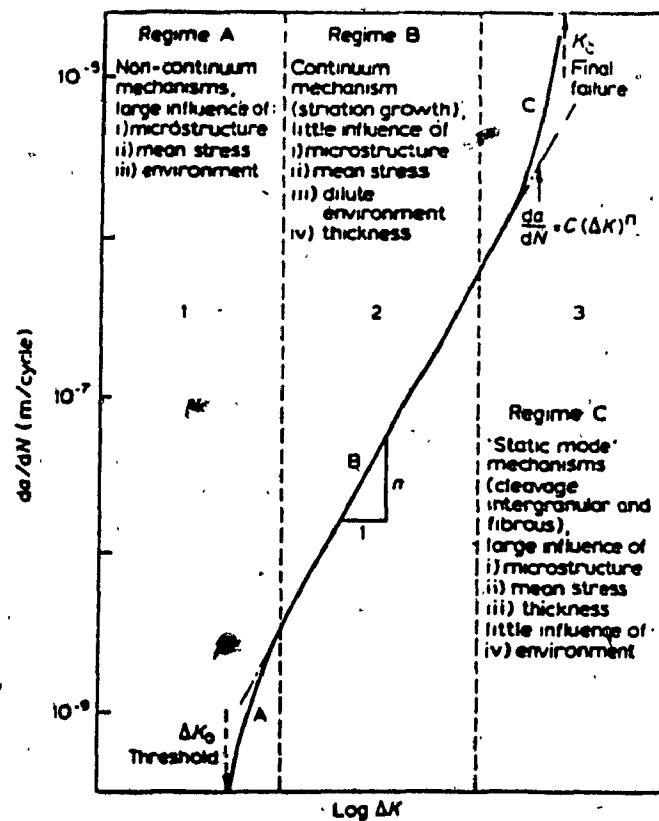
Figure 17

Typical fatigue crack growth curve (log da/dN versus log ΔK) [32]

(fast final failure) of the general description of the fatigue phenomena.

As Ritchie summarized [33] "In stage I the crack propagation mechanism is characteristic of a non continuum medium. The microstructure has a large influence, as well as the stress ratio R and environment. In stage II crack propagation mechanisms are typical of a continuum medium. The microstructure, R, environment, thickness had little influence on FCP. In stage III crack, propagation mechanisms are similar to those in a static mode. The microstructure, R, and thickness have large influences but not the environment."

A) Linear propagation models (no load interactions)
The second stage can be described mathematically by formula:

$$\frac{da}{dN} = C(\Delta K)^n$$

This formula is known as the Paris-Erdogan law. A large amount of work was done to establish accurate values for c and n, and several models were proposed. Irving and McCartney [34] made a classification of models based on comparing the value of n.

"1) Models based on instantaneous value of crack opening displacement (COD) and these lead to values of n about 2.

2) Models based on damage or strain accumulation and

these can predict the onset of rapid acceleration as K approaches K_{IC} and give values of n about 4.

3) Models based on energy balance concepts within a crack tip process zone where values of n in the range of 2 to 4 are obtained, depending on the plastic zone size used." Broek, Schijve and Walker realized that the Paris equation is valid only for fixed R (mean stress ratio), while the FCP rate function is really $da/dN=f(\Delta K, R)$. Therefore a new model, known as Walker model has been proposed.

$$\frac{da}{dN} = C \frac{\Delta K^{m+n}}{(1-R)^n}$$

Further Foreman tried to develop on equation taking account that the FCP rate curve is not a straight line, when the crack size becomes so large that $K_{max} = K_{IC}$. In other words the Foreman model tries to extend into the stage III where da/dN becomes infinite when the fracture occurs:

$$\frac{da}{dN} = \frac{C\Delta K^n}{(1-R) \, K_{IC} - \Delta K}$$

Brown and Cowling [32] showed that very few models provide a good fit for the threshold region (stage I). Schijve proposed a model which takes into account the apparent threshold stress intensity level:

$$\frac{da}{dN} = \frac{C \, (\Delta K - \Delta K_{threashold})^m}{(1-R) \, K_C - \Delta K}$$

B). Load interaction models

The mathematical models became more complicated if they take into account the overload retardation effect. Three models will be summarized:

    a) Wheeler model

    b) Willenborg model

    c) Elber model

a) The Wheeler model proposes an estimation of the retardation of crack growth rate by using a retardation factor: C_p

$$C_p = \left[\frac{R_y}{a_p - a}\right]^m \qquad \text{for } (R_y + a) < a_p$$

$$C_p = 1 \qquad \text{for } (R_y + a) \geq a_p$$

For identification of terms see Figure 18; m is a shape-fitting parameter that must be experimentally determined for each condition of material, loading and environment.

b) The Willenborg model does not use an empirical shape factor, but uses the material yield stress to compute the plastic zone size. Willenborg model corrected by Gallagher
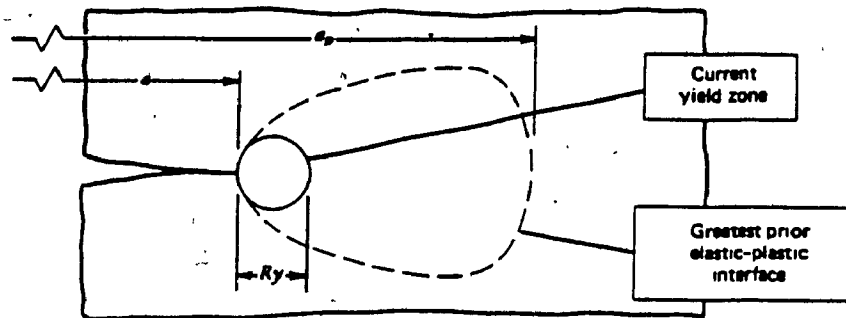
Figure 18

Description of Wheeler model for crack growth retardation.
[3]

can be written as: $K_R^W = K_{max}^{OL}\left(1 - \dfrac{\Delta a}{Z_{OL}}\right)^{1/2} - K_{max}$

where

K_R^W is the Willenborg residual stress intensity factor.

K_{max}^{OL} is the maximum stress intensity for the overload cycle.

K_{max} is the maximum stress intensity for the current load cycle.

Δa is the crack growth increment between the overload cycle and the current cycle (see Figure 19).
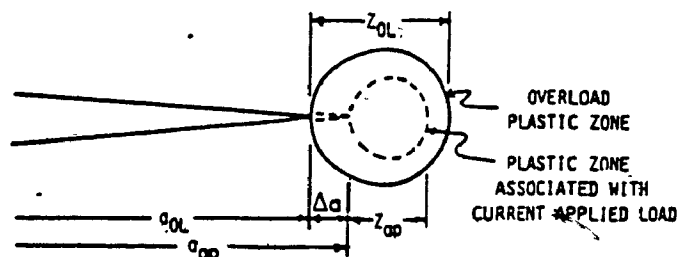
Figure 19

Plastic zones at the crack tip as described by Gallagher.

39

c) The Elber model is based, as described before, on the crack closure effect and uses a closure factor which is determined from constant amplitude data.

$$\frac{da}{dN} = C\left(\Delta K_{eff}\right)^m$$

or

$$\frac{da}{dN} = C\left(U\Delta K\right)^m$$

where U = effective stress range ratio

$$U = \frac{S_{max}-S_{op}}{S_{max}-S_{min}} = \frac{\Delta S_{eff}}{\Delta S}$$

and where

S_{max} = maximum applied stress

S_{min} = minimum applied stress

S_{op} = stress level at which the crack is just fully open

It must be emphasized that numerous other models have been proposed, the majority of which are really modifications of these classical models. As an example "The Multi-parameter yield zone model" (MPYZ) proposed by Johnston [35]

40

is a derivation of Willenberg model to account for "such recognized load interactions as retardation caused by previous overloads, acceleration due to current overloads and underload effects."

C) Submicroscopic models

Kanninen and co-workers [21] described the sequential process used to propose a model based on a new approach, that of dislocation distribution at the crack tip. First they synthesized the basic features that are generally accepted as playing an essential role in the F.C.P. process:

1. The interaction between the plastic deformation produced by the current load and the residual plasticity created in previous load cycles.

2. The connection that exists between the local deformation at the crack tip—as characterized by the crack-tip opening displacement—and the crack growth increment.

3. The impingement (closure) of the crack faces during the unloading portion of the load cycle.

While most models take into account one of these features, no model is currently known to incorporate them all. Based on this idea and on the criteria described in section 2.3.1 Kanninen and co-workers proposed the superdislocation model.

The basic element in this new model was the
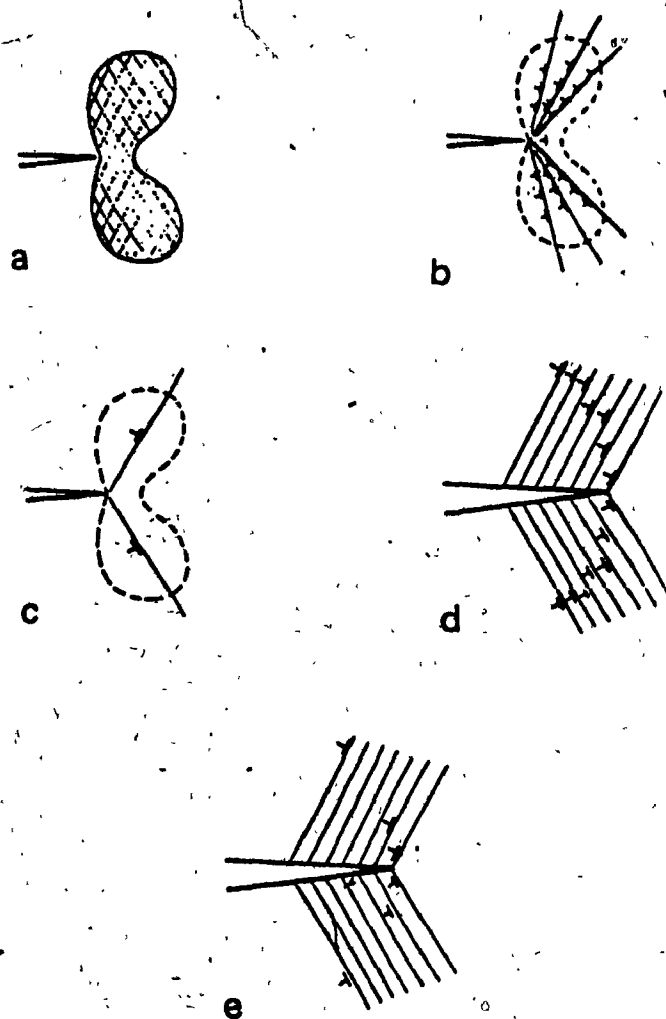
(a) Plane strain plastic deformation at the tip of a crack under fixed load.
(b) Representation of crack-tip plasticity by dislocation arrays.
(c) Representation of crack-tip plasticity by a superdislocation pair confined to slip planes emanating from the crack tip.
(d) Representation of crack-tip plasticity during fatigue by superdislocations.
(e) Representation of crack-tip plasticity during fatigue by combination of super-dislocations and super-superdislocations.

Figure 20

Evolution of a fatigue crack growth model using the inclined superdislocation representation of the crack tip plastic zone.

42

consideration that the macroscopic plasticity could be considered in terms of disloctions arrays. Figure 20 illustrates the sequential process of the model evolution. Figure 20a shows a typical plastic enclave surrounding a crack tip under plane-strain conditions. Figure 20b shows an equivalent way of characterizing crack-tip plasticity by using the dislocation arrays. This was the base of Bilby and Swinden's [36] approach of inclined dislocation slip plane. Atkinson and Kay [37] substituted the dislocation array by the concept of superdislocation Figure 20c. The superdislocation is considered to be a dislocation of an arbitrary strength on a given slip plane that represents the net effect of the entire plastic zone. Figure 20d shows the same concept applied for each cycle during FCP. Figure 20e represents the applicability of the superdislocation concept to display the loading history plastic zones in the wake of the crack tip . A synthesis of the advantages and disadvantages of different models in respect to the superdislocation model is given in table 3.

A recent publication [38] presents a general classification and chronology of FCP models, table 4.

In conclusion it is worthwhile to emphasize that none of the multitude of proposed models and concepts can be employed with complete success. However for practical use, in the aircraft industry, the Wheeler and the Willenberg models are

Table 3

Analytical procedures for the predictions of fatigue crack growth. [21]

Technique	Investigators	Strong Points	Weak Points
Semiempirical extensions of linear elastic fracture mechanics	Wheeler, Willenborg, Engle and Wood, Elber	Gives simple relations that are easy to apply; offers insight into controlling mechanisms	Lack of firm fundamental basis; difficulty in treating complicated histories; cannot easily be generalized
Dugdale strip yield model with cumulative crack-opening displacement criterion	Rice, Weertman, Bilby and Heald	Gives closed-form result for steady-state growth rate	Cannot distinguish load history effects; crack closure does not occur
Inclined strip-yield superdislocation model with critical crack-opening displacement criterion	Kaninen	Plastic deformation in different load cycles is distinguishable; closure effects handled directly; can be generalized to treat wide range of situations	Computations for complicated load histories may require lengthy computation
Elastic-plastic finite-element analysis	Newman and Armen	Highly accurate; can be used to treat wide variety of situations; useful for examining details of crack growth process	Very time-consuming computations so only a few load cycles can be treated; crack extension criterion must be arbitrary

— Accuracy / Convenience —

Table 4

Chronology and classification of fatigue crack growth models. [38]

YIELD ZONE MODELS	CLOSURE MODELS
WHEELER 1970	ELBER (CONCEPT) 1969
WILLENBORG, ENGLE, WOOD 1971	BELL (GENERALIZED CLOSURE) 1974
	NEWMAN (FINITE ELEMENT) 1974
VROMAN 1971	DILL AND SAFF (CONTACT STRESS).... 1976
PORTER 1971	KANNINEN, PEDOERSON, ATKINSON (SUPER-DISLOCATION) 1976
GRAY (GENERALIZED WHEELER)..... 1972	
GALLAGHER AND HUGHES (GENERALIZED WILLENBORG) 1974	ELBER (MODEL) 1976
	PARIS 1976
JOHNSON 1981	BUDIANSKY AND HUTCHINSON 1978
CHANG ET AL...... 1981	DE KONING 1980

the most used as a result of their incorporation in the CRACKS routines for crack propagation analysis. At Canadair, during the Challenger certification, the CRKGRO program option was selected. CRKGRO is a program incorporated in RASSP (Rockwell Automated Stress Spectrum Program) system. "CRKGRO is based on the modified Walker equation for positive stress ratio and the Chang equation for negative stress ratio. It includes an improved load interaction model that accounts for retardation and acceleration effects. This interaction model is essentially the generalized Willenborg model...modified for compressive effects by the overload interaction zone concept proposed by Chang."[4]

2.3.2 Macroscopic aspects of F.C.P.

The general macroscopic appearance of a fatigue fracture is usually characterized by typical circular or eliptic markings called "beach marks." These marks, which are associated with the crack arrest, are considered to be generated by differences in corrosion attack at the moment when the crack is stopped, or by changes in the applied loading.

In addition, macroexamination of failed components subjected to different loading conditions, different stress intensities and different directions of loading, revealed that all these parameters have also an influence on the
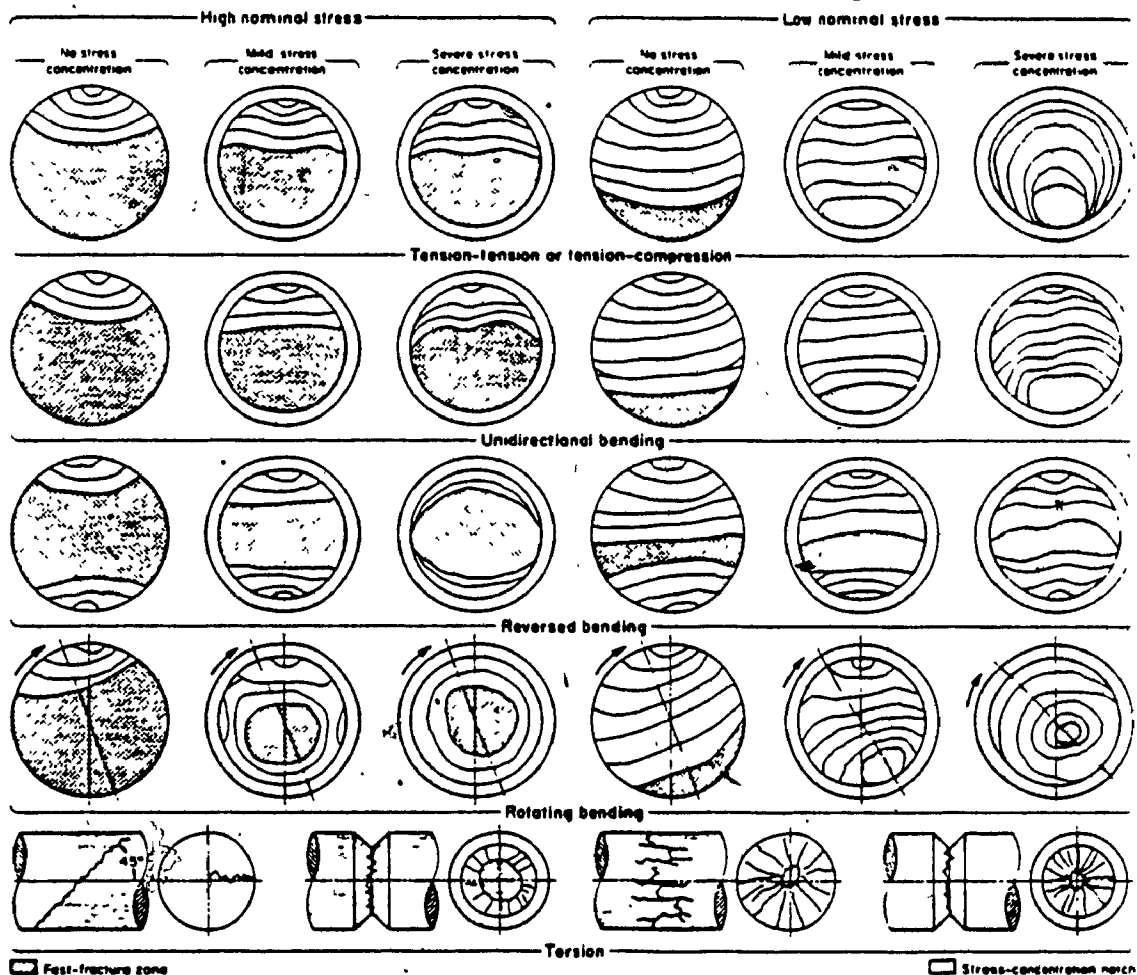
Figure 21

Schematic representation of macroscopic fatigue appearance as a function of stress, stress concentration and mode of loading. [39]

general macroscopic appearance of the fracture. A synthesis of these typical appearances is given in Figure 21.

Beside these typical fatigue macroscopic markings, the fractures of fatigue specimens can be rather different in respect to the fracture plane inclination. These changes in

46

the fracture plane inclination are strongly related to the stress factor and to the plastic zones created at the crack tip. It has been observed that when the stress intensity factor is low (as a result of a low applied stress and/or a small crack size), and then the plastic zone created at the crack tip is small compared to the large component thickness, plane strain conditions prevail and a flat fracture is observed. By subsequent propagation, the crack length increases and therefore the stress intensity factor and the plastic zone increases. If the plastic zone size is large compared to the component thickness, then plane stress conditions prevail and a slant fracture is expected, Figure 22.

The microscopic irregularities have an important influence on the plastic zone of the crack tip and the macroscopic and microscopic crack behaviours are strongly dependent on this effect. Recent research [40 ,41] done by Forsyth attempt to correlate the crack behaviour with these microscopic irregularities. In an attempt to explain the phemomena of crack front tunnelling (the crack front assumes a curved shape and propagates faster in the middle of the specimen than on its edges) and subsequent tensile jumping this work considers that in addition to the stress intensity factor and the plastic zone, another controlling parameter, the total crack front length, must be taking into
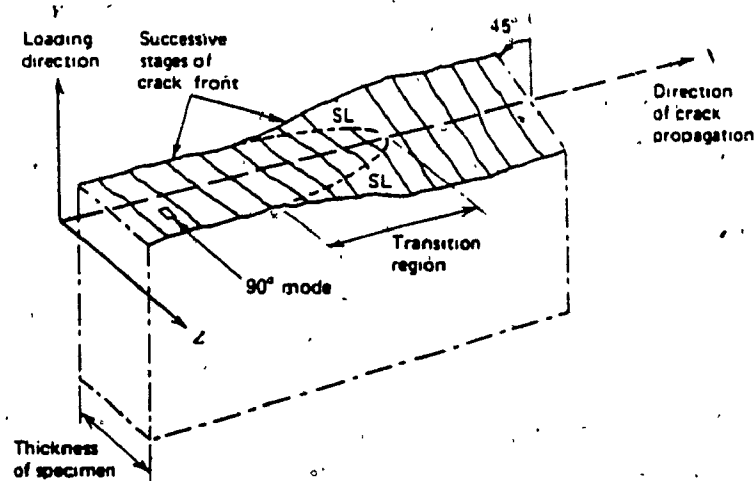
Figure 22

The inclination of the fracture plane in respect to the
specimen thickness. [13]

consideration in both micro and macroscopic crack behaviour.

A general equation which considers this parameter has been

established:

$$\frac{\sqrt{a}}{L} = \frac{K_{IC}}{1.1 \cdot L_0 \cdot \sigma_{max} \cdot \sqrt{\Pi}}$$

where a = maximum depth of crack

L = crack front length

L_0= plate thickness = shortest possible

crack-front

The experiments performed showed that "when the crack

front is greater than the equlibrium length, then rapid

fatigue growth can take place with the ductile striation mode

48

in evidence, but where the crack front is less than the
equilibrium length either small tensile jumps or fatigue
crack growth with brittle "cleavage like" striations occurs"
[16]. In other words, "fatigue cracks try to maintain an
equilibrium shape (which represents an energy distribution)
for the stress and constraints that exist. "Temporary
perturbation of this shape by other influences is
subsequently countered by local changes in fatigue crack
growth rate" [40]. This research also revealed that in any
non-homogenous material such as most commercial alloys
"microstructural features cause break up of the front into
segments that relate to elemental blocks operating with some
degree of independence from their neighbours, but under
general influence of the macroscopic crack of which they are
a part. These segments of crack front develop their own
curvature, the radius bearing a close relationship to the
lateral dimension of the element concerned." [41] It must be
emphasized that an important effect of this segmentation of
the crack front is the "considerable local differences in
fatigue growth rate and a considerable increase in the total
crack front length." [41].

2.3.3. Microscopic aspects of F.C.P.

On the microscopic scale, fatigue cracking is
characterised by a typical feature called fatigue striations

49

Figure 23.   The fatigue striations are parallel lines oriented in the general direction of the advancing fatigue crack front. These microfeatures must not be confused with the macrofeatures called "beach" marks.   Hundreds or even thousands of fatigue striations can be concentrated between two beach marks.   The fatigue striations represent the crack advances, whereas the "beach" marks represent a crack arrest over a number of low stress cycles.

Consequently, the understanding of the mechanism of the striation formation, their different appearances, the relation between the applied spectrum of loads and the succession and of spacing striations became the object of numerous studies.   The result of these studies helped the understanding of the whole process of fatigue cracking.
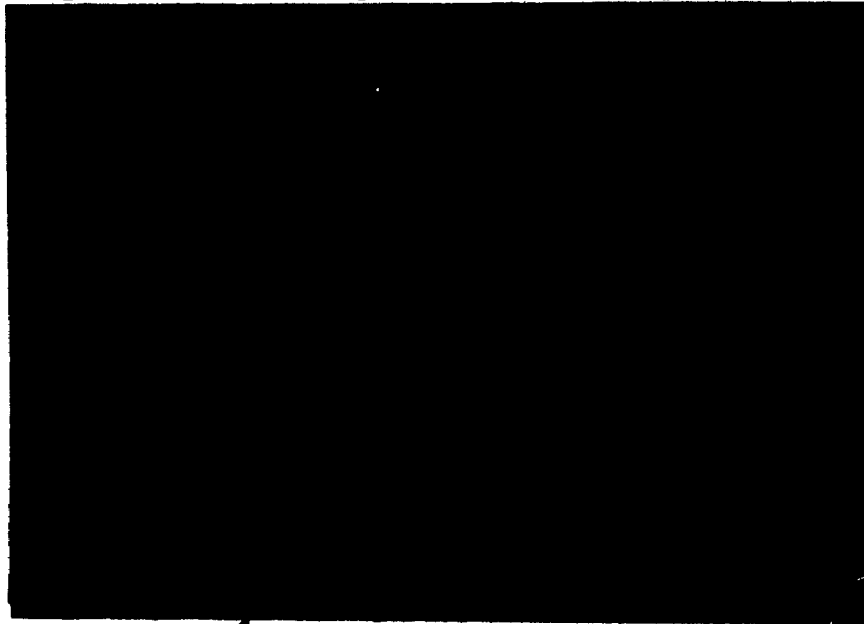
Figure 23

Typical fatigue striations. [42]

2.3.3.1. Striation formation

Basically two models have been proposed to explain striation formation:

1) The blunting - resharpening model proposed by Laird [8]

2) The crystallographic model proposed by Hertzberg [43]

The plastic blunting process as proposed by Laird is depicted in Figure 24.   The analysis begins with the cracked specimen at zero load, Figure 24a. When the tensile load stage of the cycle begins, the small double notch at the crack tip serves to concentrate slip zones along planes at 45 deg. to the plane of the crack and to maintain a square geometry of the
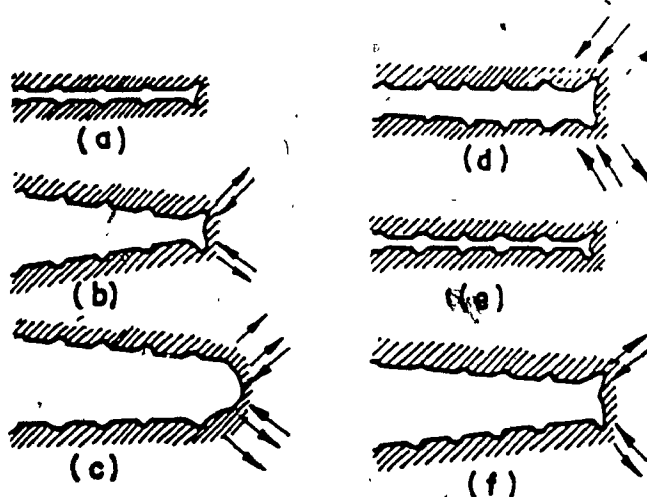
Figure 24

Fatigue crack growth by plastic blunting mechanism: (a) zero load; (b) small tensile load; (c) maximum tensile load; (d) small compressive load; (e) maximum compressive load; (f) small tensile load.   The loading axis is vertical. [8]

51

tip Figure 24b. At the moment of maximum tensile strain, the

stress concentration effect is reduced, the slip zones are

extended, and the crack tip blunts to a semicircular

configuration, Figure 24c. When the compression load stage

of the cycle begins, the slip direction is reversed, Figure

24d, and the "hinge" effect forces the crack faces to touch

each other. New crack surfaces are created in tension and

the crack plane is partly folded by buckling at the tip into

new notches, Figure 24e. The formation of these notches

represents the resharpening stage of the crack tip.

One criticism of this model is that it would explain

only the striation formation in a tension-compression type of

loading. However, as it has been demonstrated in previous

sections, even in tension-tension or tension-zero loading,

compression loads appeared due to the crack closure

phenomena. Extensive experimental evidence is given by Laird

[8] to support his blunting-resharpening model of striation

formation even in loading spectra other than tension-

compression. Another criticism of the above model is that

the plastic blunting model would explain only the formation

of those striations which matched peak to peak and valley to

valley. Hertzberg showed [13] that "the striations are

considered to be undulations of the fracture surface with:

a) peak-to-peak and valley-to-valley matching of the two

surfaces

b) matching crevices separating flat facets

c) peak-to-valley matching"

A representation of some of these morphologies is given in Figure 25. Figure 25a and c represents peak-to-peak and valley-to-valley matching. Figure 25b represents matching crevices separating flat facets and Figure 25d represents the peak-to-valley morphology. Laird [8] demonstrated that both morphologies peak-to-peak and peak-to-valley can be explained by his model.
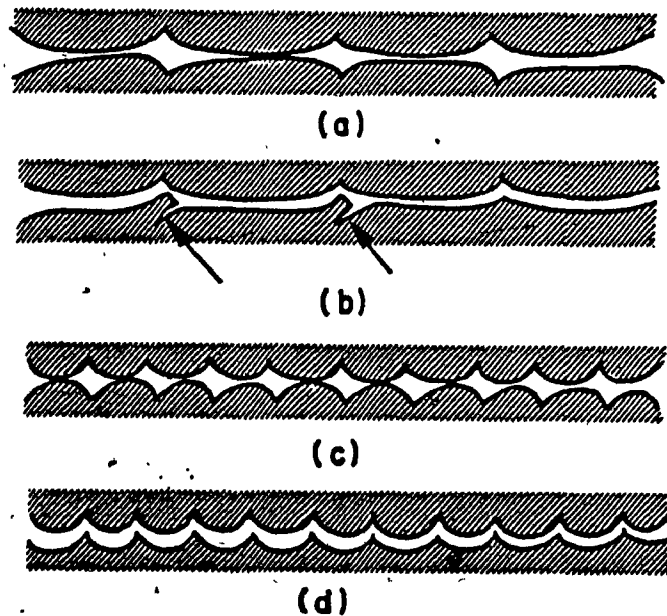
Figure 25

Various types of morphology exhibited by striations on ductile fatigue fracture surfaces, viewed in profile. The stress axis is vertical. [8]

Hertzberg showed [13] that Laird's model involves plastic

blunting of the crack tip regardless of the material microscopic slip characteristics. He proposed [43] another model of striation formation which takes account of crystallographic considerations. Hertzberg stated that when metals plastically deform only specific slip systems are operative. For example, in the FCC metals, the slip will occur only on {111} <110> type systems. The {111} planes would be the fracture planes while only two of the three possible slip directions would be operative. But the direction of slip is not parallel to the direction of crack propagation. Consequently, the fracture surface should exhibit presence of slip markings on the fatigue striations which are not parallel to the direction of crack growth. Hertzberg produced [43] the experimental evidence of these slip markings, Figure 26. This model explains why in a given material sometimes very well defined fatigue striations are seen and in other situations the fatigue striations are poorly resolved or can not be seen at all. The favourable crystal orientation is the answer to that.

In conclusion, the predominance of one or another of these two mechanisms depends probably on the ΔK level. It is very probable that at low ΔK levels, the crystallographic mechanism dominates striation formation and the fact that few slip systems are operative at such ΔK levels can be the
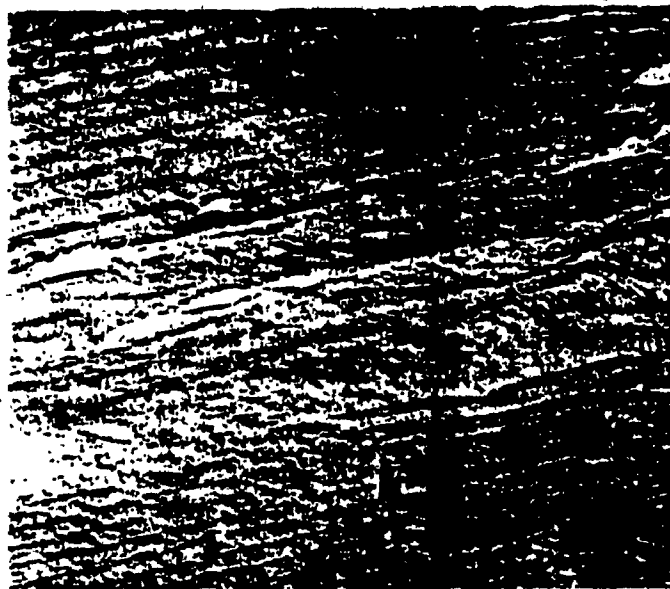
Figure 26

Fractograph of 7075-T6 aluminum alloy showing slip markings
on side of striation wall which are most parallel to the
direction of crack propagation (arrow). Magnification x8900.

reason for poorly defined or non-existent striations close to
the initiation site.   At high ΔK levels, the plastic blunting
of the crack tip probably dominates the striation formation.
These observations are exactly in accordance with the
observations made by Ritchie (see section 2.3.1.4) with
respect to the influence of different parameters on stage I
and stage II of F.C.P.

2.3.3.2. Influence_of_various_parameters_on_the_fatigue
striations

    Examinations of numerous fatigue fracture surfaces
revealed that fatigue striations have two different
appearances:
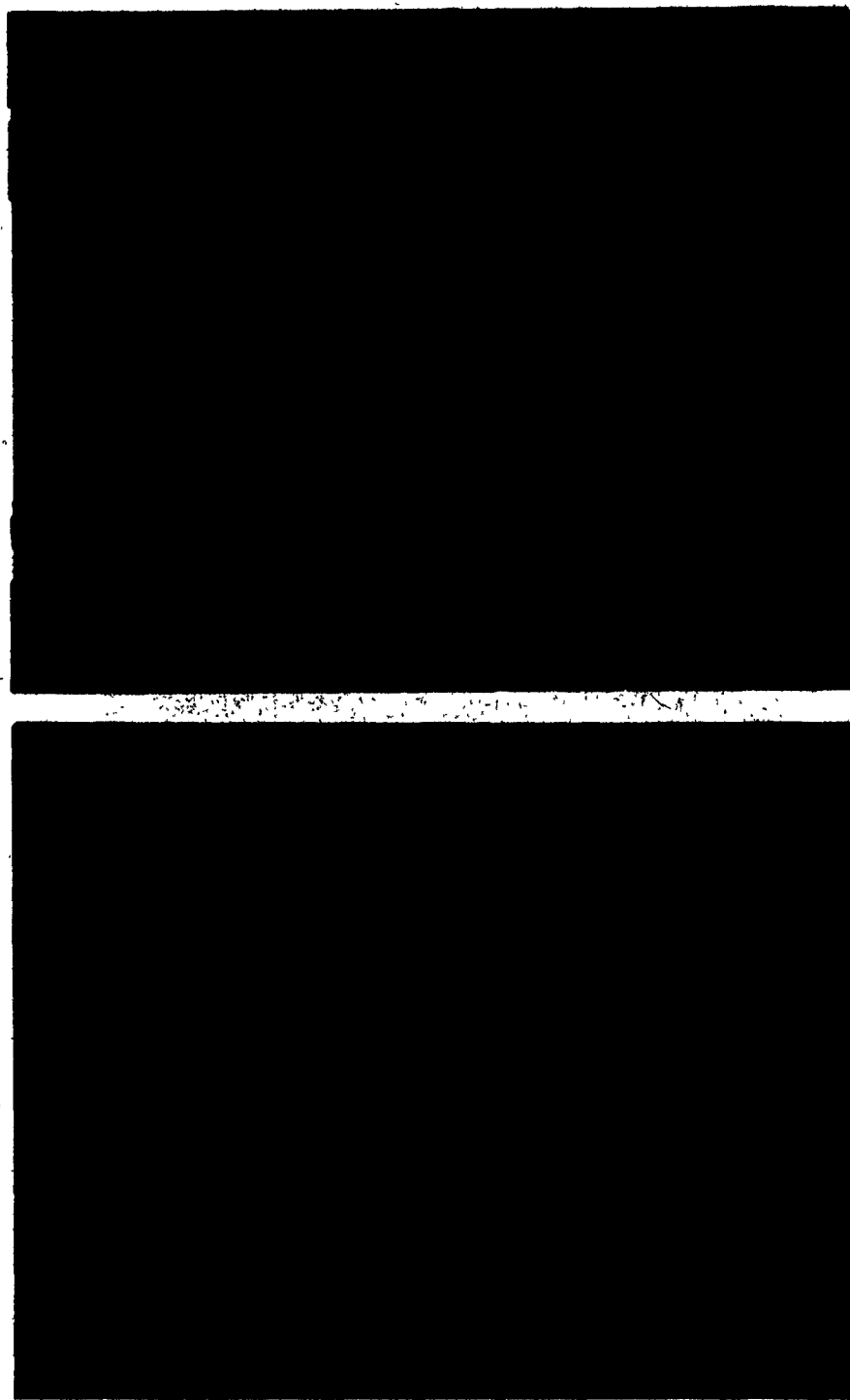
Figure 27

a) High density "ductile" fatigue striations
   Magnification 4000x [44]
b) High density "brittle" fatigue striations
   Magnification 2300x [44]

56

"brittle" or "ductile", Figure 27.

Laird was one of the first investigators who observed the differences in appearance between the two kinds of fatigue striations and defined them [45] as:

- The "brittle" appearing or cleavage-like striations are characterized by very flat fracture facets and by river patterns running parallel to the direction of crack propagation.

- The "ductile" appearing striations are characterized by a good definition, and uniformity.

The formation of either brittle or ductile fatigue striations was found to be related to the following three parameters:

- Stress intensity factor, ΔK

- Environment

- Metallurgical factors

2.3.3.2.1. Influence_of_ΔK

An extensive search of the influence of ΔK on the appearance of fatigue striation was done by Hertzberg and Mills [46]. Basically this work revealed that a strong relationship exists between the fatigue cracking micromorphology and the level of ΔK. This relationship is best illustrated in Figure 28. At low ΔK levels (close to ΔK threshold) which corresponds to ultra low crack growth regime ($da/dN \sim 10^{-7}$ mm/cycle), the fracture micromorphology has a

cleavage-like appearance with facets oriented parallel to
[111] slip plane. Hertzberg believes that this faceted
appearance results from a glide plane decohesion mechanism
where reversed slip on a limited number of slip planes ahead
of advancing crack front weakens the cohesive strength of
atomic bonds in this region. When the slip planes have
weakened sufficiently, low tensile stresses initiate local
separation, thereby resulting in a crystallographic
appearance. At medium ΔK levels and low crack growth rates
($da/dN \simeq 10^{-6}$ mm/cycle) a series of parallel lines appear on the
fracture surface. These lines are not fatigue striations
(they are much too large to correspond to crack advance
during one cycle). Their spacing would seem to be roughly
constant ($\simeq 5 \times 10^{-5}$ mm). The mechanism of generation of these
parallel fracture markings is unknown, however Gell and
Leverant [47] proposed that markings represent slip offsets
produced in the wake of the crack front and are not related
to any crack growth increment.

At medium ΔK levels and medium crack growth rates ($da/dN \simeq$
$10^{-5} - 10^{-4}$ mm/cycle) well defined "ductile" fatigue striations
are produced, whereas at high ΔK levels and high crack growth
rates ($da/dN \simeq 10^{-3}$ mm/cycle) the fatigue striations become
coarser and secondary cracking can be seen. The final fast
failure is typical of overstress loading. Hetrzberg showed
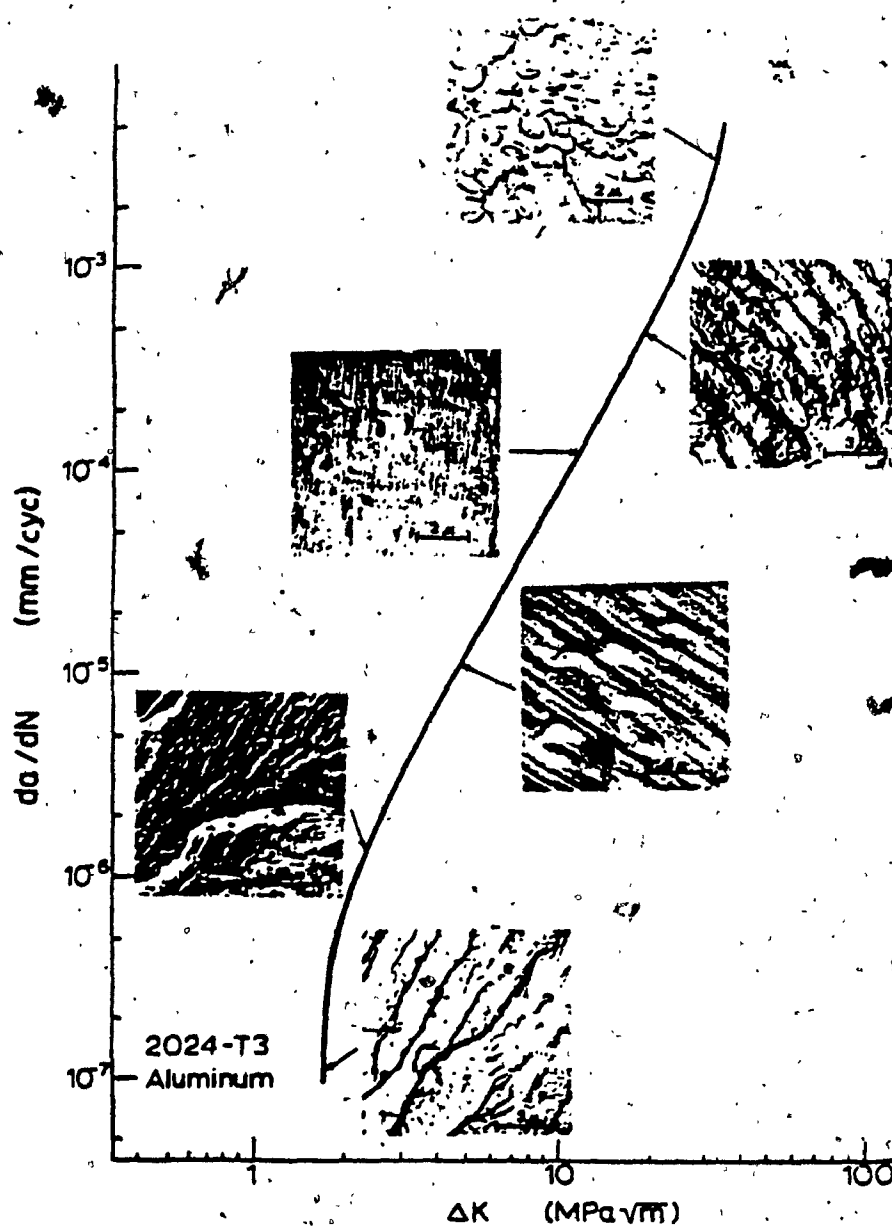
Figure 28

Composite photograph showing fatigue fracture surface
micromorphology at various points on the da/dN versus ΔK
curve for 2024-T3 aluminum alloy. [46]

even more dependence of striation appearance with respect to
ΔK.   In the case of an overload application, it has been
shown before (section 2.3.1.3.) that the phenomena of delayed
retardation occurs.   The F.C.P. rate decreases and if this
decrease is drastic, a faceted fracture surface results
(characteristic of ultra low growth rate), despite the fact
that the original F.C.P. rate was in the range of 10
mm/cycle, Figure 29.   The dependence of
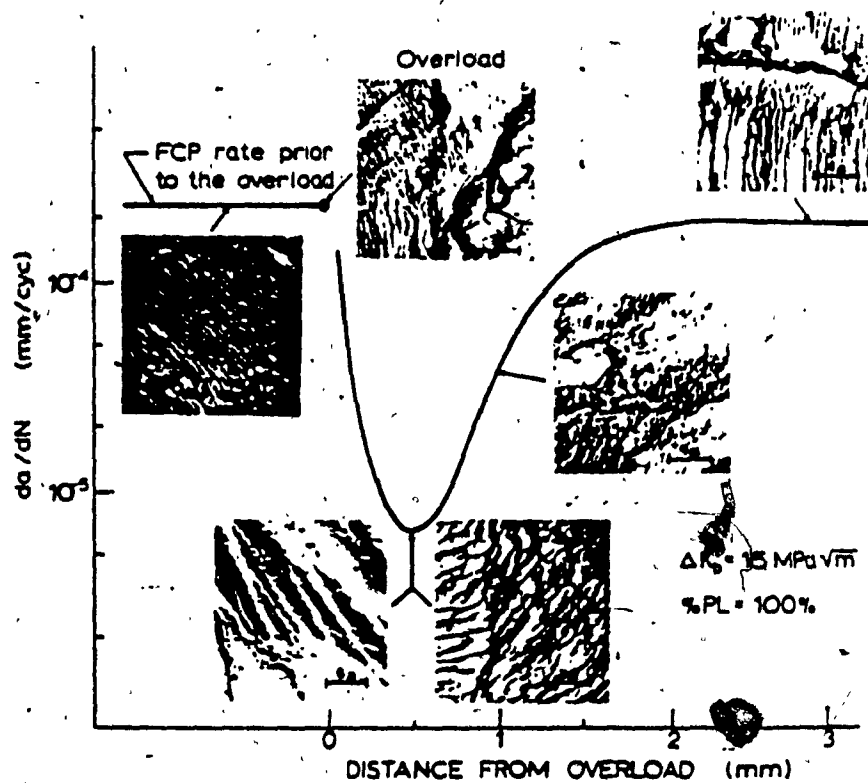
Figure 29

Fatigue crack propagation behaviour following an overload
with electron micrographs representing fracture surface
morphology at various positions from where the overload was
applied 2024-T3 aluminum alloy. [46]

60

fatigue striation appearance on ΔK level has an important
effect on fractographic examination. The failure analysis
investigator, often is faced with variations in striation
micromorphology and must decide if these variations are due
to overloading or due to the normal crack advance. It will
be shown later that this task is extremely difficult and only
minor indications provide some help in this dilemma.

Forsyth and Bowen tried to establish the influence of ΔK
level on the general macro and microscopic topography of
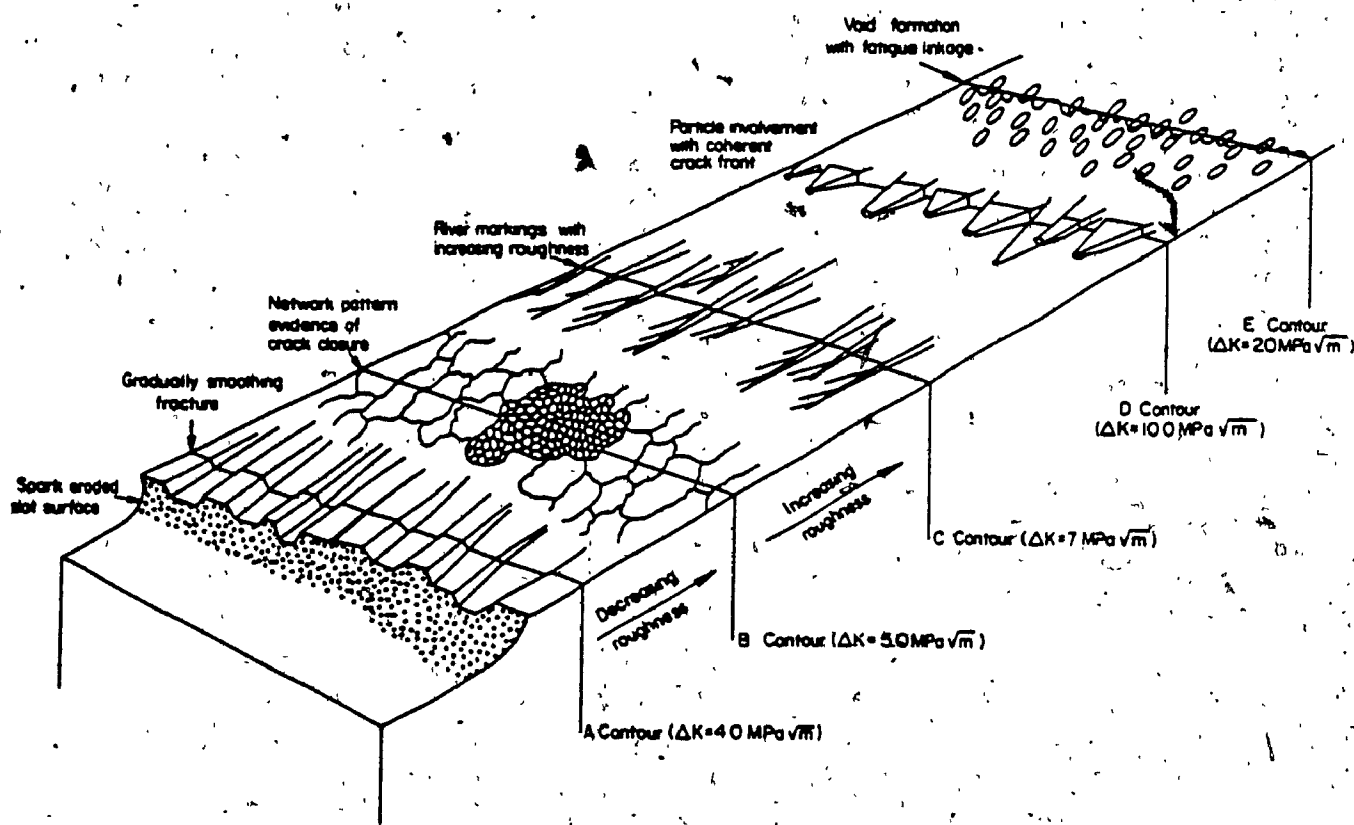
Figure 30

Schematic illustration of the cracking sequence in peak aged
7178 aluminum alloy; R = 0.1. [48]

the fracture. Figure 30 shows schematically, the changes in the roughness and in the fracture morphology of 7178 Aluminum alloy, peak aged, for a ΔK range of 4.0 - 20.0 MPa$\sqrt{m}$.

A numerical solution to quantify the relationship between the striation spacing and ΔK was given by Bates and Clark [49]:

$$S = 6\left(\frac{\Delta K}{E}\right)^2$$

where   S = striation spacing

             E = Young's modulus of elasticity

This empirical correlation allows the estimation of ΔK based on fractographic examiation for most metallic alloys, Figure 31. Similar empirical relationships were proposed by Hahn [50].

$$S \approx \frac{da}{dN} = 8\left(\frac{\Delta K}{E}\right)^2$$

and Hertzberg [51].

$$S \approx 24\left(\frac{\Delta K_{eff}}{E}\right)^2$$

However, it has been concluded [31] "for practical applications of failure analysis, the simple Bates-Clark expression which is independent of load ratio is adequate."
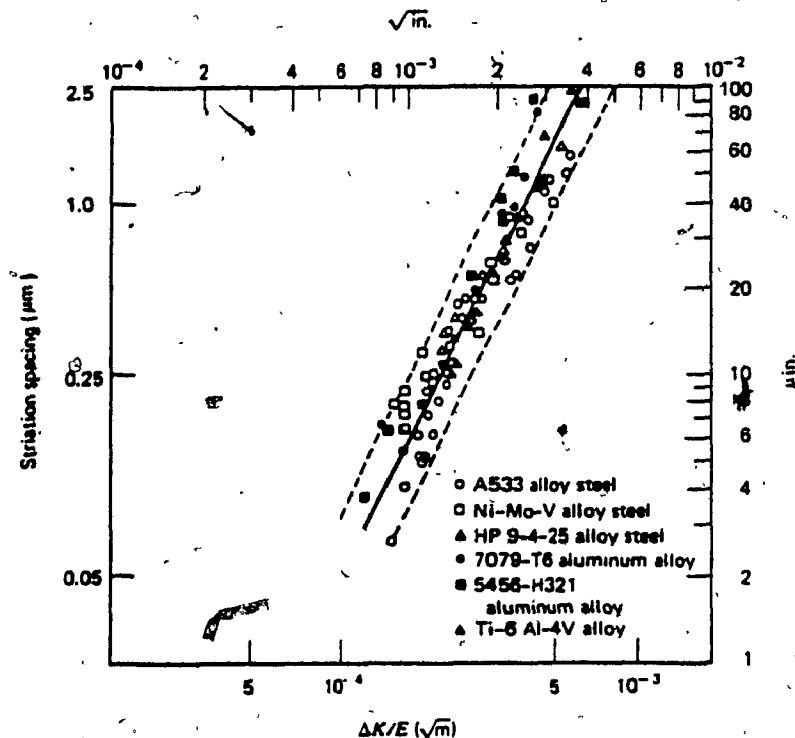
Figure 31

Correlation of fatigue striation spacing with ΔK normalized
with respect to elastic modules. [13]

2.3.3.2.2. Environment

Extensive research have been and are being carried out

to demonstrate the influence of the environment on F.C.P.

rates, and implicitly over fatigue striation appearance.

Despite the fact that this correlation is extremely important

on aircraft components due to the large range of

environmental conditions to which the airframe is subjected,

it was considered beyond the purpose of the present thesis to

pursue a deeper investigation into this field. A few of the environmental parameters which play a role in modification of the F.C.P. rates are: Temperature, Humidity, Agressivity.

Obviously these parameters can influence the F.C.P. rates and implicitly the fatigue striations appearance and spacing, in different ways depending on the component base metal. For the purpose of this thesis we will examine the influence of these parameters on aluminum alloys only.

Temperature

The effect of temperature on fatigue, fatigue crack growth and implicitly on the fatigue striations was analysed/ by several authors. Christensen and Harmon [52] found that "the fatigue life and physical properties degrade as temperature increases", Figure 32. Kaufman and Santer [45] found that fatigue crack growth rates below room temperature are about the same as or lower than those at room temperature", Figure 33. However, it must be emphasized that this particular research takes into account both the temperature and humidity effect on the fatigue crack growth rate and it will be explained in the next paragraph that the increase in humidity and the decrease in temperature have a contradictory effect.

Humidity

Humidity appears to play an important role on the F.C.P. rates and on the appearance of the fatigue striations.
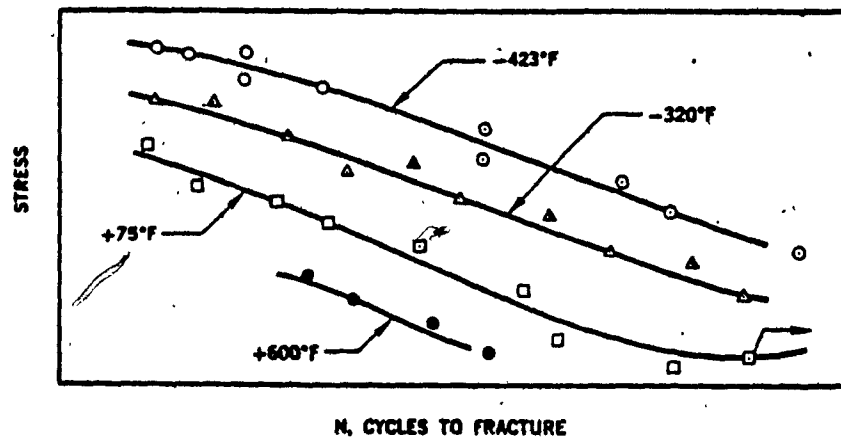
a)
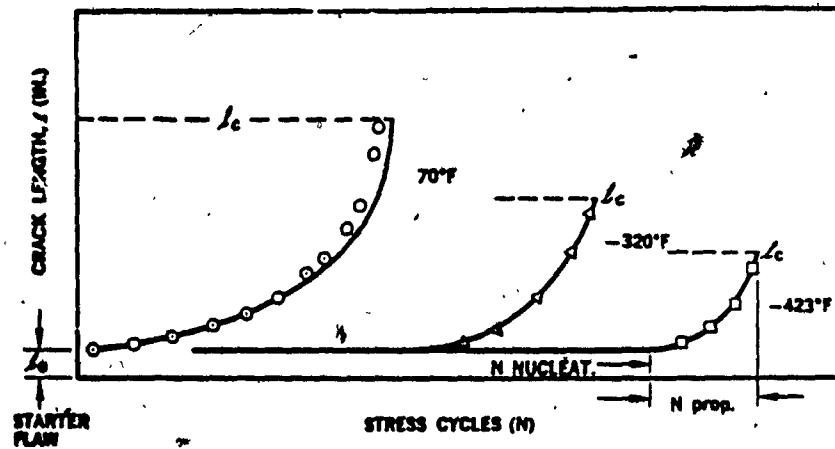
b)

Figure 32

a) Fatigue life as a function of test temperature (typical for most metals) [52]
b) Growth of fatigue cracks as a function of temperature (schematic) [52]

65

As shown in Figure 33 the F.C.P. rates for 5083-0 alloy are appreciably higher in moist air than in dry air. Similar results are indicated by other literature [13], as well.

An important contribution to the understanding of the influence of humidity on the F.C.P. rates is given by Hartman and others [53] who showed that the superiority in fatigue performance of 2024-T3 aluminum alloy versus 7075-T6 aluminum alloy is greatly minimized with elimination of moisture from the test environment. This is in accordance with the higher susceptibility to such environment of 7075-T6 than 2024-T3. All these findings would seem to indicate that the oxide induced crack closure phenomenon plays an important role. Similar conclusions are given in [26]. The morphological changes of the fatigue striations appearances due to humidity appear to be consistent with the macroscopic observations. Vogelesang [54] showed from theoretical models and confirmed by fractographic examinations that the environment "can essentially change the mechanism of crack growth." However with respect to the humidity, he showed that "a coherent crack front with blunted crack tip has been found" in specimens tested in humid air. In another work [55], Stubbington and Forsyth found that fatigue speciments tested in air exhibited only ductile type striations, whereas those tested in aqueous solutions exhibited brittle striations.
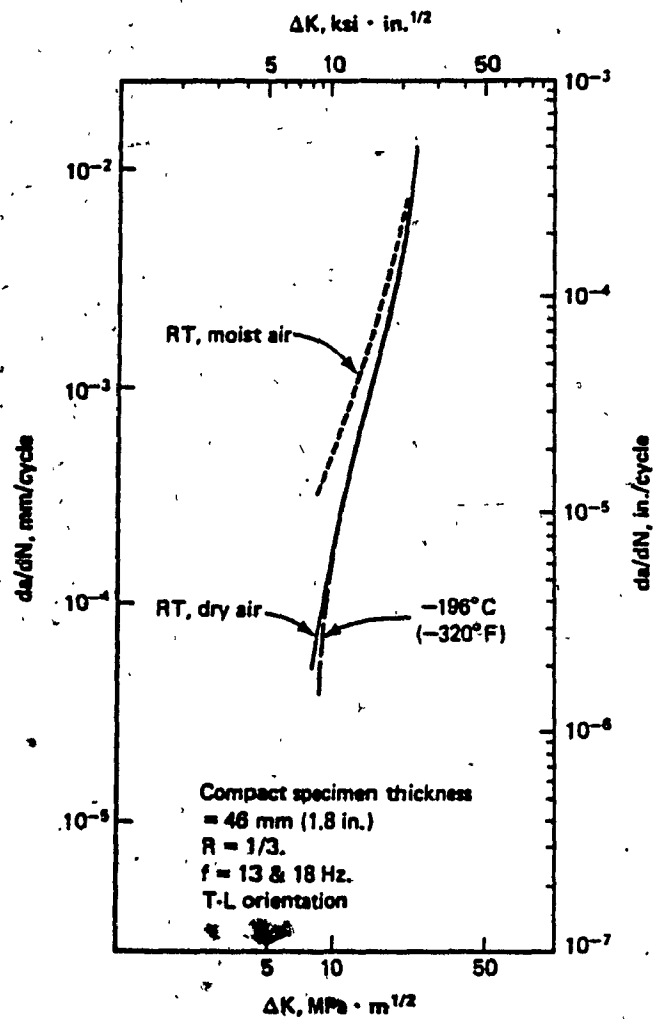
Figure 33

Effect of temperature and humidity on fatigue crack growth.
Material: 5083-0 Aluminum alloy [45]

A comprehensive analysis of the influence of the
environment (especially humidity) was performed by McMillan
and Hertzberg [6]. During the experimental program they
tested the relative effects of five environments on 7178-T6
aluminum alloy. The five environments were:

    a) desicated air (standard environment)

    b) high humidity air (90% relative humidity)

    c) distilled water

    d) aqûeus 3.5% NaCl solution

    e) hydraulic fluid (skydrol)

The results of these tests are shown in Figure 34 and they
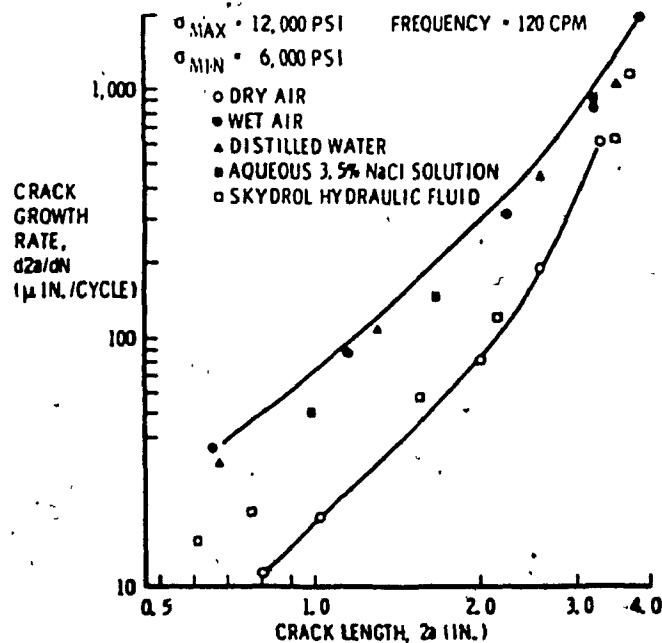
Figure 34

Effects of environments on crack growth rate of 7178-T6
aluminum alloy. [6]

68
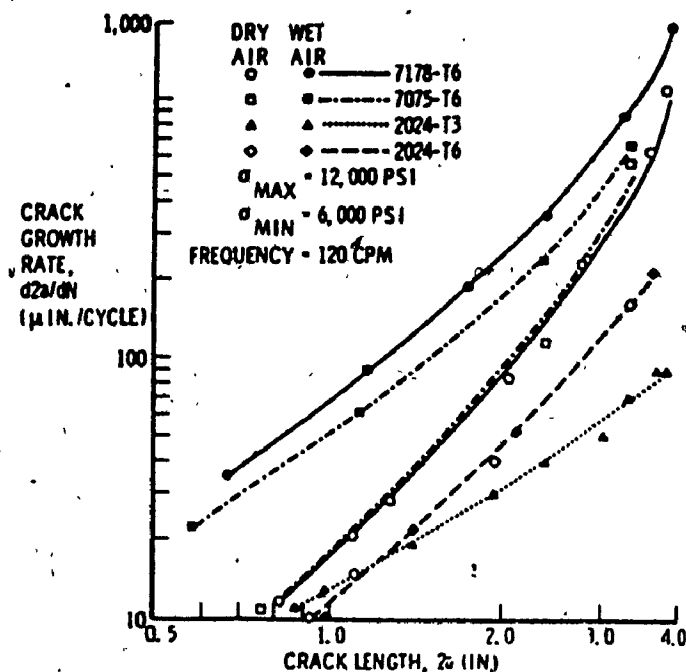
Figure 35

Crack growth rate of several aluminum alloys as a function of environment. [6]

confirm these observations: the F.C.P rates are accelerated by humidity and water. Fractographic examinations of these specimens showed that, in the case of desicated air, finely spaced ductile fatigue striations cover nearly 100% of the fracture surface. "In contrast the wet-air specimen (and the distilled water specimen) exhibit only isolated patches of ductile striations, while the remainder of the surface has a

brittle, cleavage like appearance." Hertzberg and McMillan pointed out that the changes in crack growth rates in dry and wet air are associated with a change in fracture mode from ductile to brittle striation formation. Another research program [6] determined the reaction of different aluminum alloys to dry-wet types of environments. The results given in Figure 35, confirm the results obtained by Hartman [53].

Aggressivity

The aggressiveness of the environment is also strongly associated with the modifications in F.C.P. (macroscopic) as well as changes in the fracture micromorphology. As mentioned above, Vogelesang made a comprehensive examination of the environmental effect on crack growth and even developed a model to explain the interaction between the micromorphology and the environment. His most important observations can be synthesized as follows "Fatigue crack growth rates are faster in a more aggressive environment and as soon as the environment is controlling the crack growth mechanism a more coherent crack front occurs." As a result of these observations Vogelesang stated that "more irregular and chaotic crack fronts have lower K values and as a consequence lower crack growth rates." Vogelesang and Schijve [54] also determined the correlation between other modes of failure such as stress corrosion cracking and corrosion fatigue on the F.C.P. rates. For the practical

70

purposes of fractographic examination it is shown in [56]
that "in aluminum alloys tested in a corrosive environment
(water or sea-water), the striations form on crystallographic
fracture planes and are called "brittle striations... within
each grain, the fracture path associated with corrosion
fatigue looks like a cleavage plane."

2.3.3.2.3. Influence of the microstructure

Fractographic examination of fatigued specimens of
different alloys revealed that, in similar testing
situations, the appearance of the fatigue striations differ
from metal to metal. Aluminum alloys are known to form well
defined fatigue striations. However, as shown in [56] "in
steel, fatigue striations that are formed at ordinary crack
growth rates are not always as well defined as they are in
aluminum alloys." Some attempt to explain the differences in
the fatigue striation appears had been made as early as 1963,
when McEvily and Boettner [57] explained the difference in
the curvature of striations observed in several alloys in
terms of stacking fault energy of the material. In other
papers, the appearance of fatigue striations is related to
the metal ductility [39]: "The clarity of the fatigue
striations depends on ductility of the material. Striations
are more visible at stress levels higher than the fatigue
limit: also they are more readily visible in ductile

materials." The majority of airplane structural components
are manufactured of various aluminum alloys and therefore it
was considered appropriate to study the microstructural
influence on fatigue striations and F.C.P. in these
materials.

As stated above, aluminum alloys usually form well
defined fatigue striations in inert or non corrosive
environments. However, an important factor to be accounted
for is the multitude of particles and dispersoids which one
normally expects in precipitation hardening materials. These
inclusions and precipitates will strongly affect the F.C.P.
and the fracture micromorphology. Several studies consulted
[58,59,60] pointed out the role of these microscopic features
in respect to the advancing fatigue front. Kauffman showed
[58] that there are three basic components of the structure
which play a role in fracture resistance:

  a) coarse intermetallics

  b) grain boundaries

  c) matrix containing solute or precipitates.

a) The coarse intermetallics (normally ≥ 1 μm) are normally
insoluble (such as: Al_7Cu_2Fe, Mg_2Si) or relatively soluble
(such as: $CuAl_2$, $CuAl_2Mg$); they fracture first on stressing
and become the initial sources of fatigue cracking. A
schematic [59] of tensile crack extension by coalescence of
mircovoids nucleated at particles is shown in Figure 36.
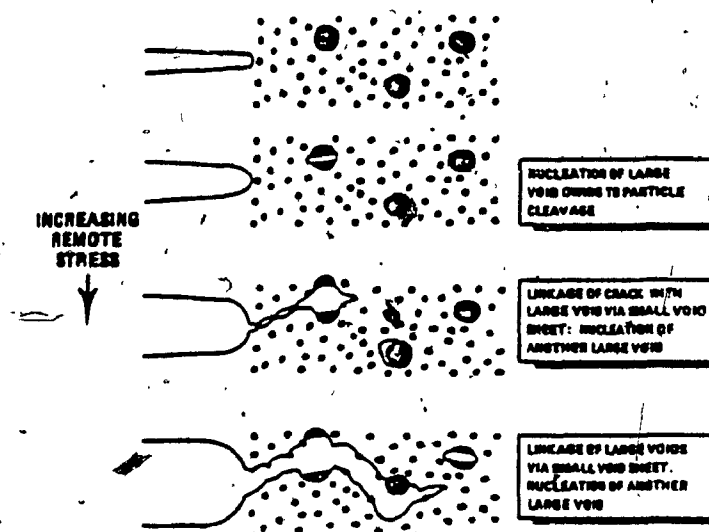
Figure 36

Schematic of tensile crack extension by coalescence of microvoids nucleated at particles and dispersoids [59].

As a result of the brittle manner in which these particles are fractured one must expect to find evidence of tensile jumping when examining fractures of aluminum alloys specimens tested under fatigue loading. Indeed this phenomena has been reported in several works [40, 41, 48 ,59] and the author of this thesis found evidence of this morphology in many cases of fatigued specimens. Another group of particles (normally 0.03 to 0.5 µm in diameter) consists of dispersoids such as $Al_{12} Mg_2 Cr$ or $Al_{20} Cu_2 Mn$ which seem to play a dual and contradictory role: they supress recrystallization and therefore minimize the grain size which is favourable to a

73

transgranular mode of failure, but also nucleate microvoids by decohesion at the matrix interface. The nucleation of microvoids produce similar effects as the coarse intermetallics.

b.) The effect of grain boundaries on the fracture toughness is related to the intergranular fracture. Embury showed [61] that features such as areal fraction of grain boundary precipitates, the size of precipitate free zone (PFZ) the extent of localized deformation in the vicinity of the boundary and others influence the balance of events at the grain boundary. One interesting finding reported by Embury [61] is the relationship between the PFZ size and the local plasticity at the crack tip.

c) The most challenging area of research is related to the influence of the smallest particles of the system (age-hardening precipitates or Guinier-Preston (GP) zones) on the fracture and fatigue resistance of high strength aluminum alloys. These particles which usually are smaller than 0.01 μm in diameter play an essential role in the strengthening mechanism of the aluminum alloys, however their role in the fatigue process is not completely understood. The size, the morphology and the interparticle distance are dependent on the quench rate and the degree of the precipitation aging. In the optimal conditions these particles have been credited for increasing the fatigue limits [62]. However in many

commercial applications, the aluminum alloys are often overaged to ensure an optimum combination of stress-corrosion resistance and high temperature mechanical properties. The overaging tends to produce coarser particles which particularly for the 7xxx alloys results in intergranular fracture and low toughness.

The general influence of particles on the fracture and fatigue resistance was studied by Laird who synthesized [20] the observations reviewed by Hahn and others with respect to the influence of various parameters on the F.C.P. rates in aluminum alloys:

1. Statically strong alloys, such as 7075-T6 can show higher growth rates than less strong but more ductile alloys such as 2024-T3.

2. Heat-to-heat variations in composition and processing, small amounts of cold work, and different heat-treatments can alter the life of a typical alloy such as 2024-T3 by as much as 100 percent.

3. Brittle fracture modes associated with inclusions or intermetallic particles can double the rate of crack propagation when the advance per cycle is large (≃ 1 μm/cycle).

Trying to explain these variations and the general poor fatigue properties of high strength aluminum alloys, Laird and coworkers concluded [63] that in the Al-Cu alloys the

•motion of highly jogged and continually interacting
dislocations causes a disorder of the general structure and a
subsequent softening of the material takes place affecting
the elastic properties of the precipitates as well.

For the case of other aluminum alloys when the hardening
mechanism is not affected, Calabrese and Laird [64] used a
different model which involves that presence of
"geometrically necessary" dislocations at the plate-matrix
interface. The basic conclusions of Laird's work [20] are
that cyclic stress-strain response of complex aluminum alloys
is dominated by GP zones and dispersoids in combination. It
may be interesting to point out that somewhat similar results
were reported by Yan and Wang [65] which proposed a mechanism
of progressive retardation of grain boundary gliding to
explain the co-existance of both ductile and brittle fatigue
striations on the same fracture surface.

With respect to the influence of the microstructure on
the striation appearance, a comprehensive description was
given by Klingele [66]. Some of his most important
observations are listed below: When the fatigue crack front
approaches a hard zone the F.C.P. showed a retardation, but
after the hard zone the F.C.P. showed an acceleration, Figure
37. As the fracture front propagates continuously on both
sides of a hard inclusion, it is stopped completely for a
number of load cycles at the inclusion. After climbing over
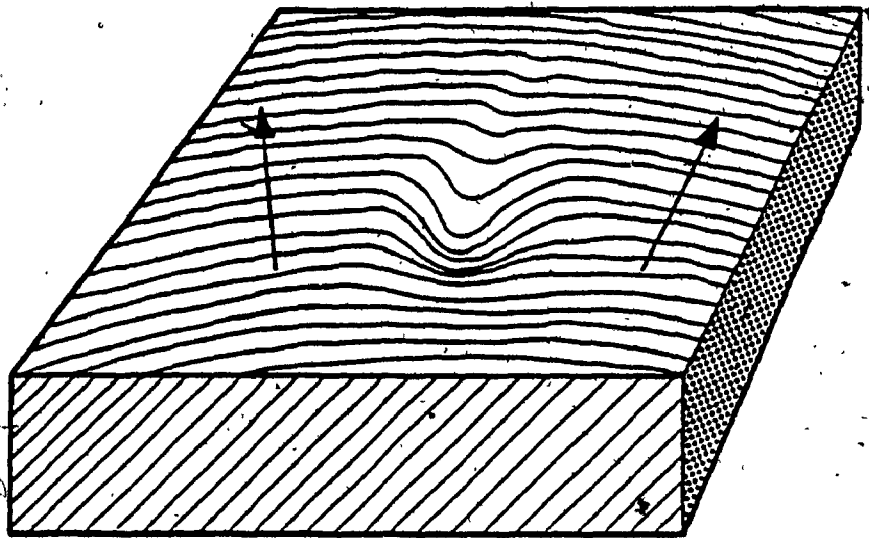
Figure 37

In a hard region the fatigue crack is retarded, i.e. the
width of the striations is smaller than on either side.
Behind the hard region the crack steps are larger than on
either side. [66]

the inclusion the fracture catches up to the main fracture in

large steps, Figure 38.   The F.C.P. accelerates when the

crack front approaches a pore and is retarded after passing

the pore Figure 39.

In conclusion, it is evident that all the above

observations on microstructural effects must be accounted in

establishing adequate quantitative fractographic techniques.

These techniques are detailed in the next section.
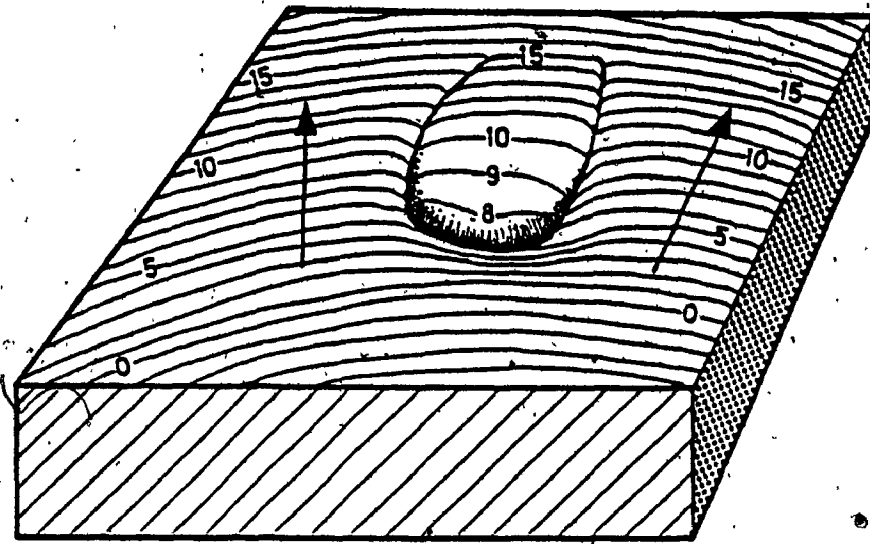
Figure 38

Hard region (obstacle) separates the fatigue crack front into
three adjacent paths with different propagation rates.
Within the hard region there is no propagation for some load
cycles. [66]
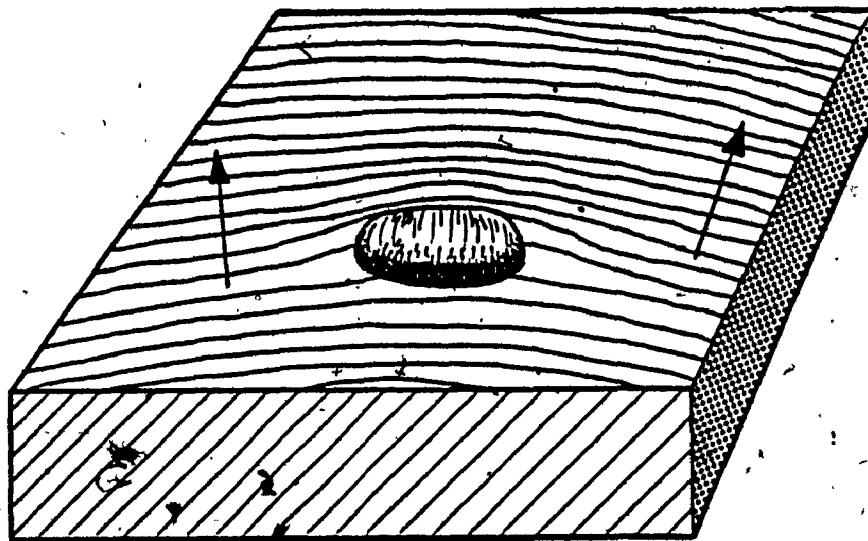
Figure 39.

When a fatigue fracture comes to a pore, it is accelerated.
Behind the pore, the fatigue fracture is retarded. [66]

78

3. FRACTOGRAPHY

3.1 GENERAL COMMENTS

The term "Fractography" as defined in 1944 [56] describes the science of studying fracture surfaces usually at high magnifications. Perhaps the name of this science is relatively new, however the science itself is centuries old. The metallurgist was always preoccupied why and how components fail and apparently the answer to this question can be found by examination of the fracture surface. The improvement of optical microscopes and especially the introduction of the electron microscope with its large depth of focus provided the investigators with the tools needed to reveal the micro and submicro-morphology of the fracture. The transmission (TEM) and scanning (SEM) electron microscope were instrumental in the extensive development of fractography as a science and in all the benefits related to the understanding of the fracture mechanisms.

The aircraft industry has been the major promotor of fractographic examination of components failed both in service and in testing. The magnitude of human and material losses in the event of an airplane accident is too high to neglect possible material or design errors. Fractographic examination in the whole context of failure analysis has as a

prime objective, of discovering these errors and avoiding
their repetition. Table 5 shows the history of changes in
certification requirements originating from major aircraft
accidents. As can be seen from this table, identification
of the mode of failure (through failure analysis) was the
force behind the changes in regulations. "Introduction /of
the damage tolerance concept is possibly the most significant

Table 5

'Changes in Certification Requirements Stemming from Accidents

Date and Place	The Accident	Cause and Resulting Regulations
August 1948 Minnesota	Martin 202, wing failure	Each of the three accidents was caused by fatigue failure.
January 1954 Italy	DH Comet 1, fuselage failure	Resulting regulations: CAR 4b, Adt 4b-3 (fatigue evaluation of airframe), 1956.
April 1954 Italy	DH Comet 1, fuselage failure	
November 1962 Maryland	Vickets Viscount, tailplane failure	Catastrophic bird impact on empennage. Resulting regulations: FAR 25, Adt 25-23 (8 lb [3.6 kg] birdproof empennage), 1970.
August 1966 Nebraska	BAC 111, empennage failure	Catastrophic unsymmetrical load, failure of T-tail. Resulting regulations: FAR 25, Adt 25-23 (unsymmetric T-loads), 1970.
March 1966 Japan	Boeing 707, fin failure	In each of the six accidents, nominally fail-safe airframes failed.
December 1968 Alaska	F27, wing failure	
May 1974 Illinois	Lockheed Civil Hercules, wing failure	
October 1974 Alaska	Lockheed Civil Hercules, wing failure	Resulting regulations: FAR 25, Adt 25-46 (damage tolerance evaluation), 1978.
April 1976 Argentina	HS 748, wing failure	
May 1977 Zambia	Boeing 707, tailplane failure	

upgrading of structural requirements in the past 40 years. Table 5 suggests it was justified." [67]

The major advantage of fractographic examination consists in the fact that practically, "the history of the fracturing process is imprinted upon the fracture surface" [68]. By careful selection, testing and examination of components failed in different loading conditions it is possible to establish a strong relationship between the fracture morphology and the mode of failure.

The fractographic examination is especially rewarding in the case of fatigue failures where qualitative and quantitative evaluation can produce an accurate time-related picture of the failure process. The increasing participation of fractographic examination in major airframe certification projects has been emphasized in many papers, [5,69,70, 71, 72, 73]. Searching for conclusion through these papers revealed that fractographic examination is considered as a significant and confident method to determine the crack growth rate curves. In addition, this method "saves considerable expenses in testing and prospectively can save analysis costs, as well." With reliance on fractographic data, there is no need for periodic crack length monitoring during the test" [71]. Additional cost-saving benefits are mentioned in [72].

3.2. OBJECTIVES AND PROCEDURES

Fractographic examination of components or test specimens which failed in fatigue has several major objectives:

1) To determine the exact origin of the crack and the direction of crack propagation.

2) To identify, on a microscopic scale, the applied loading spectrum and to establish the influence of certain spectrum loads on the advancement or retardation of the crack propagation.

3) To determine the number of spectrum loading cycles from the start of crack initiation to the end of testing, in order to substantiate the analytical crack-growth curves for the component under test.

4) To examine the crack propagation front and provide information regarding inspectable crack size, crack tunnelling, etc.

5) To provide information about possible material or manufacturing defects which could be a source of crack nucleation or which could be associated with acceleration of crack propagation. [74]

By the nature of these objectives the fractographic analysis can be classified as either: Qualitative fractography or

Quantitative fractography. Qualitative fractographic examination in the entire context of failure analysis can be defined as the study of fractured surfaces in order to determine the mode or modes of failure. In the particular case of fatigue specimens, where the mode of failure is well known, the qualitative fractographic examination provides answers regarding the initiation site, the general direction of propagation, material defects, etc. This examination employs low and high power optical microscopes, with different light sources, electron microscopes, cleaning and etching solutions, etc. The electron microscope provides both a great depth of focus, and very high magnifications (up to 100,000x) revealing the fracture surface micromorphology.

Basically the following steps are followed in a routine qualitative fractographic examination of the component failed in fatigue:

a) The as received component is examined visually and general photos are taken to record the orientation of the damage with respect to the component geometry.

b) The fractured surface exposed by the failure or broken open in the laboratory is examined with a low power (2-10x) optical microscope, to determine, where possible: the origin or origins (stage I) of the fatigue crack and its orientation with respect to the component geometry, the general direction of fatigue

cracking, the typical macroscopic marks ("beach" marks)
the extent of fatigue crack growth (stage II), and the
extent of the final fast fracture (stage III) with
respect to the entire fracture surface. The important
features are photographed. It is also important to
observe the environmental effects such as corrosion,
oxidation, heat colouration, as well as secondary
mechanical damage of the fracture surface.
c) Scanning electron microscope (SEM) examination is
carried-out next to determine the appearance, the
density and the general orientation of the fatigue
striations. If a quantitative fractographic examination
is intended a proper area is selected for this anlysis.
d Further analyses, such as x-ray energy spectroscopy
'XES , electron microprobe analysis 'EPMA , Auger
electron spectroscopy (AES and many others, can be
carried-out to determine the nature of different
inclusions or particles deposited on the fracture
surface or embedded in the material. These analyses can
provide crucial information regarding fatigue cracking
initiation from surface or subsurface discontinuities
and regarding the influence of different environmental
factors to the fatigue crack propagation. In order to
preserve the surface for these analyses the cleaning
techniques must be employed with special care. Detailed

descriptions of qualitative fractographic examination procedures and techniques are given through the literature [37, 49, 67, 84, 85, 86, 87].

Quantitative fractographic examination of fatigue failures, especially in the case of fatigue and damage tolerance testing, provides additional important information related to the crack growth rates, retardation effects, propagation fronts, inspectable crack lengths, etc; in the other words, answers to all the questions raised by the objective of constructing accurate crack growth rate curves. Detailed information about the quantitative fractographic examination procedures and techniques will be discussed in the next sections.

3.3. QUANTITATIVE FRACTOGRAPHY

Since the first report in 1951 of the fatigue striations by Zappfe and Worden, numerous attempts were made to correlate the macroscopic test parameters such as the number of loading cycles, the stress level etc, with the microscopic fatigue imprint, i.e. the striations.

Significant contributions to the answer to this problem were made by Forsyth and Ryder, Crussard, Pelloux, Schijve and many others. In 1960 Forsyth and Ryder performed a critical experiment which established that "each load

excursion was responsible for one striation" [6]. This
conclusion is the basic principle of the quantitative
fractography. Since this discovery an extensive literature
has been written on this subject. As a result of this
extensive research a better formulation of this principle can
be stated: Each striation is a result of a single load
application, however it is not necessarily that each load
excursion will produce a striation. It was already explained
in previous sections that in conditions of ultra-low crack
growth, the striations are either not resolvable or are not
produced at all. Also, the retardation effect inhibits
striation formation and cleavage-like morphology is visible.
Based on this principle adequate techniques and procedures
were developed.

3.3.1 Procedures_and_methods_of_quantitative_fractography

3.3.1.1. General_procedure

The general procedure of quantitative fractography
consists basically in striation spacing measurements at
selected locations along the fracture surface. After the
qualitative fractographic examination has been carried-out,
the selected specimen is placed in the SEM chamber. A number
of fields, located along an imaginary straight line which
passes through the crack origin are photographed and a
striation count procedure is carried-out on each of these

86

microphotographs. The striation count procedure consists in counting the number of striations in a measured length.

The striation spacing is then calculated using a simple formula:

$$\rho = \frac{1}{S} = \frac{n \cdot M}{d}$$

or

$$\frac{da}{dN} \approx S = \frac{1}{M} \cdot \frac{d}{n}$$

where ρ = striation density, cycles/mm

S = striation spacing, mm/cycle

n = number of striations as counted on the micrograph

d = measured distance containing n striations, mm

M = magnification employed

Similar formula are given in [11, 79]. The minimum total number of cycles, N_{a_i} necessary to propagate a crack over a length "a_i" can then be computed as:

$$N_{a_i} = \frac{a_i}{S_i}$$

When calculating the propagation life from a number of fields a general formula for the total number of cumulative cycles can be written as:

$$N_C = \sum_{i=0}^{i=f} N_{a_i} = \sum_{i=0}^{i=f} \frac{a_i - a_{i-1}}{S_i} \qquad \begin{array}{l} f=\text{failure} \\ o=\text{origin} \end{array}$$

87

The average crack growth rate across the examined area can be
written as:

$$\frac{da}{dN} \approx \frac{a}{N} = \frac{\sum a_i}{\sum \frac{a_i - a_{i-1}}{S_i}}$$

If the total number of applied cycles is known, the number of
cycles necessary to initiate the crack can be computed from a
simple equation:

$$N_{INIT} = N_{FF} - N_{PROP}$$

where

N_{INIT} = the number of cycles necessary to
initiate the crack

N_{FF} = total number of cycles applied to
reach the final failure

N_{PROP} = the number of cycles necessary to
propagate the crack from initiation
to final failure

It is evident that $N_{PROP} = N_C$, if a = total fatigue crack
length.

The distance of each field from the origin is measured using
the SEM stage verniers. Finally, a table containing the
following data is constructed:

a) Field identification number

b) Distance from the origin=crack length, a, [mm]

c) Striation density, ρ, [cycles/mm]

88

d) Striation spacing, S, [mm/cycle]

e) Estimated number of cycles, N, [cycles]

f) Cumulative number of cycles, N_C [cycles]

g) Average crack growth rate, $\frac{da}{dN}$, [mm/cycle]

Based on the above information the curve of crack growth rate versus the distance from the origin can be plotted, as well as the crack growth versus the number of cycles. Two such typical curves as determined during the Canadair Challenger 600/601 certification program are shown in Figure 40.

Using the crack length versus numbers of cycles curve, one may determine the first N.D.T. inspection interval which can detect the crack. The minimum inspectable crack size usually achievable in industry is considered to be in the range of 1.3 - 2.0 mm (0.05 - 0.08 in), depending on the N.D.T. technique employed and on the inspection accesibility. Therefore in the case of the curve from Figure 40b, for a crack length of 1.3 - 2.0 mm, the first N.D.T. inspection interval must take place between 310 and 335 thousand flights. This curve shows also that the failure to detect this crack will allow another 90 - 115 thousand flights before the crack reaches the critical depth.

3.3.1.2. Specific striation count techniques

In section 2.3.3.2. the influence of various parameters on the formation and appearance of the fatigue striation was described. Based on these effects, specific rules must be
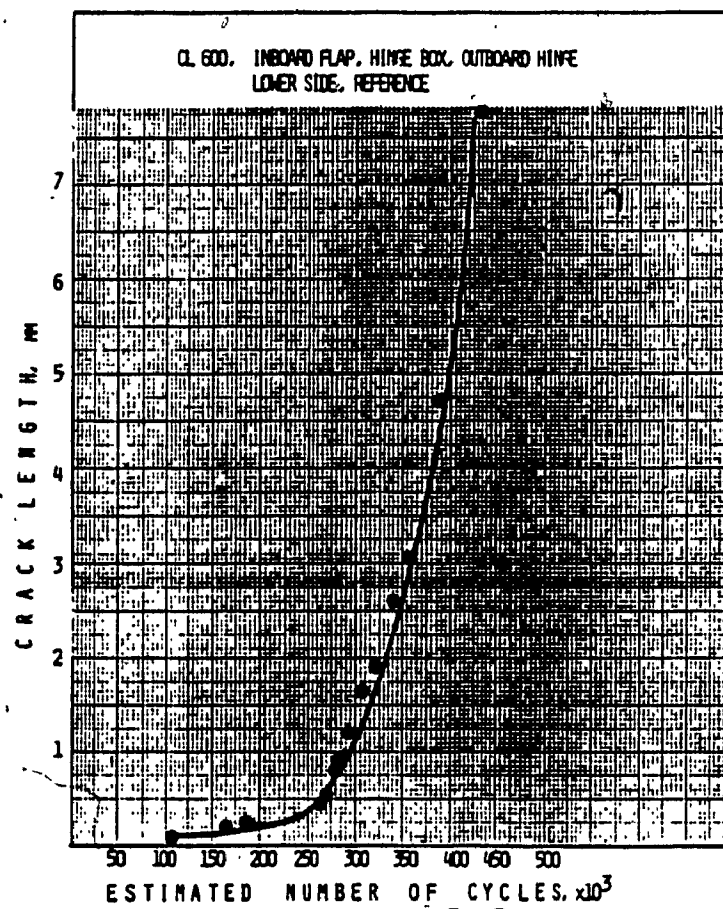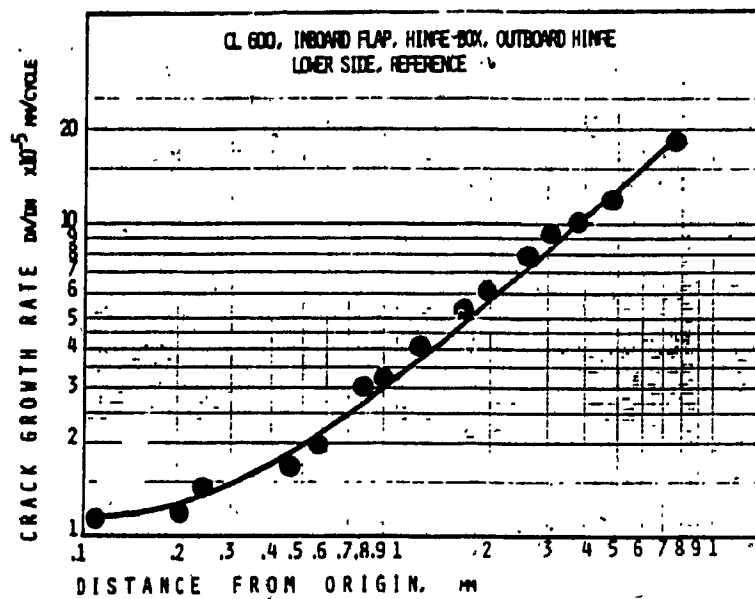
Figure 40[80]

a) The curve of the crack growth rate versus crack length.
b) The curve of the crack length versus number of cycles.

considered in the striation count technique, and these are synthesized as follows:

A) Field_Selection

   a) The areas selected for examination should be large with uniform striations [66]; a minimum of 10 relatively uniformly spaced striations must be present in each field [70]. This rule is based on the observations that for "any given fracture surface, striation spacing formed at the same nominal stress intensity can vary by a factor of two or three" [13, 70]. As Forsyth indicated [41, 81] aluminum alloys have a tendency for fatigue fracture to advance with many small crack front segments which exhibit some degree of independence from their neighbours. Therefore one may expect that adjacent fatigue striation patches created during stage II to exhibit various directions of propagation and/or variation in striation spacing. [82]

   b) The striated areas selected for examination should be oriented in the general crack propagation direction (CPD) [70]. This rule as well as the next one result from the same reasons as rule a).

   c) The areas selected should be relatively flat with a tilt angle (with respect to the CPD) of less than ± 30 deg from the macroscopic fracture plane. This condition as explained by Dainty [70] limits localized

striation spacing errors due to facet tilting deviations
to approximately 15%.

d) Selected fields must be located along an imaginary
straight line passing through the origin. When along
this imaginary line, there are obstacles such as smeared
areas etc., the line can be broken in order to avoid the
obstacle, Figure 41 [66].

e) As a general rule it is necessary to select a minimum
of two fields per each mm of crack length [70]. This
will yield sufficient data to construct a representative
fatigue crack growth curve.
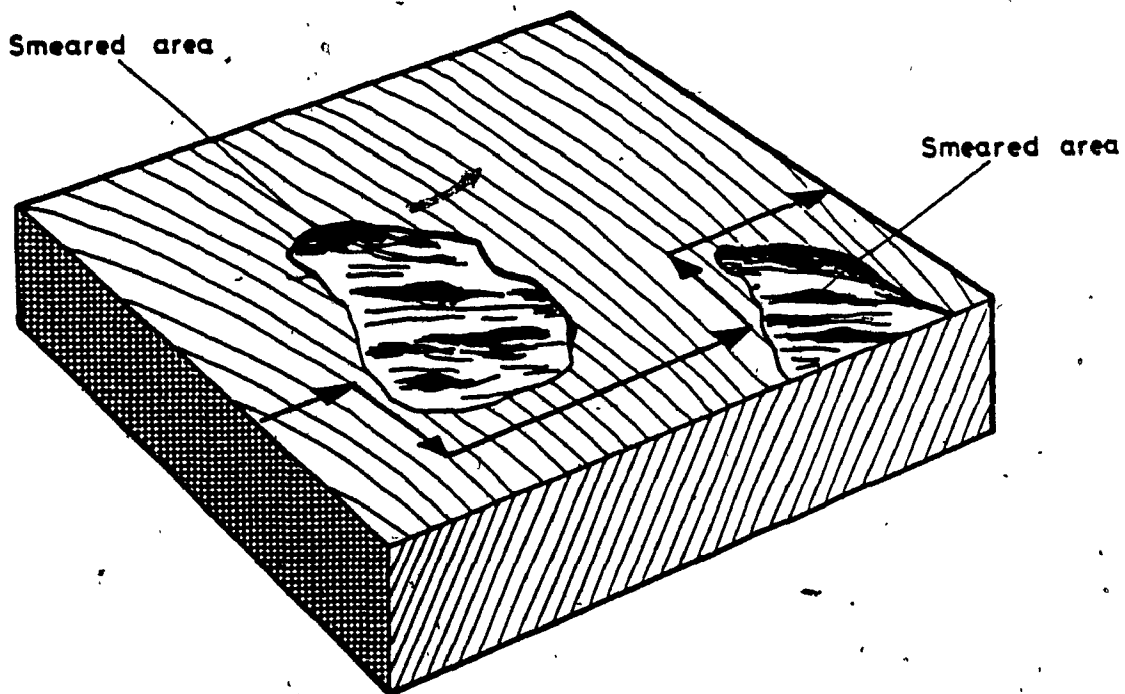
Figure 41

Broken measuring line for quantitative evaluation of
striations. [66]

f) During stage III in many occasions patches of fatigue striations are mixed with regions of rapid fast fractures. The striation count technique cannot be employed with confidence across these areas. If an estimation of the crack propagation rate across these regions is however required, one must count the individual striations and consider the overstress rupture regions as produced by one cycle [66].

B) Striation counting

The following rules are derived from the necessity to establish the true dimensions of the striation spacing for each field.

a) The specimen must be rotated or tilted in the electron microscope to produce the largest spacing between striations [82].

b) Striations should not be counted around a hard inclusion, a pore, or a hard zone, for the reasons explained in section 2.3.3.2.3.

c) Secondary cracks are not suitable for evaluation because they slow down and finally stop, Figure 42 [66].

d) Striations on a step are suitable only if they lie on crystallographically oriented planes or if they cross the step and the neighbouring areas in unbroken lines, Figures 43, 44, and 45 [66].

93
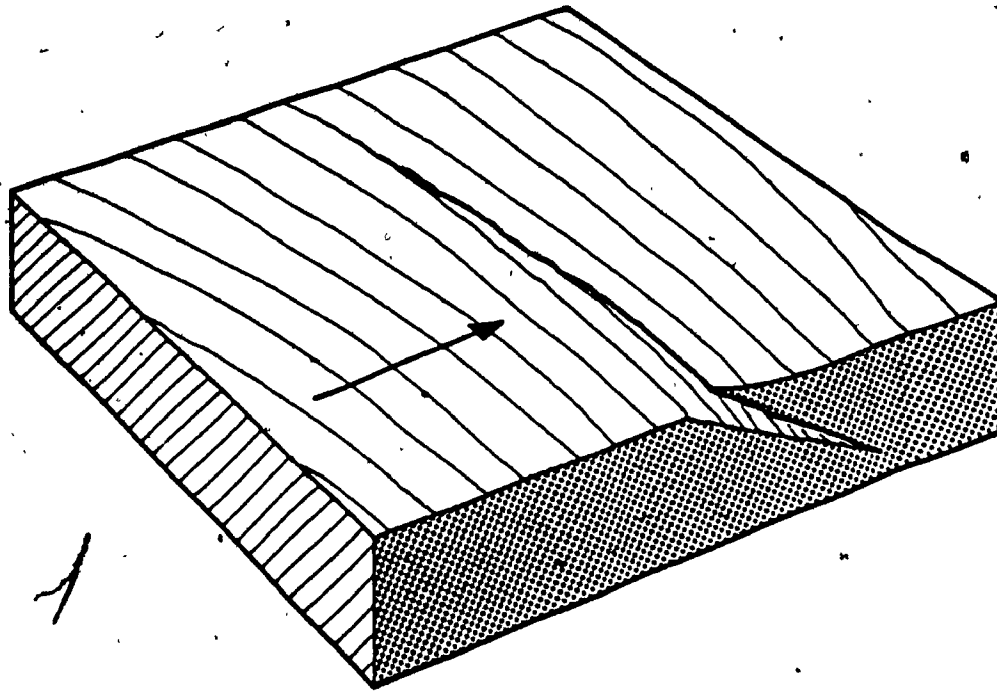
Figure 42

Narrow striations inside a secondary crack are not
appropriate for quantitative evaluation. [66]

e) If the specimen has a microstructure which contains a
lamellar phase (such as pearlite, the striation pattern
may show the width of the lamellae and not the real
propagation pattern [66].

f) Secondary cracking may not be counted as a true
striation. Featherby showed [83] that the number of
cracks and the number of true striations do not
coincide, Figure 46.

g) The striations from protected areas (steps or
depressions) [66], are likely to give the best results.
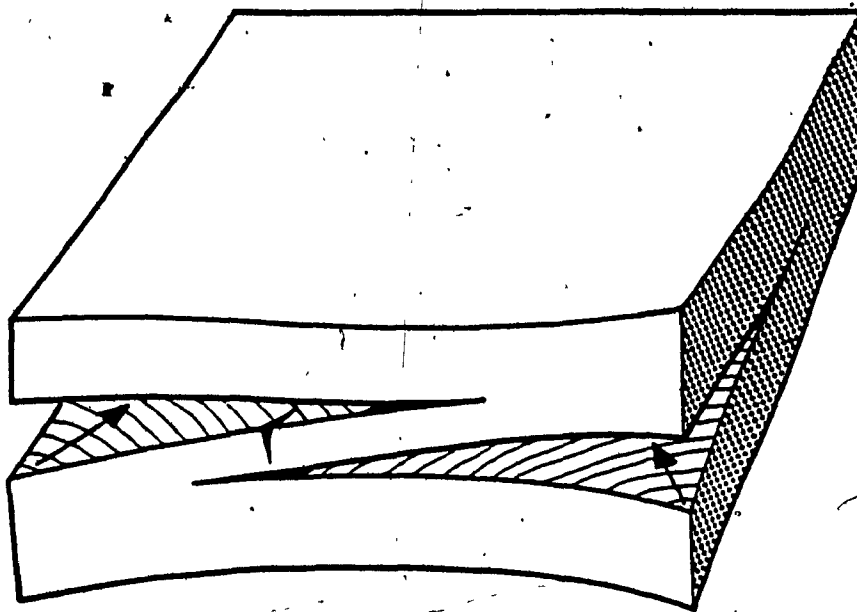
Figure 43

A secondary fatigue crack situated between two parallel
fatigue planes forms a step perpendicular to the main fatigue
plane. [66]
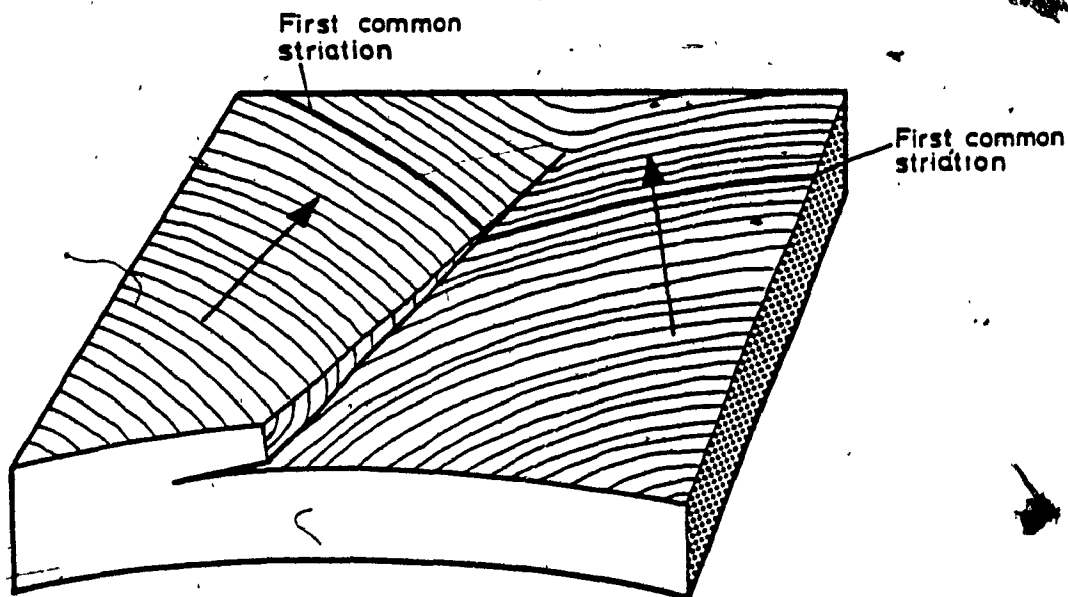
Figure 44

Striations in steps perpendicular to main fatigue plane may
only be used for quantitative evaluation if there are common
striations in adjacent paths. [66]
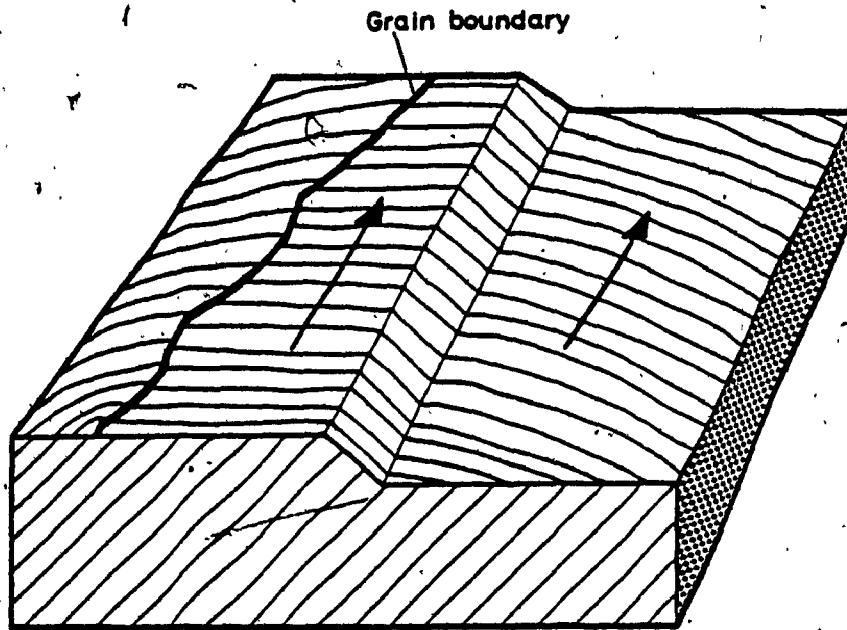
Figure 45

Crystallographic step in fatigue fracture is appropriate for quantitative evaluation of striations. [66]

Figure 46

Cracking (bottom) and true striations (top) in 2219 aluminum alloy; no apparent correlation between crack and striation spacings. Magnification 4000x [83]

3.3.2. Methods_of_quantitative_fractography

The methods of quantitative fractography can be classified with respect to the type of loading spectrum applied during the test:

    a) Uniform amplitude spectrum

    b) Block spectrum

    c) Random spectrum

A general description of typical spectra and their micrographic imprint is shown in Figures 47 & 48. Abelkis | 82| showed that determination of the loading history from the microscopic fracture imprint striation counting is rather straightforward for constant (uniform amplitude loading. However, it becomes a complex and difficult task for block and random loading spectra.

In the majority of the tests done within the Challenger 600 601 certification program, the loading spectra were chosen to represent as accurately as possible the service conditions expected to be encountered by the airplanes. Hence, the block spectrum was extensively used in comparison with the constant amplitude spectrum.

In the case of uniform amplitude spectrum the quantitative fractography is a simple evaluation of the striation spacing, whereas in the case of either block spectrum or random spectrum the first problem is recognizing the microscopic fracture imprint and only then quantitative

Loading   Testing

Constant Amplitude

Block Spectrum

FbF Random Spectrum

Service

FbF Random Spectrum
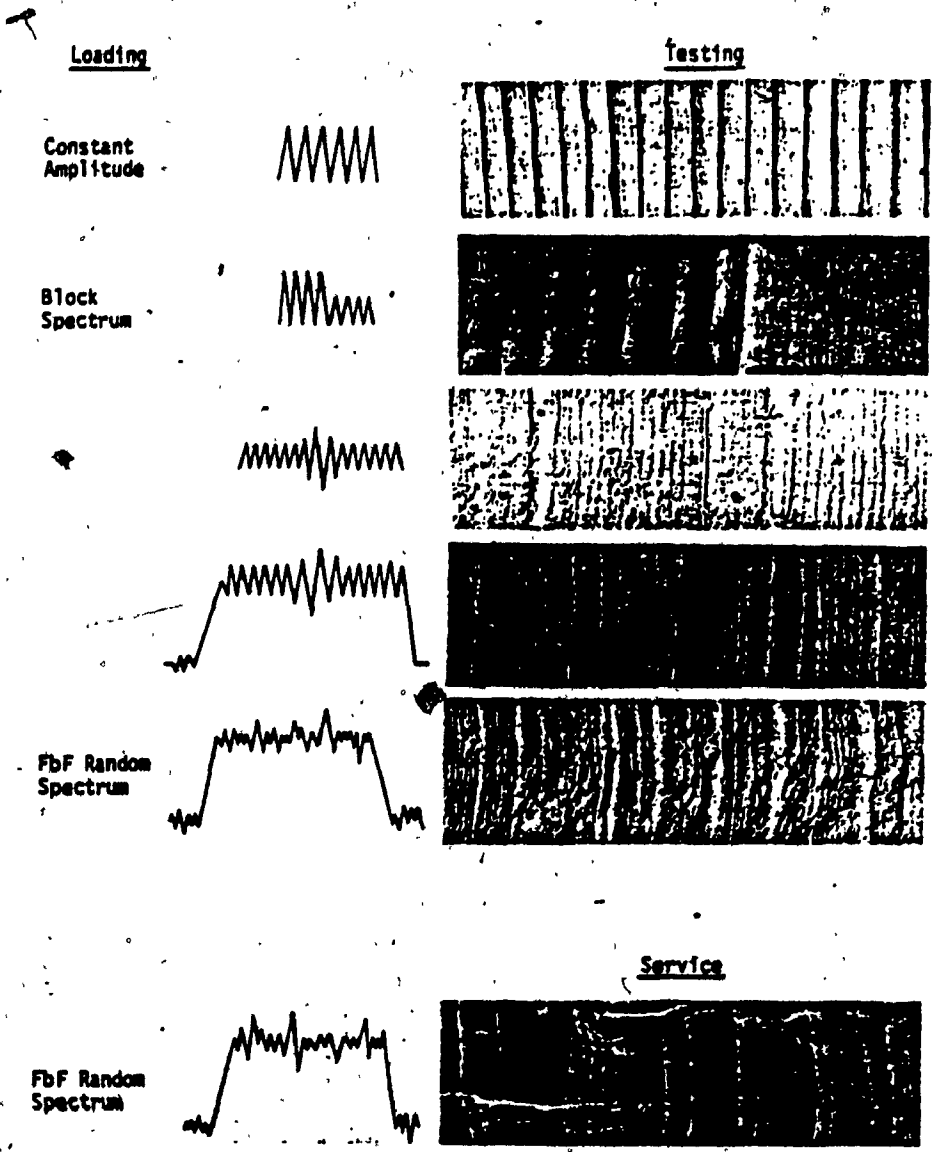
Figure 47

Examples of striation markings under various loading conditions--aluminum alloys. [82]
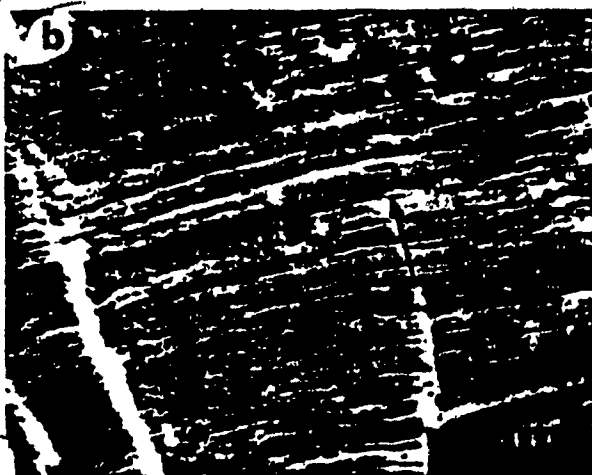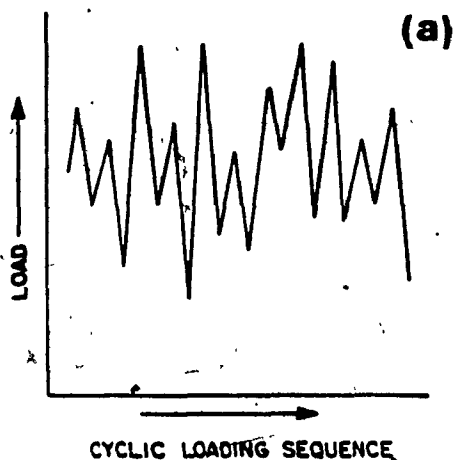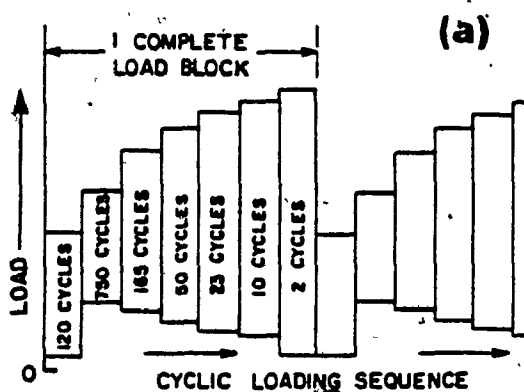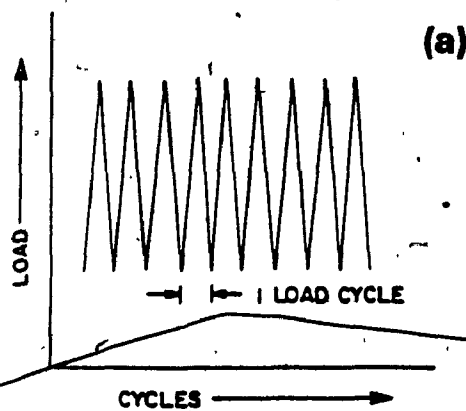
Figure 48

Typical examples of microscopic fracture imprints [70]
A - uniform amplitude, B - block spectrum, C - random
spectrum
a) loading   b) resulting microscopic fracture imprint

evaluation can be done by estimating the crack advance produced by the block or by the random cycles. Obviously special techniques must be imagined and tested to help the investigator becoming oriented to what stage of the spectrum is seen on the SEM screen at a certain moment. An example of a block spectrum is shown in Figure 49. This particular block consists of 470 cycles of loading with 8.33 KSI, followed by 1600 cycles of loading with 7.00 KSI. This experiment done at McDonnell Douglas Company was designed to demonstrate that overload retardation and acceleration phenomena in simple spectrum loading can be defined through fractographic examination. The number of cycles and the loading level were chosen such as to produce at the end of each block a crack propagation rate approaching that of the constant amplitude loading.

This analysis was extended to more complicated spectrum and the following basic observations were concluded:

a) Striation groups representing individual flights can be identified for all types of applied loading spectra.

b) Striations of individual cycles within the flight can be identified only at longer crack length. At shorter crack lengths identification is possible only for major loadings such as GAG (Ground-Air-Ground) cycle and the peak flight load. Near crack initiation, a complete flight appears

	S_{max}, MN/m^2 (ksi)		R
CA$_6$	57.46	(8.33)	.28
CA$_2$	48.27	(7.00)	.52

$a = 25.4 \longrightarrow 29.0$ mm
$= (1.00 \longrightarrow 1.14$ in.)
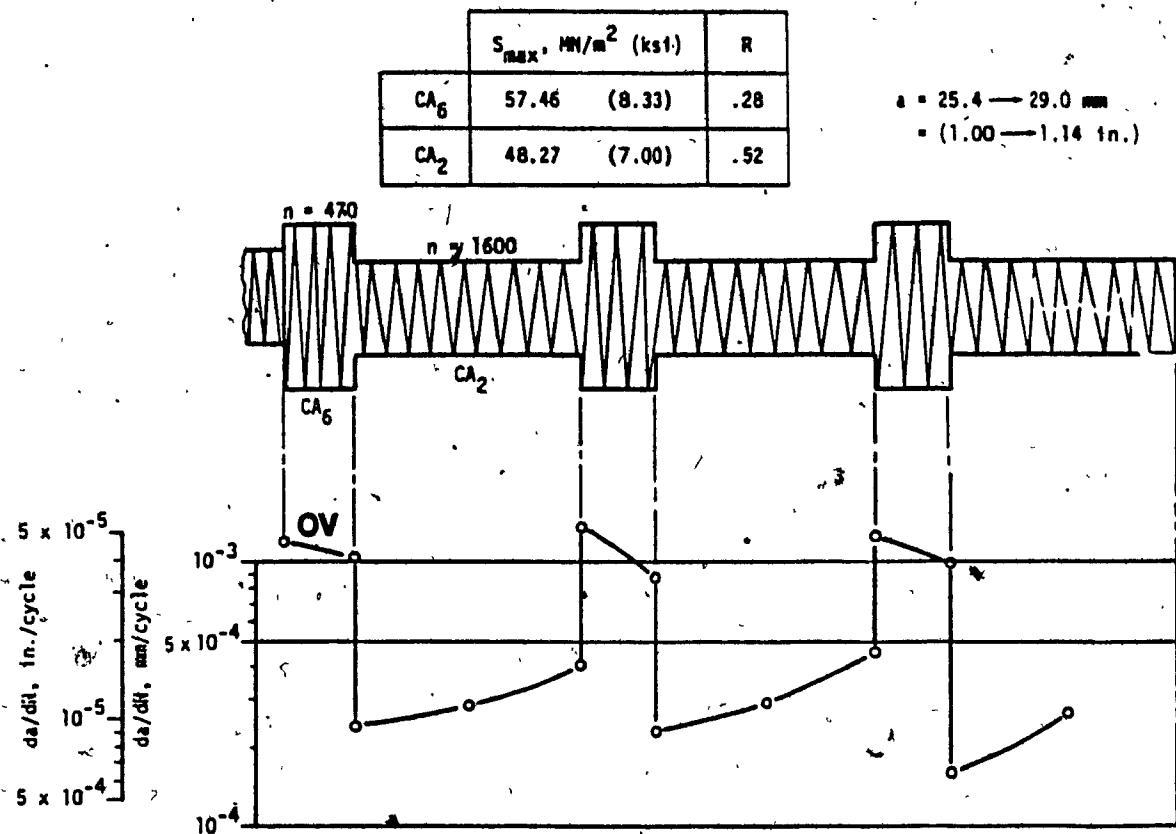
Figure 49

Loading interaction effects in crack propagation.
Fractography results. Material: 7075-T651; note the decrease
of the crack growth after application of the overload (OV).
The crack retardation effect increases with application of
succesive overloads. [82]

as one striation only.

c) Striation identification is clearer for spectra with lower
flight peak loads. Identification of individual striations
becomes more difficult for the spectra with higher peak
loads, in particular the striations due to the highest load

cycles.

d) Significant markings (deep valleys or high peaks) are associated with the GAG and the peak flight load cycles. As stated in paragraph b), these markings remain dominant in the fractographs of shorter cracks, whereas the striations of the lesser cycles become indistinguishable.

e) Increase in the crack propagation rate, as determined by quantitative fractography is primarily related to the increasing load between reversals; although the striation profile and to a certain extent the striation width are influenced by previous loadings and the unloadings.

The quantitative fractographic examinations performed during the Challenger 600/601 certification prógram followed strictly these rules as well as those described in previous sections (3.2, 3.3.1.1, 3.3.1.2).

In the situation of random loading spectrum the problem of identification between the loading spectrum and the microscopic fracture imprint become even more complicated. The technique which has been developed over the years to solve this problem and which is well documented in the literature makes use of "block markers". A typical block marker is shown in Figure 50. The block marker is usually a defined number of successive cycles of a constant amplitude which are easily recognized on the fracture surface. In other words they are landmarks to help establish the
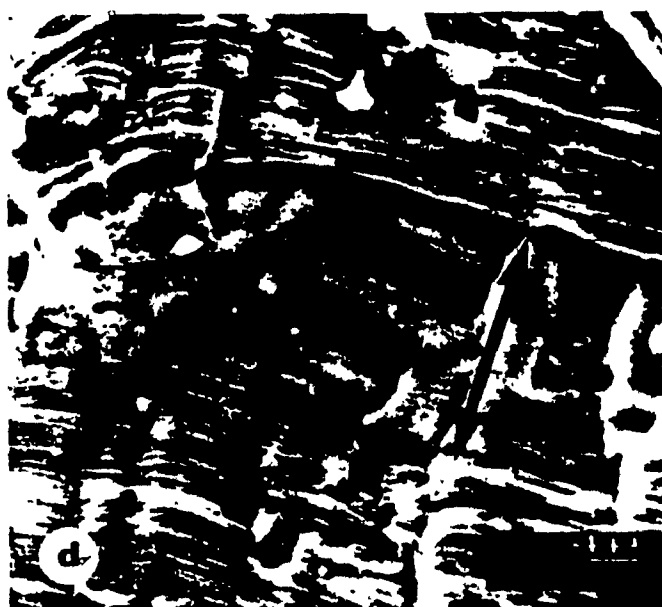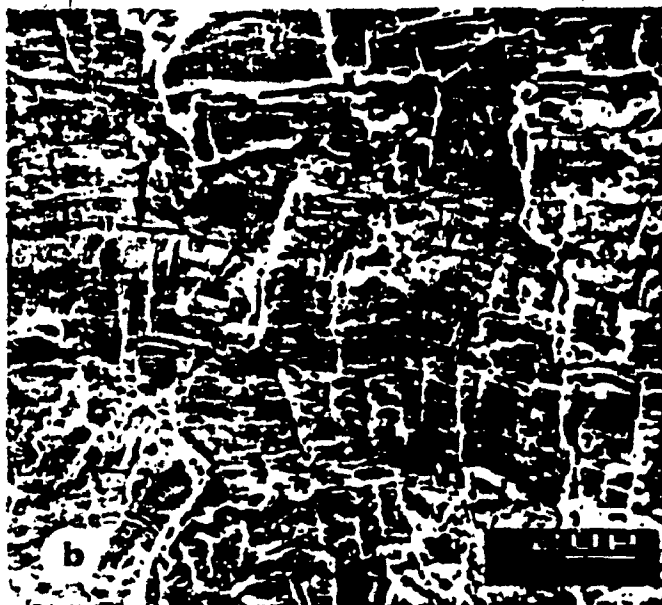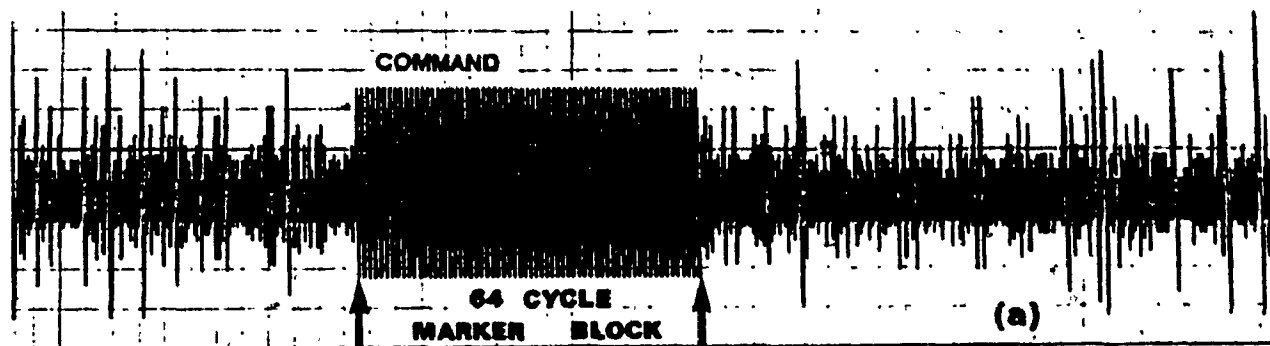
Figure 50

(a) Snowbird load spectrum with marker block (b) to (e)
Marker band as viewed on increased modifications.

correlation between the sequence of random loads and crack advances. As in the previous case several rules to be followed in this technique have been established. Anderson and McGee synthesized [72] some of the rules used at Lockheed-Georgia Company in the developing of marker blocks technique for a full-scale cargo airplane wing testing. This technique must comply with the following specifications. Each marker block should:

- produce micro rather than macro growth
- have relatively few cycles
- exhibit unique features of striation width
- have little or no influence on
  subsequent crack growth

In conclusion to this study a marker load procedure is recommended. Some of these recommendations are listed below:

a The marker loads should be constant amplitude cycles with the maximum stress equal to the maximum tensile stress in the flight spectrum and the minimum stress equal to the maximum compressive stress in the spectrum.

b) An interval of 100 flights between sets of marker loads would be adequate.

c) Each set of marker loads should have a unique number of cycles (minimum seven cycles) in order to provide maximum accuracy in the final fractographic analysis.

d) A continuous real-time record should be made of the

entire load application history to aid the final
fractographic correlation. It must be emphasized that
this technique has been extensively used at N.R.C. -
N.A.E. - Ottawa in the full scale fatigue tests of
different airplanes. One of the most representative
procedures (Snowbird load spectrum) shown in Figure 50
was applied to a Canadair Cl-41 Tudor trainer.
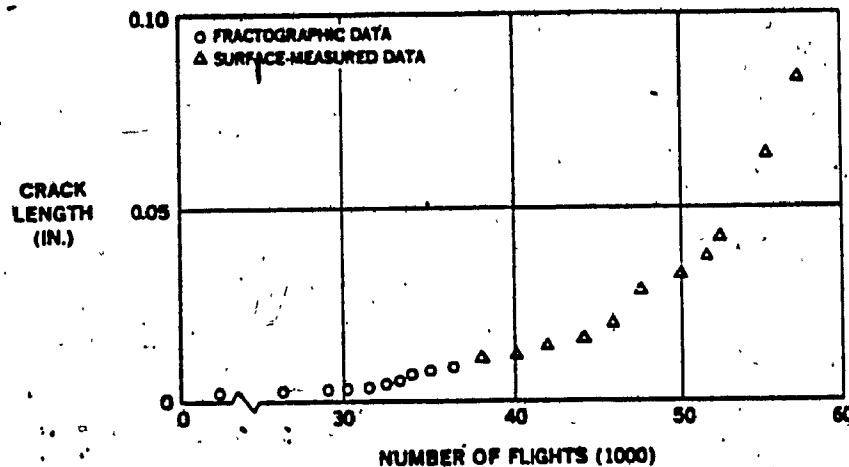
Figure 51

Results of combined micro- and macro corner crack growth data
for a countersink hole specimen. [73]

3.3.3. Reliability of quantitative fractography

Extensive experimental work has been done to demonstrate
the reliability of quantitative fractography. Some of these
studies made a simple correlation between the crack growth
curve as determined fractographically and the crack growth

curve as plotted from data obtained by visual measurements
during the crack monitoring. For example Wang [73] showed an
excellent correlation between the microcrack growth curve and
the macrocrack growth curve Figure 51. Wiebe and Dainty [69]
estimated the accuracy of the fractographic analysis at any
point along the fatigue crack propagation curve to be within
4-6% of the macroscopic observations.

Another way to verify the reliability of the
fractographic examination is to plot the crack growth da/dN
versus the stress intensity factor, ΔK, as determined by
striation count and compare it with both macroscopic
determination and theoretical estimate using one of the
F.C.P. models. An extensive study providing the above
comparision was performed by Au and Ke [84] for a AMS 6265
steel. A typical diagram obtained during this study is shown
in Figure 52. The basic conclusions of this study can be
synthesized as follows:

a) There was good correlation between macroscopic crack
growth rate and fatigue striation spacing for crack growth
rates ranging from 10^{-4} to 10^{-3} mm/cycle, Figure 53.

b) The correlation between macroscopic crack growth rate
and fatigue striation spacing was not affected by the stress
ratio, frequency, environment or carbon content (Figure 54).
Similarly with respect to 2219-T851 aluminum alloy Albertin
and Hudak [31] found that: "at growth rates above
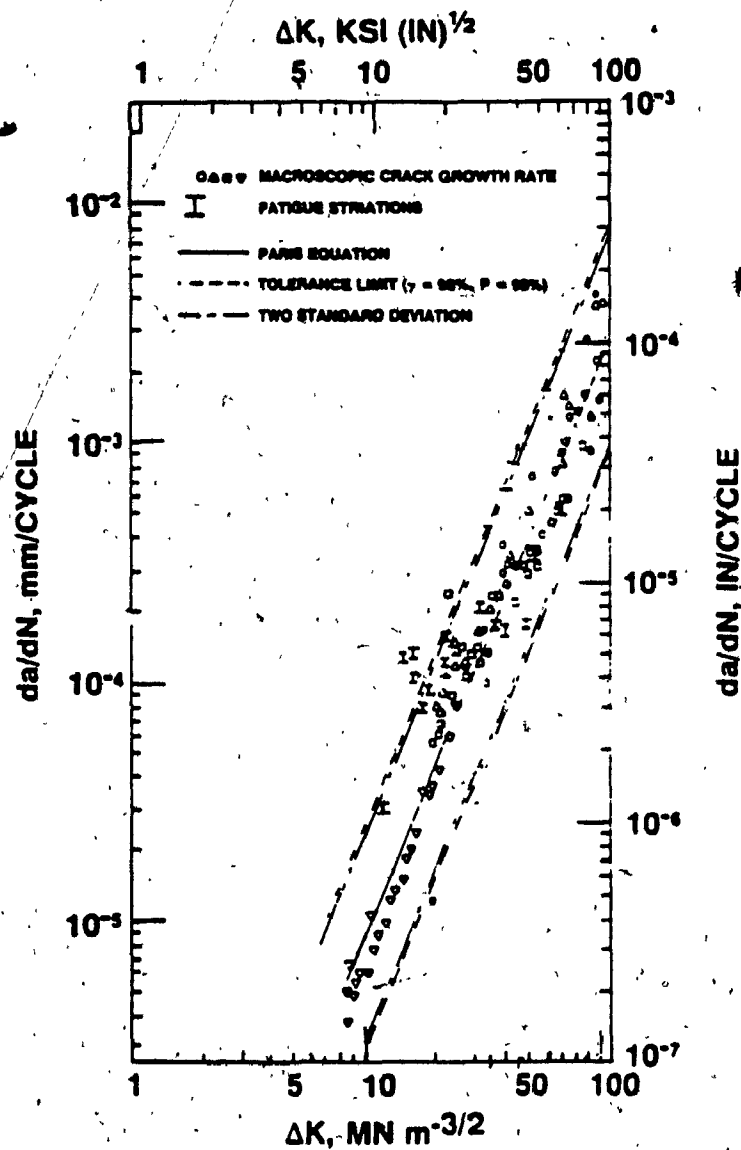
Figure 52

Fatigue crack growth rate of noncarburized AISI 9310 as a function of stress intensity range when tested in dry air, 3.4 Hz, and R = 0.05. [84]

107
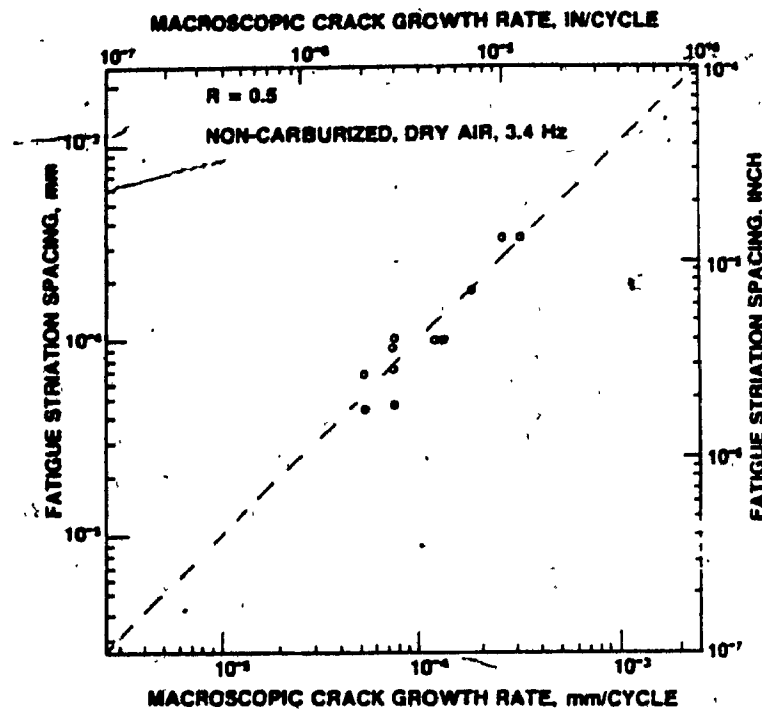
Figure 53

Correlation of macroscopic crack growth rate with fatigue
striation spacing for R = 0.5. [84]
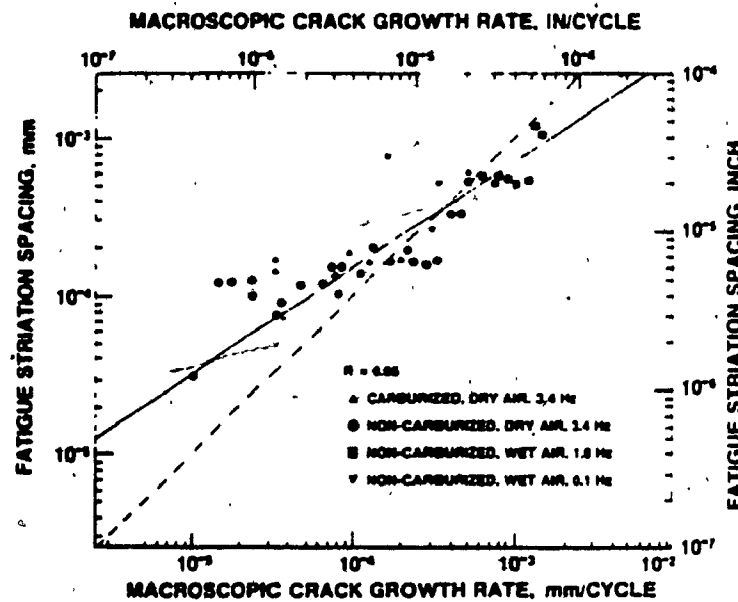
Figure 54

Correlation of fatigue crack growth rate with fatigue
striation spacing for R = 0.05. [84]

0.025μm/cycle a one-to-one correspondance exists between microscopic striation spacing and macroscopic fatigue crack growth rates provided supplementary static cracking modes are absent", Figure 55.

Another way to prove the reliability of fractographic examination is to compare the stress intensity factor ΔK obtained by striation counting and employing the Bates & Clark formula (see section 2.3.3.2.1) with the ΔK obtained by linear fracture mechanics methods. Several reports [84, 49], (Figure 56) provided the experimental evidence validating the Bates-Clark equation which implicitly proved the reliability of quantitative fractographic examination. The studies which employed block markers to determine F.C.P. curves reported similar results [72], Figure 57a and b demonstrating the applicability of fractographic examination in the case of random loading spectrum, as well.

It is clear that there is sufficient theoretical and experimental evidence to justify the employment of the quantitative fractography as a useful method in determination of realistic crack growth curves within the Challenger 600/601 certification program. However, despite all this evidence we undertook the task of verifying once again the validity of this method; consequently the first part of our experimental program was dedicated to this objective.
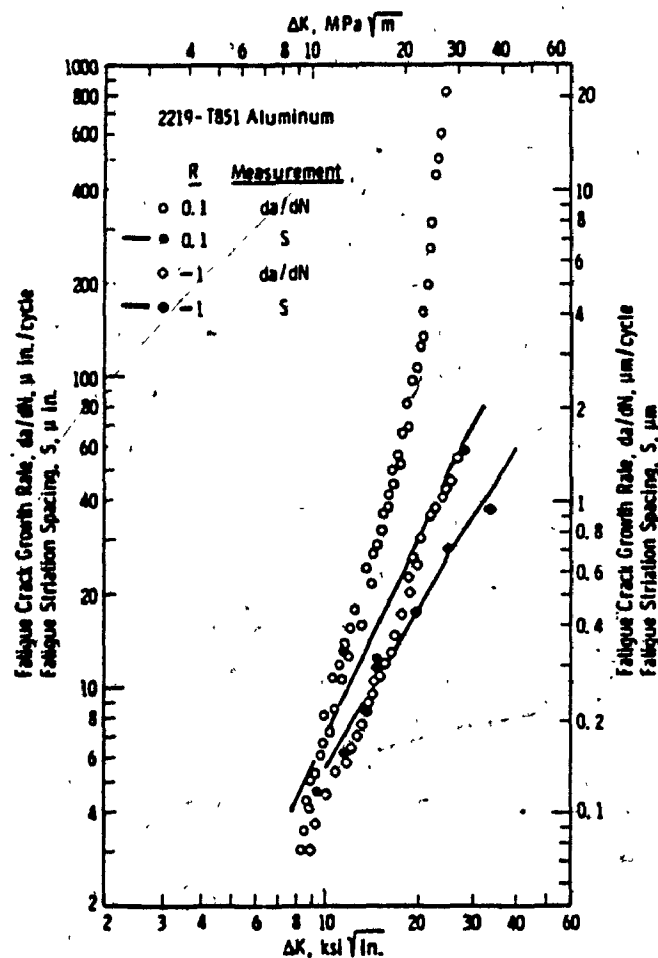
Figure 55

Comparison of microscopic fatigue striations spacing and macroscopic fatigue crack growth rates in Type 2219-T851 aluminum at load ratios, R, of 0.1 and -1. [31]
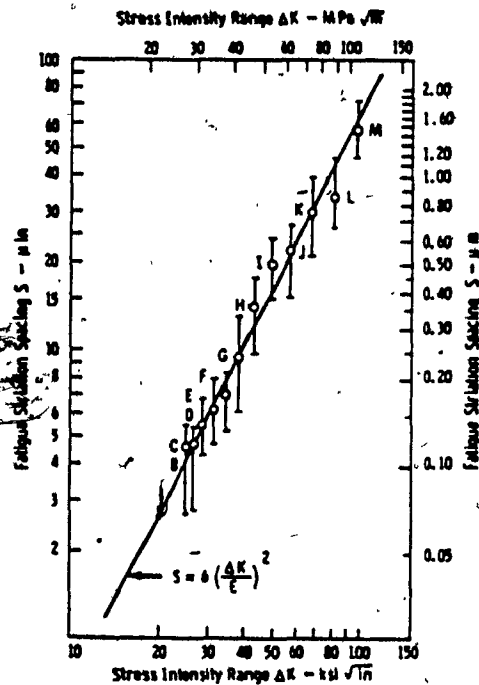
Figure 56

Comparison of fatigue striation spacings from fractography
(points on the diagram) with the Bates-Clark equation
(continuous line). [49]

3.3.4 <u>Criticism of quantitative fractography</u>

'As in all other engineering methods and processes, there

are some aspects of the quantitative fractography which can

be criticized.   Some of the disadvantages of this method are

related to the limitations of the method itself and of the

equipment employed.   Other disadvantages are related to the

human aspect of the method and finally some disadvantages are

related to the inherent material characteristics and

environmental effects.
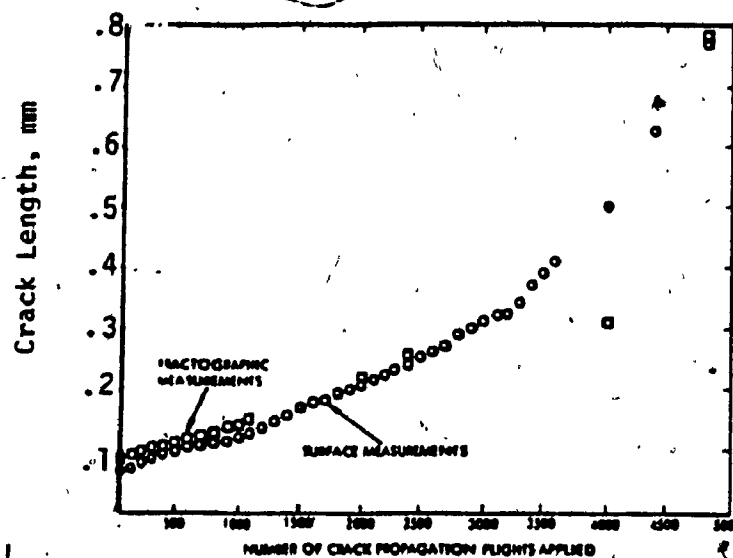
a)

Crack growth curve plotted from fractographic location of markers and similar curve from surface measurements for the low stress specimen.
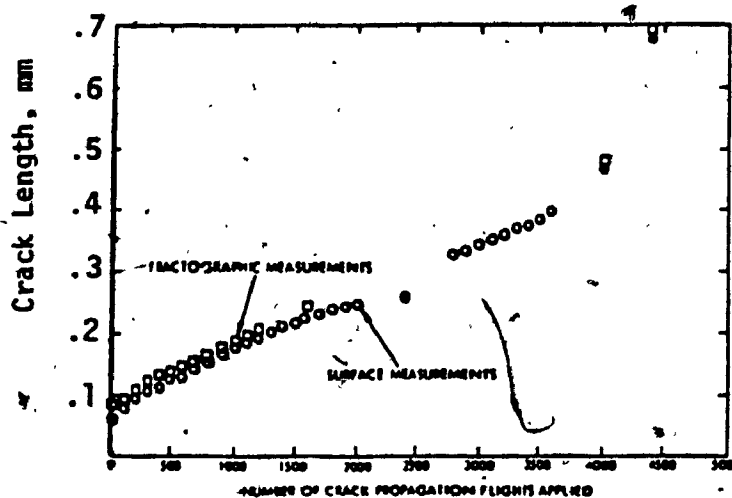
b)

Crack growth curve plotted from fractographic location of markers and similar curve from surface measurements for the modified high stress specimen.

Figure 57 [72]

112

In the first place it must be understood that this method is based on the assumption that the striation spacing across a limited length of the fracture is constant which obviously is not true. To be more explicit, one must consider the schematic curve in Figure 58. The striation count technique as explained in Section 3.3.1.1. implies that the investigator measures the striation spacing at certain locations, A, B, C, etc. across the fracture. The method also implies that the striation spacing S_j as measured for example at location B is constant across the length L_j. However this hypothesis is not true and actually the striation spacing S_j represents the largest striation spacing along the length L_j. Therefore the number of cycles necessary to propagate the crack along the length L_j will be

$$N_j = \frac{L_j}{S_j} = \frac{a_j - a_{j-1}}{S_j}$$

and because S_j is a maximum (the largest striation spacing), N_j will be a minimum. Hence, when estimating the propagation life from fractographic examination one will obtain the minimum number of cycles necessary to propagate the crack.

The above inaccuracy of the method is also greatly increased by the equipment limitation, by the human factor as well as by the material characteristics and the fatigue process itself. As explained in previous sections, the striation density is extremely high immediately adjacent to

113
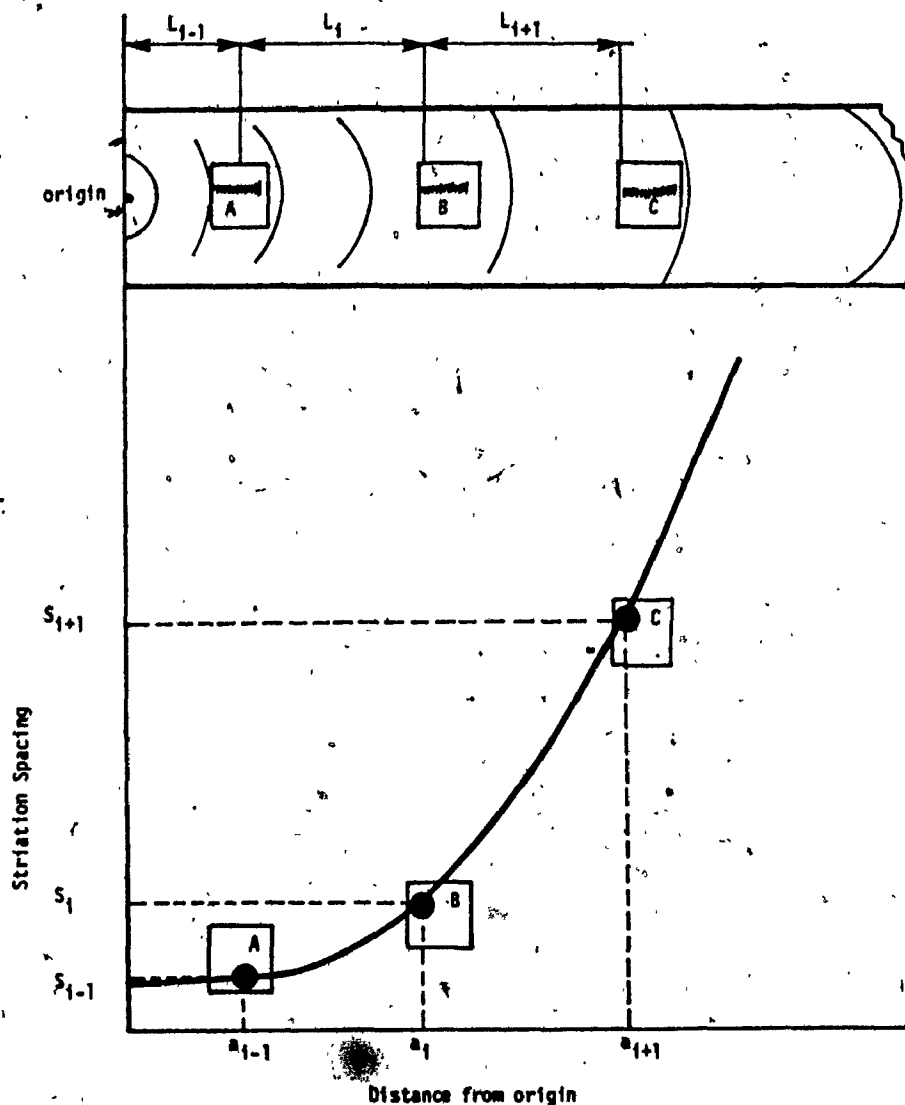
Figure 58

Curve of striation spacing versus distance from origin
(schematic)

the origin, which makes the striation resolution very

difficult or impossible. Figure 59 shows the limit of

resolution of the SEM and one must imagine that depending on

material and the test conditions there is a certain distance

114

from the origin where the striation count is impossible. Hundreds of thousands or even millions of fatigue striations can be concentrated in a small area immediately adjacent to the origin and can not be counted. Furthermore as shown in section 2.3.3.2.1, because of impossibility of resolving the finest fatigue striations the exact mechanism of fracture very close to the origin is not known. The human factor plays an important role here in sofar as an experienced microscopist is capable of obtaining micrographs from regions much closer to the origin than can an inexperienced investigator. The material characteristics can be unhelpful particularly to the novice in the field, for example some grades of steel produce poor striations compared with aluminum. Obviously, the larger the number of fields investigated the smaller the error, however one must consider the increasing cost of investigation when long fractures are examined: Given the need to select at least two fields for each mm of crack length (rule e from section 3.3.1.2) one must obtain and analyze a minimum of 50 micrographs for each inch of crack. Despite the expense this is the usual number of photographs we have taken in our investigation.

Another important factor to be considered is the quality of the fracture surface. Corrosion products, fretting oxides, dirt and especially mechanical damage (smearing, rubbing, etc) can obliterate the microfeatures partially or
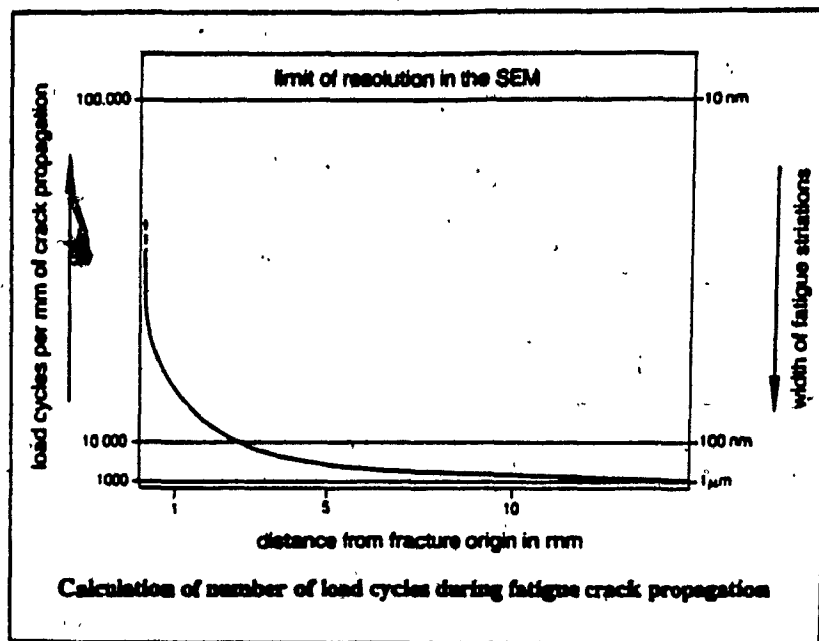
Figure 59

Quantitative evaluation of striations [11]

completely. These problems are always more extensive in the

case of service failures than in the case of test specimens.

Again the microscopist's experience in cleaning fracture

surfaces, as well as his ability to find well-resolved

patches of fatigue striaions are essential to an accurate

quantitative examination.

With adequate consideration of the limitations of the

method it can be concluded beyond any doubt that the

fractographic examination of fatigue and damage tolerance

test articles is an extremely important method of verifying

reliability during a certification program of a modern

aircraft.

4. EXPERIMENTAL RESULTS

4.1. GENERAL COMMENTS

Two experimental programs are presented:

Program #1: Studies the fractographic examination of standard-fatigue specimens tested under a constant amplitude loading spectrum.

Program #2: Studies the fractographic examination of real aircraft components. The experimental work presented consisted basically of the findings of the most representative analysis performed on different components from CL 600/601 Challenger fatigue and damage tolerance tests. These tests were conducted under flight simulated loading (Block Loading).

Both programs were carried out at Canadair Ltd., Materials & Process Engineering Laboratory between 1982-1985.

4.2 QUANTITATIVE FRACTOGRAPHIC EXAMINATIONS OF SAMPLES TESTED UNDER CONSTANT AMPLITUDE LOADING SPECTRUM

4.2.1. Objectives

The test was carried out to verify the applicability of fractographic examinations in determination of data necessary to construct the F.C.P. curves. The fractographic examination must determine the average crack propagation rates and the estimated number of cycles necessary to

117

propagate the crack to a certain depth by measuring the striation spacings at selected locations along the fracture. Another objective was to demonstrate the validity of the Bates and Clark formula to calculate the stress intensity factor ΔK, from the striation spacing measurements (see section 2.3.3.2.1.).

Recommended Thickness: $\frac{W}{20} \leq B \leq \frac{W}{4}$

Minimum Dimensions: W = 25 mm (1.0 in)

$a_n = 0.20W$

Note 1 – Dimensions are in millimetres (inches)

Note 2 – A-surfaces shall be perpendicular and parallel as applicable to within 0.002 W, TIR

Note 3 – The intersection of the tips of the machined notch (a_n) with the specimen faces shall be equally distant from the top and bottom edges of the specimen to within 0.005 W

Figure 60

Standard Compact-Type (CT) Speciment for Fatigue Crack Growth Rate Testing.

118

4.2.2. Procedure

The test was carried out using Standard Compact - CT
type specimens, fabricated in accordance to the requirements
of ASTM E399 -" Standard Test Method for Plane-Strain
Fracture Toughness of Metallic Materials", Figure 60. The
provenience and the principal material characteristics of the
four specimens examined are given in Table 6.

Table 6

Material characteristics

Lab. Code	Vendor Code	Aluminum Alloy	Chemical Composition					Yield Strength -ksi-	Modulus of Elasticity x10³ ksi
			Zn %	Cu %	Mg %	Zr %	Cr %		
1	Alcoa "A"	7050	6.11	2.06	2.36	0.12	-	72.1	10.2
2	Alcoa "K"	7475	5.62	1.68	2.14	-	0.24	61.9	10.2
3	Cegedur "F"	7050	6.35	2.05	2.48	0.11	-	70.3	10.2
4	Cegedur "G"	7475	5.66	1.55	2.35	-	0.21	57.0	10.2

The specimens were loaded on a fatigue testing machine Satec
Sonntag SF-1U and the crack extension was measured with a
travelling microscope during the test. The loading spectrum

119

consisted in a succesion of equal amplitude tension-tension cycles with P_{MAX} = 500 kgf and P_{MIN} = 450 kgf. Each sample was loaded until the crack extended between 4.5 and 5 mm long. Then the fatigue cycling was stopped and the specimens were broken open using a tensile machine Satec Baldwin.

The exposed fracture surfaces were prepared and then examined by means of a Scanning Electron Microscope SEMCO Nanolab 7. The quantitative fractographic examinations were carried out in accordance with the rules and techniques explained in section 3.3 of this thesis.

The visual measurements of the crack extension with the associated number of cyles necessary to produce such a crack depth, were then used to compute both the macroscopic crack growth rate da/dN and the macroscopic stress intensity factor ΔK. To make easier these computations a computer program was adapted for the CDC Cyber 835 of Concordia University Computer Center. This version was developed using an original program given in ASTM E647. The program is listed in Appendix #1.

Then the fractographic measurements were used to compute the fractographic crack growth rate da/dN. The fractographic stress intensity factor, ΔK, was calculated using the Bates & Clark equation:

$$\Delta K_{FRACT} = 0.408E\sqrt{S}$$

where   E = Young's modulus of elasticity
          S = striation spacing

4.2.3. Results

The crack advance as measured macroscopically (with a travelling microscope along the specimen sides) and the corresponding number of cycles are shown in Tables 7-10. In, these tables are shown also the results of the seven point incremental polynomial method used in the computer program for determing the crack growth rate da/dN, as well as the values of stress intensity factor ΔK as computed from the linear elastic stress analysis equations. For each of the four specimens used, the fatigue-cracking was halted 10 times and the crack advance was measured on the specimen side. All tests were conducted at room temperature and with a mean stress ratio of R=0.053.

The results of quantitative fractographic analysis are tabulated in Tables 11-14. The results of the striation counting are given for the deepest crack penetration point and therefore when compared with the macroscopic results one must expect to see higher crack propagation rates for fractographic measurements than for macroscopic measurements. Indeed when the crack growth curves versus the number of cycles were plotted for both the macroscopic and the fractographic observations, Figures 61-64, these curves show that the F.C.P. rates as calculated by means of quantitative fractography give higher values than the F.C.P. rates as calculated from the macroscopic observation. The explanation

TABLE 7

SEVEN POINT INCREMENTAL POLYNOMIAL METHOD FOR DETERMINING DADN

SPEC. NO.   1   NO. POINTS = 10

CT SPECIMEN   B = 1.505IN. W = 3.002IN.   AN = 1.260IN.
PMIN = .110KIPS   PMAX = 2.090KIPS   R = .053
TEMP = 76.F

OBS NO	CYCLES	A(MEAS)	A(REG)	M.C.C	DELK	DA/DN
1	150000.	1.272				
2	180000.	1.285				
3	200000.	1.298				
4	225000.	1.305	1.310	.986255	6.04	.614E-06
5	250000.	1.333	1.324	.971650	6.22	.753E-06
6	290000.	1.350	1.357	.977068	6.32	.117E-05
7	315000.	1.380	1.389	.978500	6.50	.145E-05
8	325000.	1.410				
9	340000.	1.435				
10	350000.	1.444				

*DATA VIOLATE SPECIMEN SIZE REQUIREMENTS

TABLE 8

SEVEN POINT INCREMENTAL POLYNOMIAL METHOD FOR DETERMINING DADN

SPEC. NO.   2   NO. POINTS = 10

CT SPECIMEN   B = .505IN.   W = 3.004IN.   AN = 1.257IN.
PMIN = .110KIPS   PMAX = 2.090KIPS   R = .053
TEMP = 76.F

OBS NO	CYCLES	A(MEAS)	A(REG)	M.C.C	DELK	DA/DN
1	160000.	1.323				
2	200000.	1.332				
3	220000.	1.347				
4	245000.	1.362	1.361	.987140	6.33	.551E-06
5	280000.	1.382	1.384	.997852	6.56	.585E-06
6	290000.	1.392	1.388	.995505	6.63	.593E-06
7	325000.	1.407	1.409	.995895	6.68	.608E-06
8	350000.	1.422				
9	375000.	1.440				
10	400000.	1.457				

*DATA VIOLATE SPECIMEN SIZE REQUIREMENTS

TABLE 9

SEVEN POINT INCREMENTAL POLYNOMIAL METHOD FOR DETERMINING DADN

SPEC. NO. 3   NO. POINTS = 10

CT SPECIMEN   B = 1.496IN.   W = 3.002IN.   AN = 1.252IN
PMIN = .110KIPS   PMAX = 2.090KIPS   R =   .053
TEMP = 76.F

OBS NO	CYCLES	A(MEAS)	A(REG)	M.C.C	DELK	DA/DN
1	101000.	1.277				
2	125000.	1.297				
3	145000.	1.312				
4	153000.	1.320	1.323	.996245	6.17	.104E-05
5	175000.	1.352	1.347	.995689	6.33	.119E-05
6	200000.	1.377	1.379	.994775	6.55	.143E-05
7	215000.	1.397	1.401	.983361	6.62	.191E-05
8	225000.	1.417				
9	235000.	1.437				
10	245000.	1.477				

*DATA VIOLATE SPECIMEN SIZE REQUIREMENTS

TABLE 10

SEVEN POINT INCREMENTAL POLYNOMIAL METHOD FOR DETERMINING DADN

SPEC. NO.   4   NO. POINTS = 10

CT SPECIMEN   B = 1.502IN   W = 2.999IN   AN = 1.255IN
PMIN = .110KIPS   PMAX = 2.090KIPS   R =.053
TEMP = 76.F

OBS NO	CYCLES	A(MEAS)	A(REG)	M.C.C	DELK	DA/DN
1	122000.	1.275				
2	161000.	1.290				
3	193000.	1.300				
4	203000.	1.311	1.307	.978617	6.15	.474E-06
5	248000.	1.330	1.331	.981777	6.18	.545E-06
6	285000.	1.345	1.352	.976288	6.29	.657E-06
7	303000.	1.373	1.362	.963294	6.50	.773E-06
8	362000.	1.400				
9	375000.	1.430				
10	383000.	1.455				

*DATA VIOLATE SPECIMEN SIZE REQUIREMENT

123

TABLE 11

Specimen: #1
ALCOA "A"
Material: 7050 Al Alloy

Pos	Dist from Origin -mm-	-in-	*1) Am -in-	Striation Count No. cycles	Length -mm	Magn. -x-	Striation Density cycle/mm	Striation Spacing x10-5 mm/cycle	x10-6 in/cycle	Est. No of cycles min	Cumm. cycles min	Avg. da/dN x10-5 mm/cycle	x10-6 in/cycle	ΔK ksi√in
1	0.90	0.035	1.2950	CL*2)	-	-	>10^5	<1.0	<0.40	90000	90090	<1.0	<0.4	<0.80
2	1.53	0.060	1.3200	11	13	20000	16965	5.89	2.32	24448	114448	1.34	0.5	6.33
3	2.98	0.1170	1.3770	9	10	16000	14400	6.96	2.74	20833	135881	2.19	0.9	6.88
4	5.26	0.2070	1.4670	16	15	9000	9600	10.41	4.10	55609	191490	2.75	1.1	8.42
5	6.10	0.2400	1.5000	5	4	7100	8875	11.30	4.40	19090	210580	2.90	1.1	8.72
6	7.61	0.2990	1.5590	6	4	3800	5700	17.50	6.90	8628	219208	3.47	1.4	10.92

*1) Am = An+a where An = machined notch = 1.260 in.

*2) CL = Cleavage (ultra-low growth regime)

TABLE 12

Specimen: #2
ALCOA "K"
Material: 7475 Al. Alloy

Pos	Dist from Origin -mm-	-in-	*1) Am -in-	Striation Count No. cycles	Length -mm	Magn. -x-	Striation Density cycle/mm	Striation Spacing x10-5 mm/cycle	x10-6 in/cycle	Est. No of cycles min	Cumm. cycles min	Avg. da/dN x10-5 mm/cycle	x10-6 in/cycle	ΔK ksi√in
1	0.82	0.032	1.289	CL*2)	-	-	>10^5	<1.0	<0.40	82000	82000	1.00	<0.4	<0.8
2	1.05	0.040	1.297	9	10	20750	18675	5.31	2.10	4331	86331	1.22	0.5	6.02
3	1.42	0.055	1.312	6	8	14750	11062	9.02	3.55	4101	90432	1.57	0.6	7.83
4	2.45	0.096	1.353	8	10	13700	10960	9.12	3.59	11293	101725	2.41	0.9	7.88
5	3.25	0.127	1.384	9	10	11430	10288	9.72	3.82	8230	109955	2.96	1.2	8.13
6	4.24	0.166	1.423	16	15	9000	9600	10.41	4.09	9510	119465	3.55	1.4	8.41
7	4.34	0.170	1.427	16	15	9000	9600	10.41	4.09	960	120425	3.60	1.4	8.41
8	5.87	0.231	1.488	6	8	9600	7200	13.90	5.47	11007	131432	4.47	1.8	9.72

*1) Am = An+a where An = machined notch = 1.257 in.

*2) CL = Cleavage (ultra-low growth regime)

TABLE 13,

Pos	Dist from Origin -mm-	-in-	*1) Am -in-	Striation Count No. cycles	Length -mm-	Magn. -x-	Striation Density cycle/mm	Striation Spacing x10⁻⁵ mm/cycle	x10⁻⁶ in/cycle	Est.No of cycles min	Cumm cycles min	Avg. da/dn x10⁻⁵ mm/cycle	x10⁻⁶ in/cycle	ΔK ksi√in
1	0.72	0.028	1.280	CL*2)	-	-	>10⁵	<1.0	<0.4	72000	72000	<1.0	<0.4	<0.8
2	2.71	0.110	1.362	3	4	21800	16340	6.12	2.41	32516	104516	2.59	1.0	6.45
3	4.25	0.173	1.425	3	4	19600	14700	6.8	2.70	22647	127163	3.34	1.3	6.83
4	6.32	0.257	1.509	6	8	10400	7800	12.8	5.00	16171	143334	4.41	1.7	9.30
5	8.33	0.340	1.592	7	8	7400	6475	15.4	6.10	13051	156385	5.33	2.1	10.27
6	11.06	0.451	1.703	7	9	7800	6066	16.5	6.50	16545	172930	6.40	2.5	10.60

*1) Am = An+a where An = machined notch = 1.252 in.

*2) CL = Cleavage (ultra-low growth regime)

TABLE 14

Pos	Dist from Origin -mm-	-in-	*1) Am -in-	Striation Count No. cycles	Length -mm-	Magn. -x-	Striation Density cycle/mm	Striation Spacing x10⁻⁵ mm/cycle	x10⁻⁶ in/cycle	Est.No of cycles min.	Cumm cycles min	Avg. da/dn x10⁻⁵ mm/cycle	x10⁻⁶ in/cycle	ΔK ksi√in
1	0.08	0.003	1.258	CL*2)	-	-	>10⁵	<1.0	<0.4	8000	8000	<1.0	<0.4	<0.8
2	0.48	0.018	1.273	CL*2)	-	-	>10⁵	<1.0	<0.4	40000	48000	<1.0	<0.4	<0.8
3	0.66	0.026	1.281	6	10	33000	19800	5.06	1.99	3557	51557	1.2	0.5	6
4	2.36	0.093	1.348	6	10	25500	15300	6.55	2.57	25954	77511	3.04	1.2	6.66
5	3.73	0.147	1.402	6	9	15500	10330	9.70	3.81	14123	91634	4.07	1.6	8.11
6	5.34	0.210	1.465	5	5	7000	7000	14.30	5.62	11258	102892	5.19	2.0	9.86
7	6.08	0.240	1.495	9	9	6600	6600	15.20	5.98	4868	107760	5.64	2.2	10.17

*1) Am = An+a where An = machined notch = 1.255 in.

*2) CL = Cleavage (ultra-low growth regime)
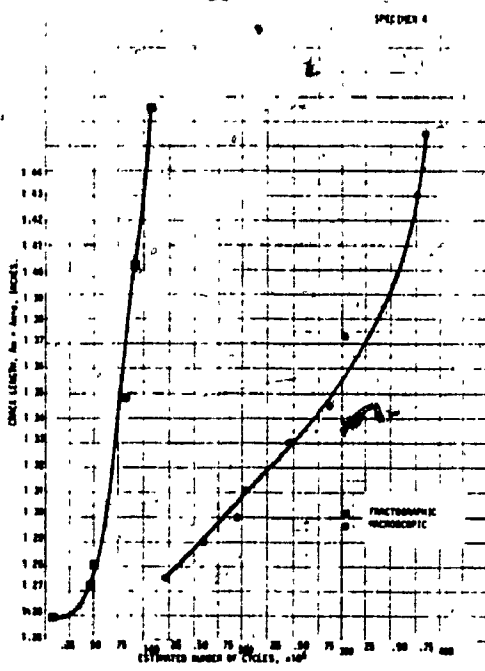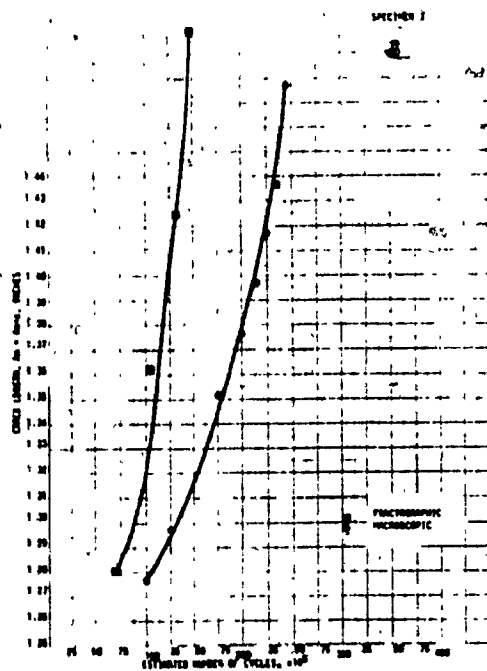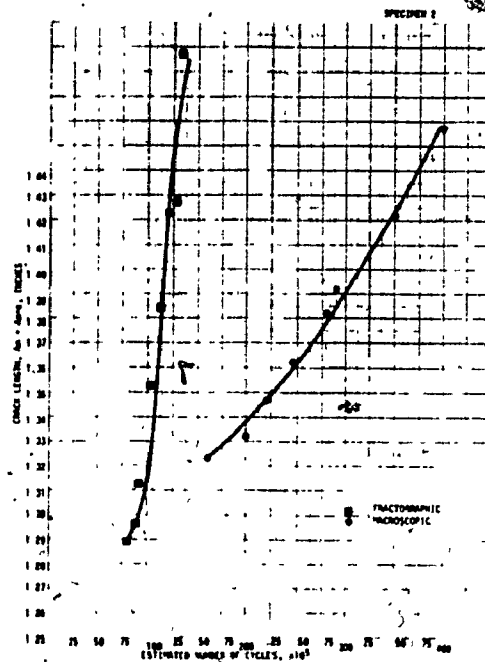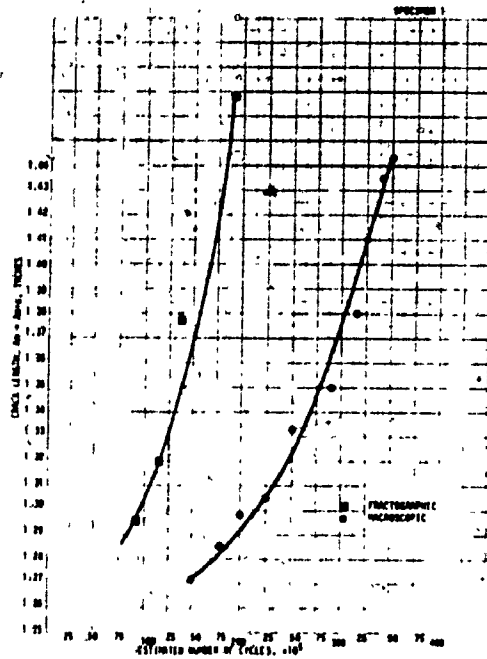
Figure 61-64

Fatigue crack growth curves of the four specimens as
constructed based on both the fractographic analysis and
macroscopic data.

of this difference can be found in consideration of the phenomenon of crack tunnelling which is easily visible on all four specimens examined, Figure 65. One can also observe that specimens #2 and #4 (7475 Al Alloy) exhibit a more pronounced tendency for crack tunnelling than specimens #1 and #3 (7050 Al Alloy). The explanation can be found if one calculates the plastic zone size for plane stress (at the specimen edges, see Figure 10). By using the Irwin's model the plastic zone radius may be computed as:

$$r_y = \frac{1}{2\pi} \cdot \frac{K^2}{\sigma_{ys}^2}$$

Using the σ_y values given in Table 6 and considering the other parameters as identical in both cases:

$$R_{ALCOA} = \frac{r_{y7050}}{r_{y7475}} = \frac{(1/72.1)^2}{(1/61.9)^2} = 0.73$$

and

$$R_{CEGEDUR} = \frac{r_{y7050}}{r_{y7475}} = \frac{(1/70.3)^2}{(1/57.0)^2} = 0.65$$

The results revealed that the size of the plane stress plastic zones created at the specimen sides are larger in the case of 7475 Al Alloy than in the case of 7050 Al Alloy and therefore the crack will propagate slower at the specimen sides in the case of 7475 Al Alloy than in the case of 7050 Al Alloy. This will create a more pronounced crack tunnelling for 7475 Al Alloy than for 7050 Al Alloy.

Based on the above observations, it was considered that

127

the fractographic examination provided more realistic results than the crack monitoring during the test.

The second objective, to verify the accuracy of the Bates and Clark equation for calculating the stress intensity factor ΔK from the striation spacing measurements was carried out as well. Comparative results of the two methods to compute ΔK are shown in Figures 66-69 where ΔK was plotted versus the distance from the origin as calculated from both fractographic examination and from macroscopic observations. The comparison revealed a quite good correlation between the two methods for the ΔK range examined. However, it must be emphasized that in the regions adjacent to the initiation the macroscopic observations cannot provide accurate data due to the small crack length visible on the specimen edges and due to the phenomena of crack tunnelling and it is rather obvious from the Figures 66 - 69 that fractographic examinations can provide a much accurate estimation of the stress intensity factor, ΔK, in these regions.

With respect to the Bates and Clark equation it was demonstrated again that it is an accurate numerical tool to estimate the stress intensity factor from the striation spacing.
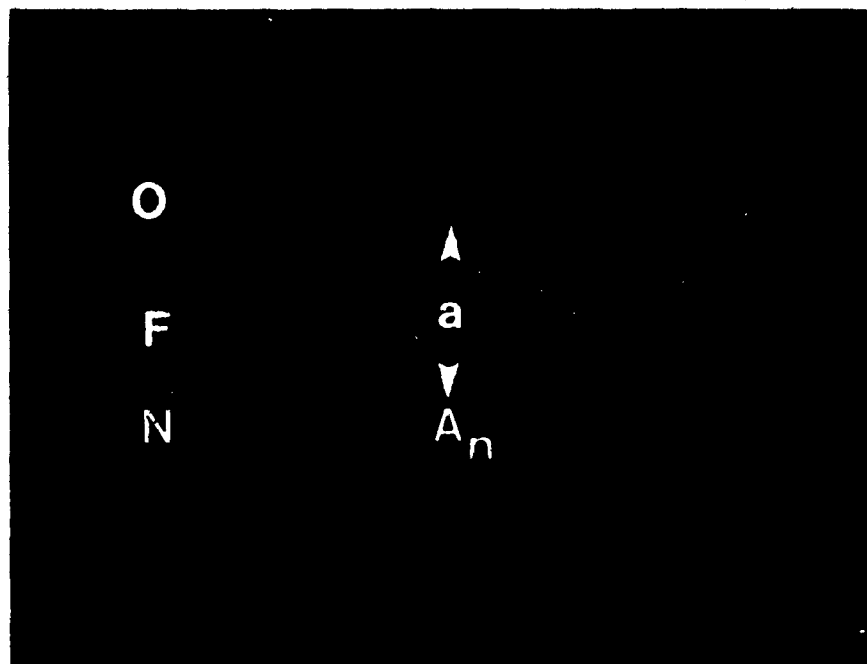
Figure 65

F = Fatigue crack   0 = Overload fracture   N= Machined notch

Evidence of crack tunnelling; deeper crack penetration in the center than on the edges.
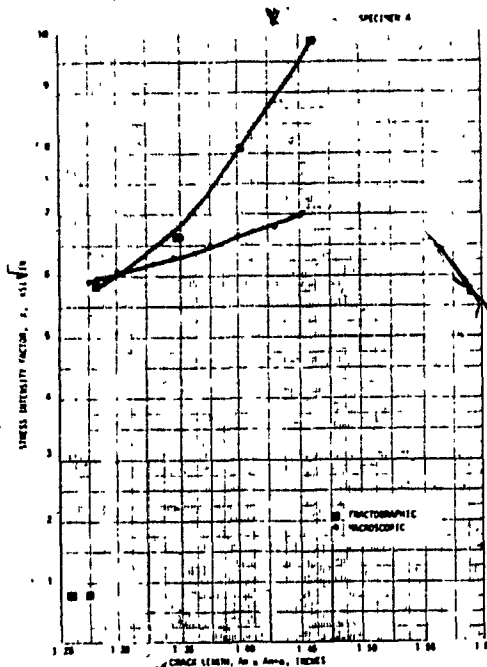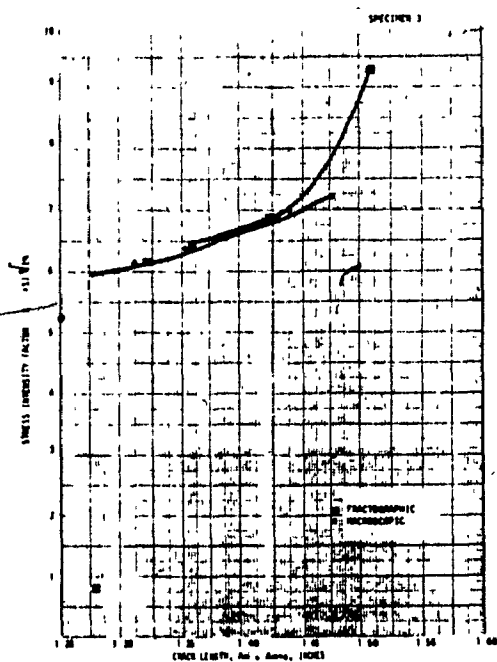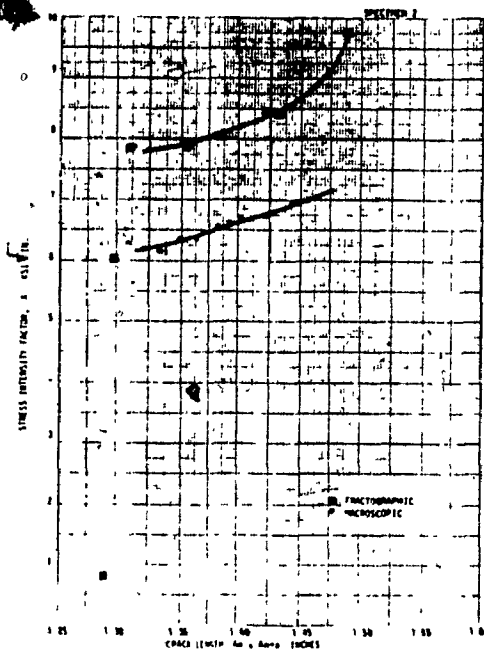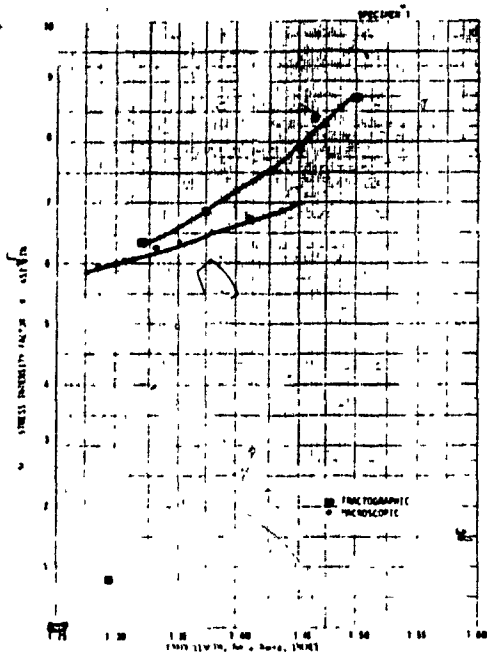
Figure 66-69

The variation of the stress intensity factor ΔK with the
crack length as determined by fractographic measurements (and
using the Bates and Clark formula) and compared with the
stress intensity factor computed from linear elastic stress
analysis.

4.3 QUANTITATIVE FRACTOGRAPHIC EXAMINATION OF AIRCRAFT COMPONENTS SUBJECTED TO FLIGHT SIMULATED LOADING SPECTRUM

4.3.1. Flap/value assembly

4.3.1.1. Objectives

The general objective of the test was "to determine the fatigue and damage tolerance characteristics of the inboard and outboard flap and vane assemblies and their attachment to the wing box structure" [85,86]. The test specimens used in these tests consisted of:

- a complete flap and vane assembly including flap arms, hinge box assemblies, vane supports and wing attachment fittings manufactured as per the latest design modifications to the standard requirement for CL 600 601 production aircraft.

The schematic loading arrangements are shown in Figures 70 & 71. Figure 72 shows the loading arrangement on the test rig. The applied loading spectra [87] are tabulated in Table 15.

131
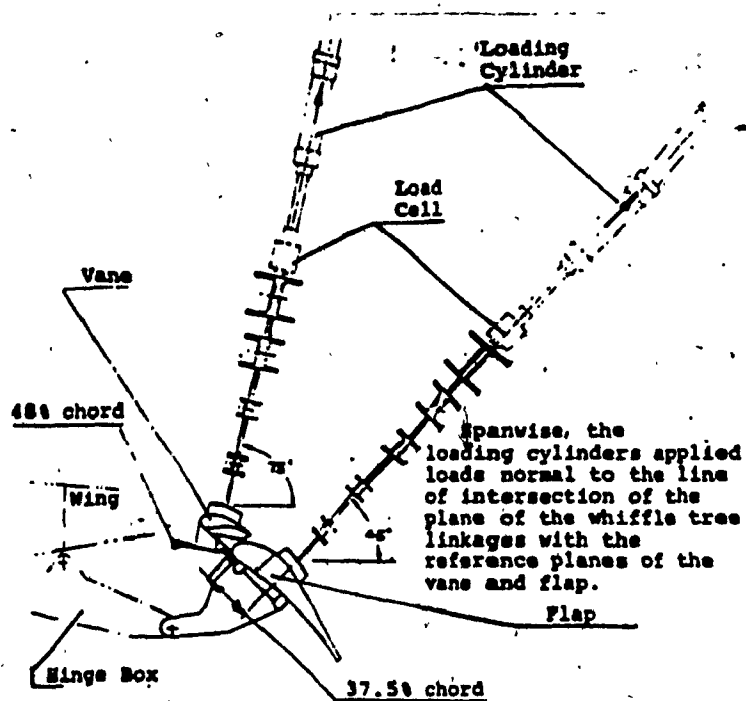
Figure 70

Outboard flap/vane fatigue and damage tolerance test, loading
arrangement.

Spanwise, the loading cylinders
applied loads normal to the line
of intersection of the plane of
the whiffle tree linkages with
the reference planes of the
vane and flap.
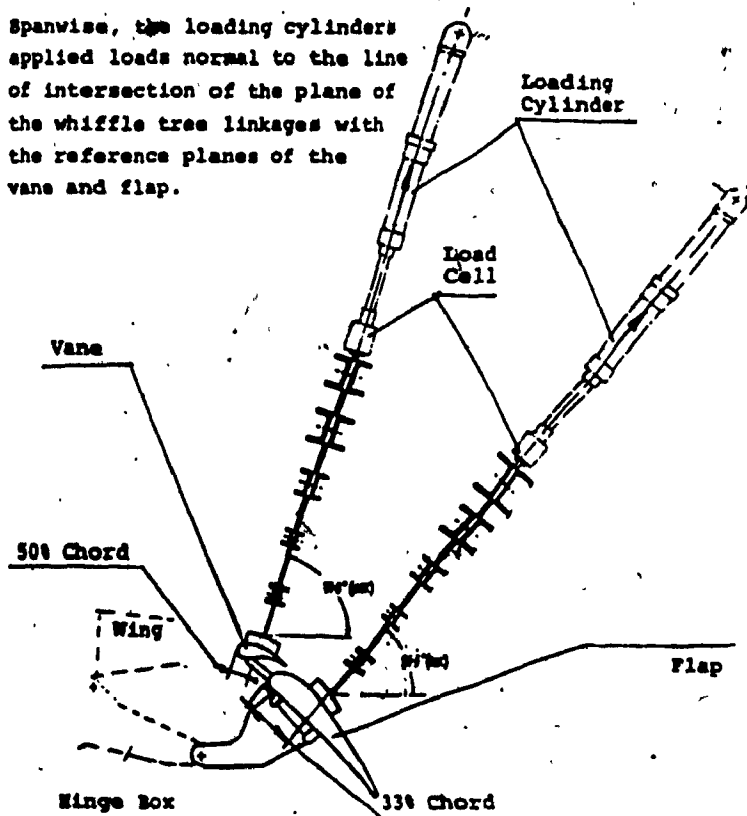
Figure 71

Inboard flap/vane, fatigue and damage tolerance test, loading
arrangement.

Figure 72

A general view of the test rig. The encircled numbers
indicate the approximate location of each of the four parts
examined. The fuselage is visible in the background.

Table 15

Loading Spectrum Applied During The Flap /Vane Assembly's,
Fatigue Test
LOADING_SPECTRUM_OF_ONE_BLOCK

Outboard Flap & Vane Assembly

Loading sequence	No. of Cycles	Vane Loading Cylinder		Flap Loading Cylinder	
		Min	Max	Min	Max
		(lbs)		(lbs)	
a	20	0	536	0	1860
b	66	0	701	0	2432
c	14	0	879	0	3052
d	15	0	1745	0	2120
e	63	0	2002	0	2447
f	22	0	2304	0	2800
Total per 1 Block	200				

Inboard Flap & Vane Assembly

Loading Sequence	No. of Cycles	Vane Loading Cylinder		Flap Loading Cylinder	
		Min	Max	Min	Max
		(lbs)		(lbs)	
a	20	0	531	0	2268
b	66	0	695	0	2966
c	14	0	871	0	3720
d	15	0	1651	0	2437
e	63	0	1906	0	2813
f	22	0	2180	0	3218
Total per 1 Block	200				

200 cycles = 100 flights = 1 block

As stated above the test objectives was the
determination of fatigue and damage tolerance characteristics
of the assembly. Some components use tests for fatigue life
and other componenets were tested for damage tolerance,
depending on the design philosophy used. In the case of the
components tested for damage tolerance after a long period of
fatigue testing without any visible natural cracking
occuring, "saw cuts" were introduced at critical locations,
to facilitate the crack initiation. The cuts were produced
with a very fine jeweler's saw, approximately 0.008" wide.
The intended saw cut depth was in the range of 0.050". The
crack-free period was 72000 flights on the outboard flap/vane
assembly and 92400 flights on inboard flap/vane assembly. At
these points the test was halted and the saw cuts were
introduced.

The objectives of the fractographic exmination were: 1
to identify the predominant loading spectrum 2) to provide
the necessary data to construct the F.C.P. curves and to
determine the first N.D.T. inspection intervales.

The fractographic techniques used to achieve these
objectives are described in the next paragraph.

With respect to the results of the quantitative
fractographic examination it must be reminded that there is a
basic differentiation between the interpretation of these
results.

In the case of fatigue testing (no saw cuts) where the initiation stage plays an important role, the number of cycles determined by the fractographic examination was normalized by a safety factor. Because the selection of these safety factors were not in the responsability of Materials and Process Engineering Laboratory, the real values of the fatigue life and the first N.D.T. inspection interval as submitted to the flight safety authorities are not presented in this thesis. However, the reader must be perfectly aware that this procedure was carried out and the fatigue life of each component was determined conservatively and was considered to be safe.

In the case of damage tolerance testing components with saw cuts it must be emphasized that the fatigue life was artificially shortened and in real life service we expect longer lives than those determined in testing.

The entire program of fractographic examinations of the broken components from these fatigue and damage tolerance tests represents an effort which was extended over a three-year period. Clearly, it is beyond the scope of this thesis to cover all the aspects of this program. A selection of the most representative parts examined during this program is tabulated in Table 16, and the fractographic analysis of the above parts is detailed in the following sections.

Table 16

Representative parts of fractographic examination program.

Pos.	Assembly	Ref.	Part Name	Cracking	Representative of:
1	Outboard Flap/Vane	88	Forward Outboard Lug, Hinge Box Assembly	Natural	•Identification of the Loading Spectrum
2			Flap Arm, Hinge Arm Assembly	Saw Cuts	•Identification of the Loading Spectrum. •Retardation and Acceleration
3	Inboard Flap/Vane	89	Vane-Actuator Cradle Assembly	Natural & Saw Cuts	•Identification of the Loading Spectrum. •Comparison Between Natural and Artificial (Saw Cut) Initiation
4	Inboard Flap-Hinge Box	80	Hinge Box	Natural	•Identification of the Loading Spectrum. •Crack Front Tunnelling and Tensile Jumping.

4.3.1.2. Fractographic techniques and loading spectrum identification

The general fractographic technique followed strictly the principles and the rules detailed in previous sections. Majority of the fractured parts, submitted for examination exhibited clean fracture surfaces without significant mechanical or corrosion damage.

As shown in Table 15, the flap/vane assembly was subjected to loading from two sources: flap loads and vane loads. Due to the assembly complexity, it was difficult to visualize the interaction between these different loads and

137

their influence on each component. Therefore one of the major tasks of the fractographic examination was to determine for each component the source of stresses (vane originated or flap originated) in order to verify the accuracy of the theoretical analysis. The source of stresses can be determined based on the identification of the microscopic fracture imprint with the loading spectra.

The analysis of the loading spectra given in Table 15 revealed that one must expect to see two different types of microscopic fracture imprints:

- One type will exhibit crack advancess due to all loading sequences (from "a" to "f"). This microscopic fracture imprint will be produced when the flap loading prevailed because the loading succession is such that no major retardation effect is expected. Some minor retardation is expected to be seen between cycle "f" and "a" and between cycle "c" and "d". A typical microscopic fracture imprint of this type is shown in Figure 73.

- The second type will exhibit crack advances due to loading sequences "d", "e" and "f" only. This microscopic fracture imprint will be produced when the vane loading prevailed because the highest peaks loading ("d", "e", "f") will create a plastic zone large enough to retard the minor loadings ("a", "b", "c"). A typical fractographic imprint of this type of loading is shown in Figure 74.

Figure 73

The identification of the loading spectrum with the
microscopic fracture imprint. The direction of propagation
is from the bottom to the top. The letters represent the
corresponding sequence (see Table 15) of the spectrum. All
loading sequences contributed to the crack advance and only
minor retardation was found. (Flap loading condition
prevailed).

Figure 74

The identification of the loading spectrum with the
microscopic fracture imprint. The direction of propagation
is from bottom to the top. The letters represent the
corresponding sequence (see Table 15) of the spectrum. The
sequences "a", "b" and "c" were almost completely retarded by
the high loading of sequence "f". (Vane loading condition
prevailed).

After this identification, the block count (rather than striation count) technique was carried-out, following, as stated before the rules established in literature. Two specific techniques were developed:

- when the block density was high and it was not possible to measure each individual block, a general micrograph at lower magnification was taken and the block count was carried out on this micrograph.

- when the block density was relatively low and it was possible to measure each individual block, this was done by using the microscope micrometer. These results were then used in constructing the F.C.P. curves.

The microfractographic measurements were done in the metric system because the SEM is calibrated in this system. A conversion to the American system was done in the building of the F.C.P. curves.

4.3.1.3. Forward_outboard_lug,_hinge_box_assembly_W.S._178.0
Failed at: 87400 flights

A general view of the part as received is shown in Figure 75. The part contained two fractures, both originated at the inner circumference and propagating outwards. The fracture marked as #1 (upper crack) originated at the indicated corner and propagated diagonally in respect to the part thickness. The fracture plane was smooth and relatively

flat; Figure 76. The fracture marked as #2 (lower crack)
originated from multiple origins and propagated radially.
The fracture plane was curved, but relatively smooth, Figure
77.
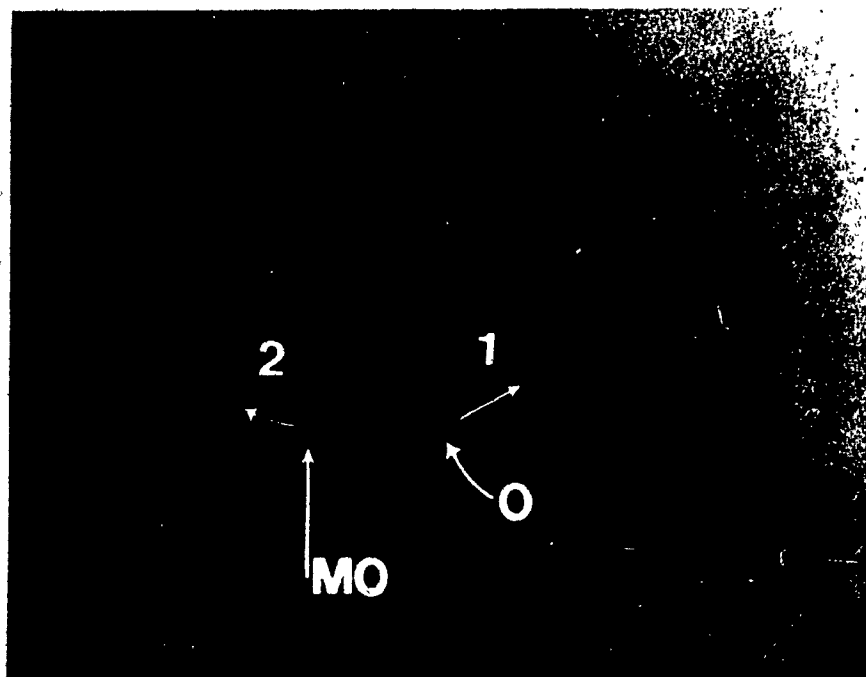
Figure 7-5   Magnification: 1.62x

General View of the Forward Outboard Attachment Lug, Hinge
Box Assembly.
0 = One Origin   MO = Multiple Origins
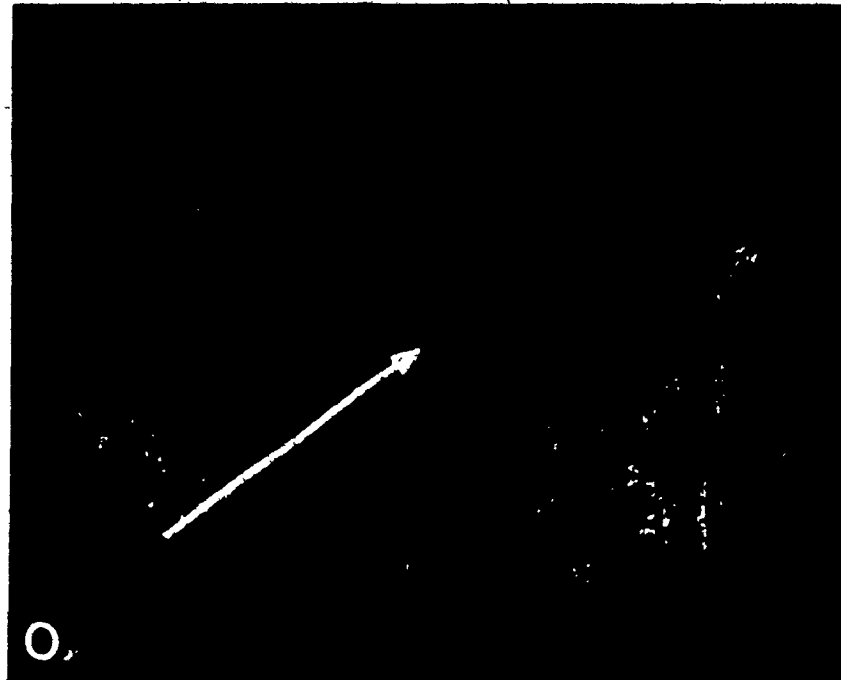
Figure 76   Magnification: 8x

General View of the Fracture #1. The origin and the direction
of propagation are indicated.
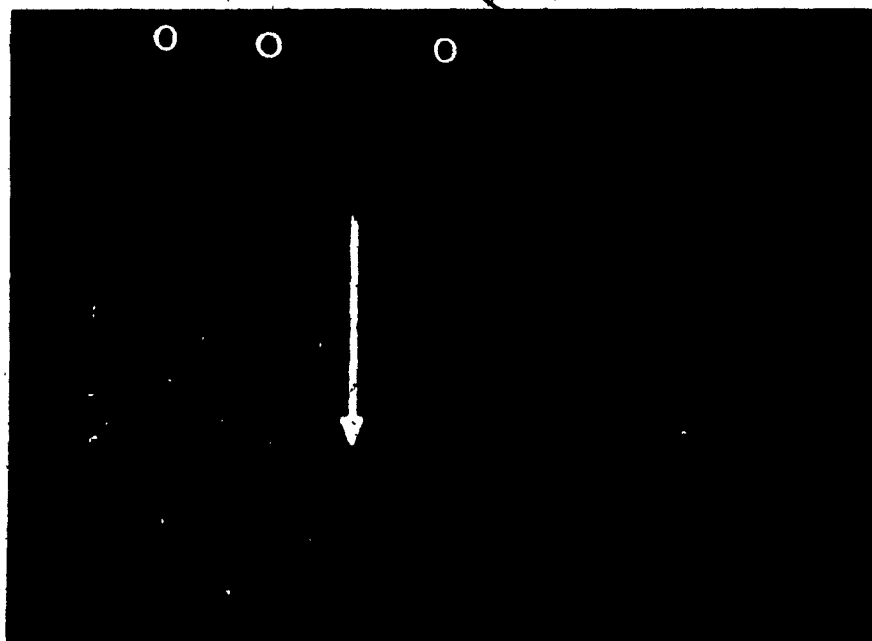
Figure 77   Magnification: 8x

General View of the Fracture #2.   Multiple origins are
indicated as well as the direction of propagation.
O = Origin

143

Scanning electron microscope examinations were carried out across both fractures. The identification of the loading spectrum with the microscopic fracture imprint revealed that the flap loading conditions prevailed over the vane loading conditions and therefore the stresses on this part were, originated from flap loading. The microscopic fracture imprint is/ shown in Figure 78. After identification of the predominant loading conditions, a quantitative fractographic examination was performed. The results of this examination, tabulated in Tables 17 & 18 revealed that a minimum of 25600 flights were necessary to propagate the crack #1 from the origin to a point located approximately 7.6 mm from the origin. In the case of crack #2, the results indicated that 2700 flights were necessary to propagate the crack from the origin to a point located approximately 4.5 mm from the origin. It is evident from these results that the stress level which generated crack #2 was higher than the stress level which induced crack #1. This is also substantiated by the presence of multiple origins of 'the crack #2 as well as the evidence of secondary cracking across the micromorphology of crack #2. It must be emphasized, however that in the case of crack #2 beyond the positon 4.5 mm a sudden increase in the striation density was observed. This sudden decrease of the crack propagation rate (and thereby, the applied loading) could be attributed to a possible transfer of load to other

144

Figure 78

This microscopic fracture imprint can be identified with a
predominant flap loading spectrum.

BLOCK COUNT

Table 17

CL-600, OUTBOARD FLAP, HINGE BOX ASSY, FWD OUTB. LUG, FRACTURE #1

Pos.	Dist from origin -mm	Block Count		Mag.	Block Density Block/mm	Block Spacing x10^{-4} mm/Block	Estimated Numer of Blocks	Cumm.	Avg. da/dn x10^{-5} mm/cycle
		No.	In length of -mm						
1	0.4826	1	0.0111	-	-	111.0	44	44	5.48
2	0.5588	6	54	910	-	99.0	8	52	5.37
3	0.5715	1	0.0117	-	-	117.0	1	53	5.39
4	0.8763	1	0.0146	-	-	146.0	21	74	5.92
5	1.4196	4	60	910	-	164.0	33	107	6.63
6	1.5367	1	0.0283	-	-	283.0	4	111	6.92
7	2.2860	3	61	950	-	214.0	35	146	7.83
8	3.0302	1	0.0273	-	-	279.0	27	173	8.76
9	3.9878	1	0.0381	-	-	381.0	25	198	10.07
10	4.3942	1	0.0330	-	-	330.0	12	210	10.46
11	5.2984	1	0.0558	-	-	558.0	16	226	11.72
12	6.2458	1	0.0660	-	-	660.0	14	240	13.01
13	6.6624	1	0.0672	-	-	672.0	6	246	13.54
14	7.3837	1	0.0914	-	-	914.0	8	254	14.53
15	7.5768	1	0.0939	-	-	939.0	2	256	14.80

Total number of cycles   51200
Total number of flights   25600

BLOCK COUNT

Table 18

CL600, OUTBOARD FLAP, HINGE BOX ASSY, FWD OUTB LUG, FRACTURE #2

Pos.	Dist from Origin -mm	Block Count		Mag.	Block Density Block/mm	Block Spacing x10^{-4} mm/Block	Estimated Number of Blocks	Cumm.	Avg. da/dn x10^{-5} mm/cycle
		No.	In Length of -mm						
1	0.4089	1	0.208	-	-	2080	2	2	102.2
2	0.8077	1	0.165	-	-	1650	3	5	80.77
3	1.3970	1	0.330	-	-	3300	2	7	99.79
4	2.8397	1	0.226	-	-	2260	7	14	101.42
5	3.8430	1	0.167	-	-	1670	6	20	96.08
6	4.4729	1	0.093	-	-	930	7	27	82.83
7	5.7150	3	38	830	-	152	81	108	26.46
8	5.8445	2	47	830	-	283	4	112	26.09

Total number of cycles   22400
Total number of flights   11200

146

components of the assembly, and therefore the crack

propagation rate of the fracture #2 beyond the position 4.5

mm becomes irrelevant.   As indicated above the total number

of flights necessary to propagate the crack up to 4.5 mm from

the origin was estimated at 2700 and this number was taken

into further computations of the fatigue life.

4.3.1.3.1. Determination_of_fatigue_cracking_initiation_and

the_N.D.T._inspection_interval

Using the data obtained from fractographic analysis the

crack growth curves were plotted, Figure 79.
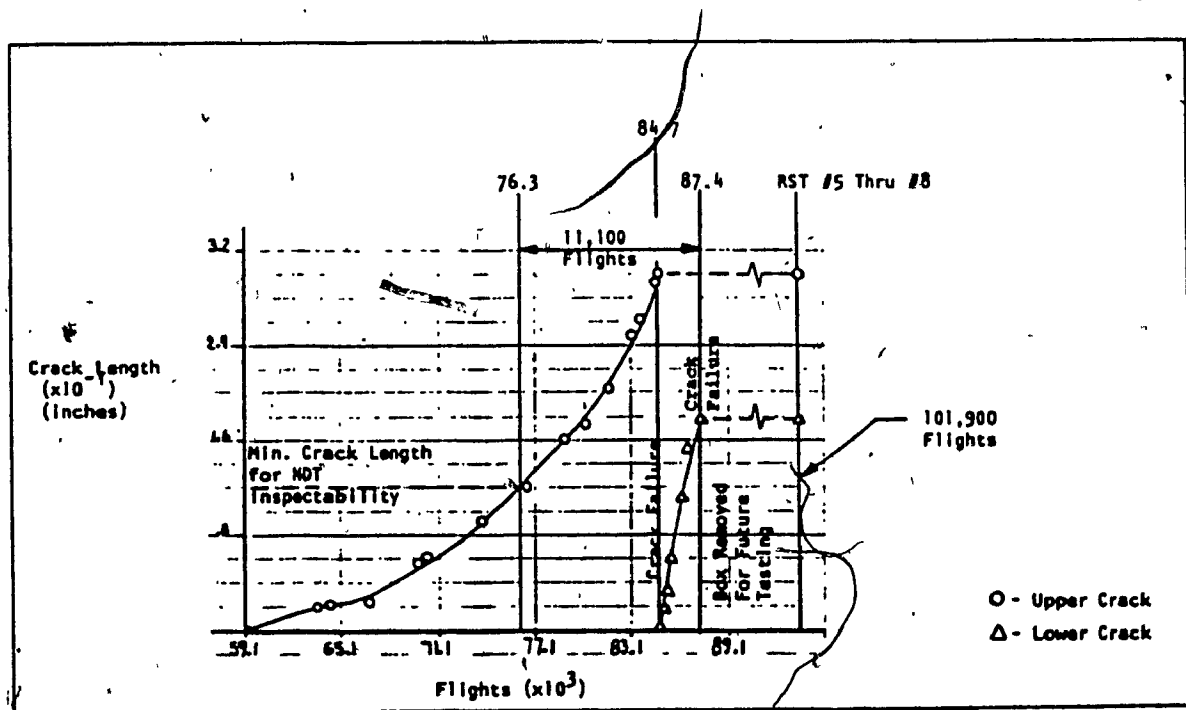
Figure 79

F.C.P. curve of the forward outboard lub, hinge box assembly,
W.S. 178.0.

The final failure of the component occurred in the lower crack at 87400 flights. The fractographic examination revealed that a higher stress level was applied on crack #2 than the stress level applied on crack #1. These findings helped in elaborating a hypothesis that the initial crack nucleation occured at the upper section (crack #1) which propagated for 25600 flights, until the residual strength of this upper cross-section became smaller than the applied load. The complete failure of the upper section produced a transfer of load to the lower cross-section (crack #2), where the crack propagated at a higher rate than did the crack #1, until final failure of the entire component. Based on this rationale the fatigue cracking initiation moment was determined by the following equations:

$$N_{FF\ COMP} = N_{FF_2}$$

$$N_{INIT\ COMP} = N_{INIT_1}$$

$$N_{FF_1} = N_{FF_2} - N_{PROP_2}$$

$$N_{INIT\ COMP} = N_{FF_1} - N_{PROP_1}$$

where $N_{FF\ COMP}$ = Total number of cycles for complete failure of the component

N_{FF_2} = Total number of cycles for failure of cross-section #2 (lower)

N_{FF_1} = Total number of cycles for failure of cross-section #1 (upper)

148

N_{PROP_1} = Total number of cycles required to propagate crack #1 (upper)

N_{PROP_2} = Total number of cycles required to propagate crack #2 (lower)

$N_{INIT\ COMP}$ = Total number of cycles to initiate the first crack of the component.

$N_{INIT\ 1}$ = Total number of cycles to initiate the cracking of cross-section #1 (upper).

Substituting the data one will obtain:

$N_{FF\ COMP}$ = 87400 (recorded in the test logbook)

N_{PROP_2} = 2700 (determined fractographically)

N_{PROP_1} = 25600 (determined fractographically)

Therefore

$N_{FF\ COMP}$ = N_{FF_2} = 87400 flights

N_{FF_1} = 87400 - 2700 = 84700 flights

$N_{INIT\ COMP}$ = $N_{INIT\ 1}$ = 84700 - 25600 = 59100 flights

Considering a minimum detectable crack size as 0.8×10^{-1} inches (2.0 mm) one can determine the first non-destructive test interval (as seen on the curve in Figure 79) as 76300 flights. The F.C.P. curve shows that the failure to detect the crack initiation will allow another 11100 flights until final failure of the component.

4.3.1.4 Flap_arm,_hinge_arm_assembly_W.S._220.0

Failed at: 81600 flights

General views of the part are shown in Figures 80-83.

Visual examination of the part revealed that cracking had initiated at the saw cuts 48A and 49A on both the bottom and the top plate. No other cracking was observed. All four cracks were broken open after visual examination, Figure 84. Visual examination of the exposed fracture surfaces revealed that fatigue cracking had initiated at all four saw cuts. The fatigue cracking propagated outwards from the saw cuts 48A and inwards from the saw cuts 49A, respectively.

Scanning electron microscope examinations were carried out along all four fractures. The first step was to identify the microscopic fracture imprint and to determine which type of loading was predominant in the crack propagation. This identification is shown in Figure 85. Based on the rationale described in section 4.2.1.2. it was evident that the microscopic fracture imprint could be identified with a vane loading spectrum, where the sequences "a", "b" and "c" did not contribute significantly to the crack advance.

However, the microscopic fracture imprint exhibited another important feature: A quite deep step in the crack advance (approximately 5% of one block advance) had occurred between sequences "e" and "f". (See Figure 85,

150

Figure 80 Magnification: .33x

General View of the Flap Arm, Hinge Arm Assembly.
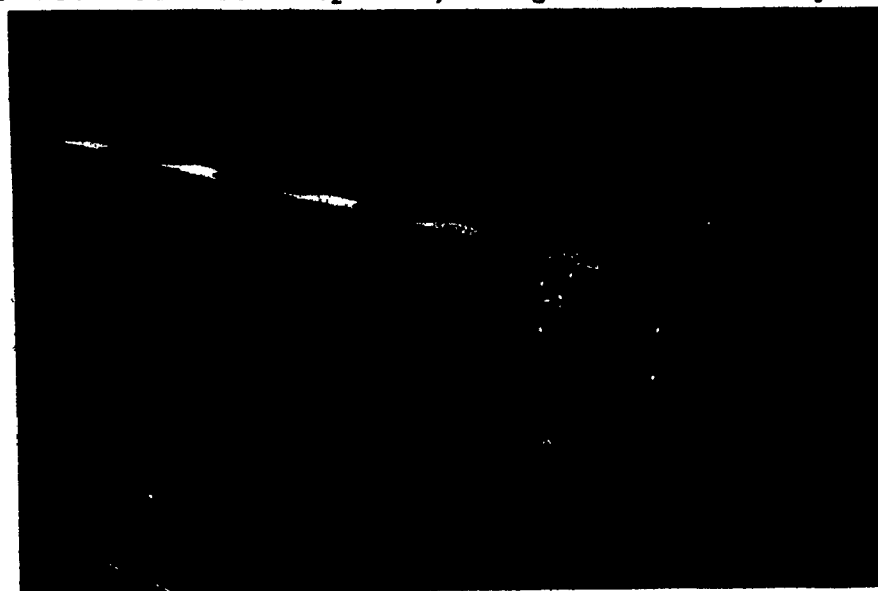
Figure 81 Magnification: .33x

Another general view of the assembly showing the position of crack originated from the saw cuts 48A & 49A.

Figure 82   Magnification: 1.25x

Enlarged view of the damaged area adjacent to saw cuts 48A
and 49A, bottom plate.

Figure 83   Magnification: 1.25x

Enlarged view of the damaged area adjacent to saw cuts 48A
and 49A, top plate.

152
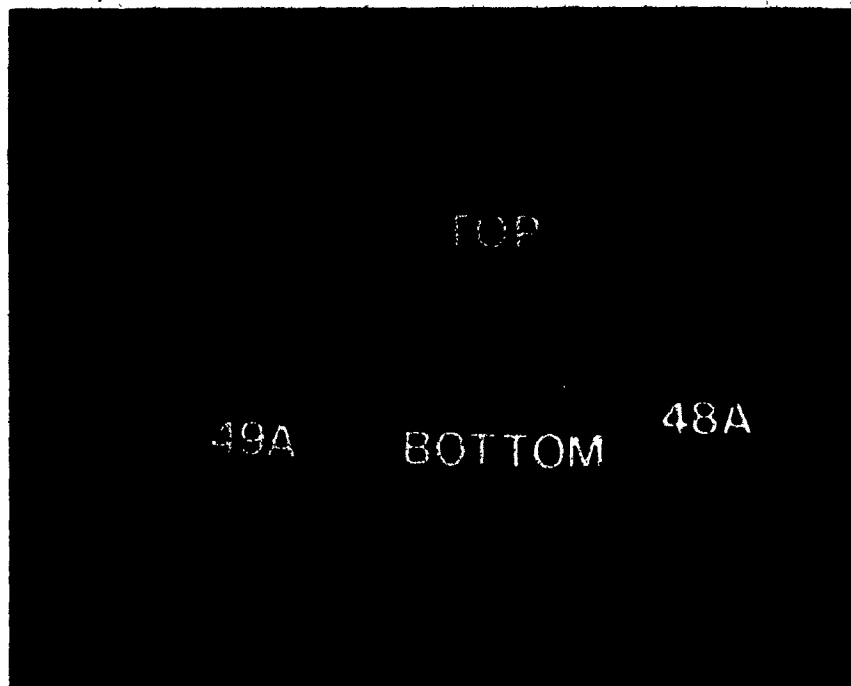
Figure 84   Magnification: 2x

General view of the four cracks after breaking open.

Figure 86

SEM Micrograph   Magnification: 230x
The fracture area immediately adjacent to the saw cut #49A
bottom plate. (The saw cut is at the top of this photo).
Note the well-defined narrow band (avg. depth 0.004").

identified with the letter "x"). This step may be considered as the first cycle of sequence "f", however no rationale could be formulated to explain the sudden acceleration of the crack advance. Several factors could produce this: an uncontrolled increase of the load at the moment when the hydraulic test equipment began sequence "f", and/or combination with other loads (such as flap loadings).

Based on this identification, a block count procedure was carried out along all four fractures. The results are tabulated in Tables 19-22.

Scanning electron microscope examination of the fractures 49A top and bottom revealed also the existance of a well defined narrow (avg. depth 0.004") band immediately adjacent to the origins, Figure 86 . The block density within this band was evidently much higher than the block density on the remainder of the fracture surface. The existance of this well defined narrow band and the higher block density within it are indicative of an initial low stress level. Subsequently a sudden overload and a higher stress level may be associated in time with the complete penetration of the part cross section by the cracks originated at the saw cuts 48A. When this complete penetration has occurred, the entire load would be transferred on the side which contained the cracks originating at the saw cuts 49A.

Figure 85

Showing a microscopic fracture imprint typical of vane
predominant loading spectrum.

BLOCK COUNT

Table 19

CL-600, OUTB. FLAP, HINGE ARM ASSY, FLAP ARM - SAW CUT 48A TOP

Pos.	Dist from origin -mm	Block Count		Mag.	Block Density Block/mm	Block Spacing x10⁻⁴ mm/Block	Estimated Number of Blocks	Cumm.	Avg. da/dn x10⁻⁵ mm/cycle
		No.	In length of -mm						
1	0.0635	1	0.0279	-	-	279	2	2	15.88
2	0.1575	1	0.0254	-	-	254	4	6	13.13
3	0.2362	1	0.0432	-	-	432	2	8	14.76
4	0.3429	1	0.0432	-	-	432	2	10	17.15
5	0.4267	1	0.0406	-	-	406	2	12	17.78
6	0.5537	1	0.0584	-	-	584	2	14	19.78
7	0.7569	1	0.0559	-	-	559	4	18	21.03
8	0.8382	1	0.0682	-	-	682	1	19	22.06

Total number of cycles 3800
Total number of flights 1900

Depth of Saw Cut = 0.047"

BLOCK COUNT

Table 20

CL-600, OUTB FLAP, HINGE ARM ASSY, FLAP ARM, SAW CUT 49A TOP

Pos.	Dist from origin -mm	Block Count		Mag.	Block Density Block/mm	Block Spacing x10⁻⁴ mm/Block	Estimated Number of Blocks	Cumm.	Avg. da/dn x10⁻⁵ mm/cycle
		No.	In length of -mm						
1	0.0812	3	13	3275	525	19.0	43	43	0.94
2	0.1651	1	0.0300	-	-	330.0	3	46	1.79
3	0.2387	1	0.0355	-	-	355.0	2	48	2.49
4	0.4546	1	0.0549	-	-	549.0	4	52	4.37
5	0.6705	1	0.0457	-	-	457.0	5	57	5.88
6	0.6908	1	0.0533	-	-	533.0	1	58	5.96
7	0.9804	1	0.0454	-	-	454.0	6	64	7.66
8	1.0998	1	0.0584	-	-	584.0	2	66	8.33
9	1.6992	1	0.0762	-	-	762.0	8	74	11.48
10	1.9405	1	0.0762	-	-	762.0	3	77	12.60
11	2.4942	1	0.0813	-	-	813.0	7	84	14.85
12	3.1597	1	0.1143	-	-	1143.0	6	90	17.55

Total number of cycles 18000
Total number of flights 9000

Depth of saw cut = 0.041"

BLOCK COUNT

Table 21

CL-600, OUTB. FLAP, HINGE ARM ASSY. FLAP ARM - SAW CUT 48A BOTTOM

Pos.	Dist from origin -mm	Block Count		Mag.	Block Density Block/mm	Block Spacing x10⁻⁴ mm/Block	Estimated Number of Blocks	Cumm.	Avg. da/dn x10⁻⁵ mm/cycle
		No.	In length of -mm						
1	0.0381	2	31	900	58.06	172.2	2	2	9.53
2	0.2006	3	72	850	35.41	282.3	6	8	12.54
3	0.3276	1	0.0330	-	-	330.2	4	12	13.65
4	0.6146	1	0.0508		-	508.0	6	18	17.07
5	0.7416	1	0.0584	-	-	584.0	2	20	18.54
6	1.0033	-	-	-	-	584.0*	5	25	20.07

*Assumed

Total number of cycles   5000
Total number of flights   2500

Depth of saw cut = 0.048"

BLOCK COUNT

Table 22

CL-600, OUTB. FLAP, HINGE ARM ASSY, FLAP ARM, SAW CUT 49A BOTTOM

Pos.	Dist from origin -mm	Block Count		Mag.	Block Density Block/mm	Block Spacing x10⁻⁴ mm/Block	Estimated Number of Blocks	Cumm.	Avg. da/dn x10⁻⁵ mm/cycle
		No.	In length of -mm						
1	0.1052	24	65	910	336.0	29.7	35	35	1.50
2	0.2382	2	56	910	32.5	307.7	6	41	2.88
3	0.4394	1	0.0330	-	-	330.0	6	47	4.67
4	0.5156	1	0.0381	-	-	381.0	2	49	5.26
5	0.6045	1	0.0457	-	-	457.0	2	51	5.93
6	0.7162	1	0.0558	-	-	558.0	2	53	6.76
7	0.8077	1	0.0381	-	-	381.0	2	55	7.34
8	0.9575	1	0.0482	-	-	482.0	3	58	8.25
9	1.1125	1	0.0660	-	-	660.0	3	61	9.12
10	1.4478	1	0.0457	-	-	457.0	7	68	10.65
11	1.6916	1	0.0533	-	-	533.0	5	73	11.59
12	2.3012	1	0.1193	-	-	1193.0	5	78	14.75
13	3.0099	1	0.1520	-	-	1520.0	5	83	18.13

Total number of cycles   16600
Total number of flights   8300

Depth of the saw cut = 0.043"

157

4.3.1.4.1. Determination_of_fatigue_cracking_initiation_and the_N.D.T._inspection_interval

The crack growth curves for all four cracks are shown in Figures 87-88. Based on the fractographic examination findings it was concluded that each pair of crack started more or less simultaneously and therefore the number of cycles necessary to initiate the first crack could be determined by employing the formula:

$$N_{INIT} = N_{FF} - N_{PROP}$$

where N_{INIT} = total cycles necessary to initiate the crack

N_{FF} = total number of applied cycles to final failure

N_{PROP} = number of cycles necessary to propagate the crack

In the case of both 48A and 49A "top" cracks

N_{PROP} = 9000 flights

N_{FF} = 81600 flights

Therefore

N_{INIT} = 81600 - 9000 = 72600 flights

Using a minimum detectable crack size of 0.075" (≈ 2 mm), the first NDT inspection interval can be determined at 76700 flights. Failure to detect the crack initiation will allow another 4900 flights to total failure of the component.

In the case of both 48A and 49A "bottom" cracks

N_{PROP} = 8300 flights

N_{FF} = 81600 flights

Therefore

N_{INIT} = 81600 - 8300 = 73300 flights

Using a minimum detectable crack size of 0.075" (≈ 2 mm); the first NDT inspection interval can be determined at 76200 flights, and another 5400 flights can be performed before final failure of the component.

It must be emphasized that the real life of this component may be longer if one accounts that all four cracks originated from saw cuts approximately 0.050 inches deep, which were introduced in the component after 72000 crack-free flights. This is also confirmed by the F.C.P. curves from Figures 87-88 which revealed that even after the introduction of the saw cuts the crack growth rate stays relatively "flat" and begins to increase only after the crack reaches 0.047"-0.048" in depth, which seems to be the critical crack size for this component and these particular loading conditions.
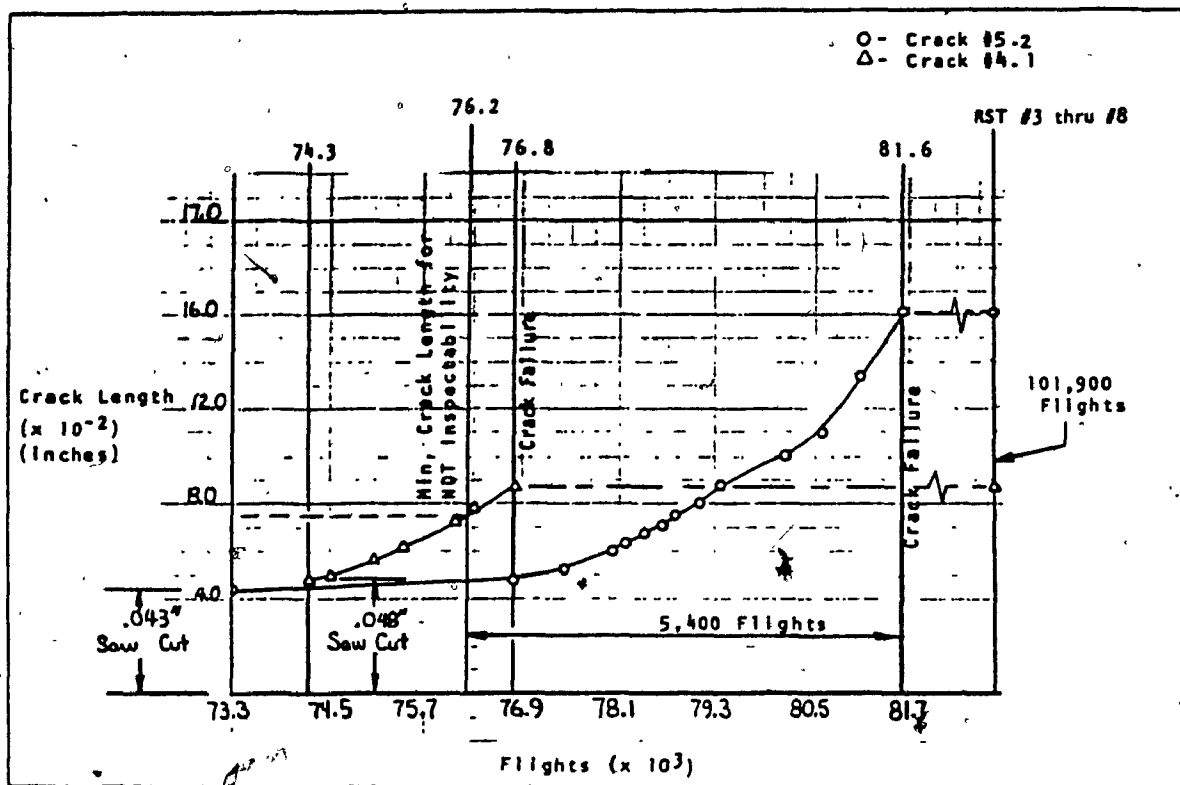
Figure 87

F.C.P. curves of the flap arm, hinge arm assembly, W.S.
220.0, bottom cracks 48A (crack #4.1) and 49A (crack #5.2).
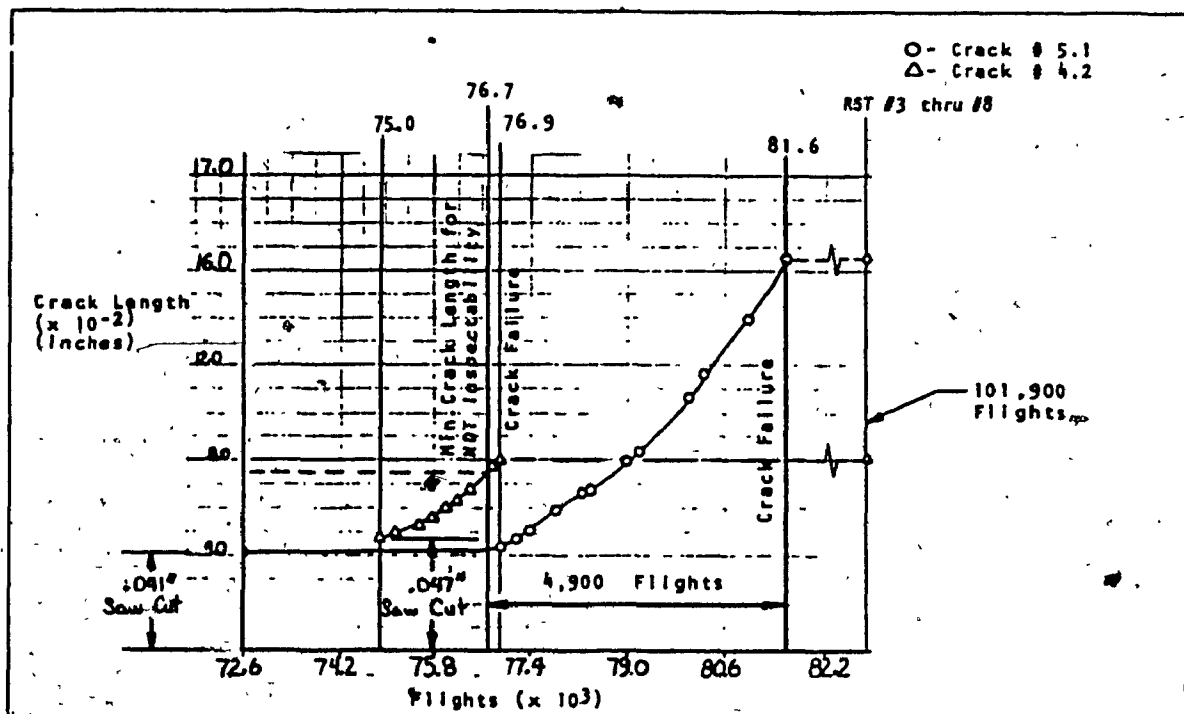
Figure 88

F.C.P. curves of the flap arm, hinge arm assembly, W.S.
220.0, top cracks 48A (crack #4.2) and 49A (crack #5.1)

4.3.1.5. Inboard and outboard sidewall members

Vane actuator cradle assembly

Failed at 119000 flights

A general view of the damaged assembly as received is shown in Figure 89. Visual examination revealed two cracks, one located on the inboard sidewall member and the other one symmetrically located on the outboard sidewall member of the cradle assembly, Figure 90.

Both cracks were broken open to expose the fracture faces. Visual examination of the outboard member fracture revealed that the fatigue cracking originated at saw cut #40 from multiple origins, and propagated diagonally through the member thickness, Figure 91. (As specified in section 4.3.1.1. the saw cut #40 has been introduced after 92400 crack-free flights). The fracture plane was inclined approximately 45 deg in respect to the saw cut, indicating that the plane stress conditions were predominant. Typical fatigue morphology covered an extensive area of the cross section, and only a narrow band immediately adjacent to the outboard side of the member exhibited a shear lip. The fatigue cracking of the inboard member originated at a symmetric position to the fatigue cracking of the outboard member, but did not initiate from a saw cut. Visual examination of the fracture revealed the existence of two separate fields of propagation each having its own
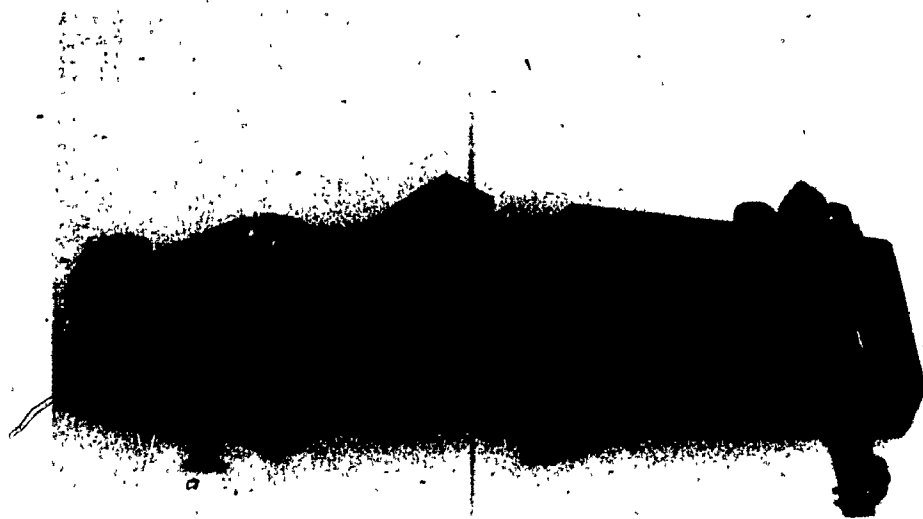
Figure 89   Magnification: .33x

General view of the cradle assembly as received.
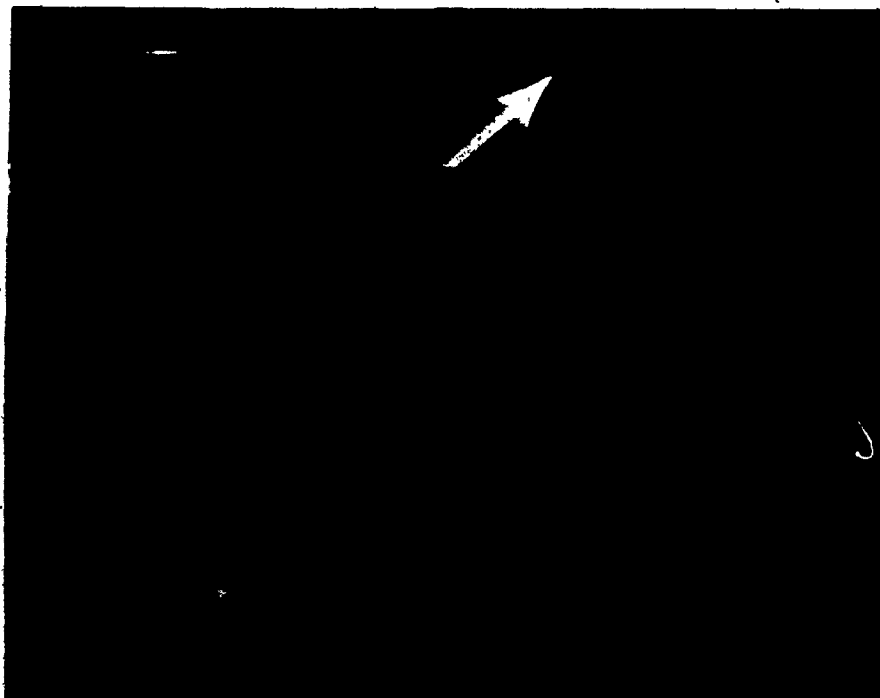
Figure 90   Magnification: 1.33x

Enlarged view of the cracked members (indicated)

initiation. One field "Pa" had initiated from multiple
origins located adjacent to the corner of the inboard side of
the member and the upper face (symmetrically oriented as saw
cut #40). The fatigue cracking which initiated from these
origins subsequently propagated parallel to the inboard side,
up to a central ridge, Figure 92.
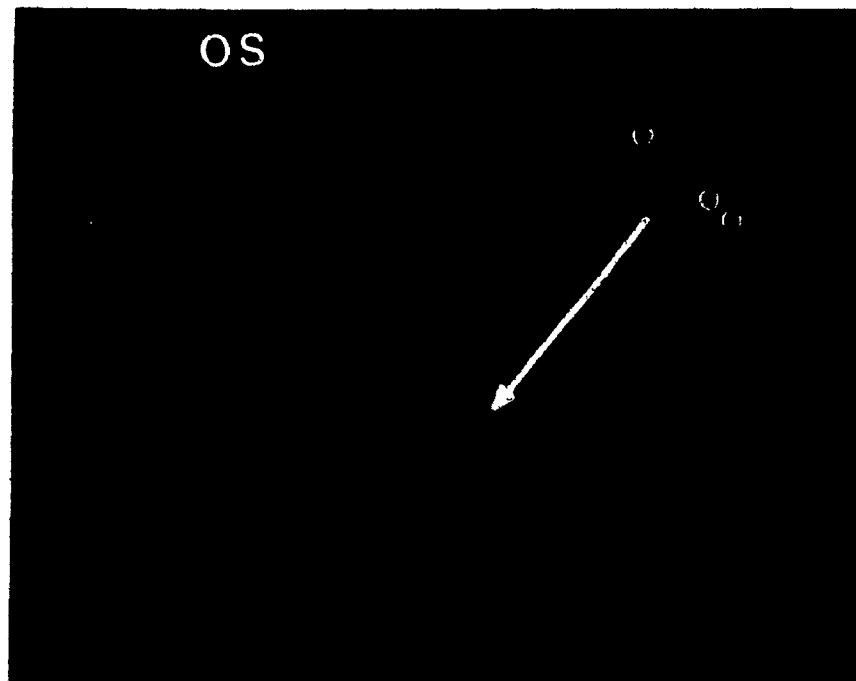
Figure 91   Magnification : 13x

General view of the outboard sidewall (OS) member.   Saw cut
#40 is at top right corner.   The direction of propagation is
indicated.
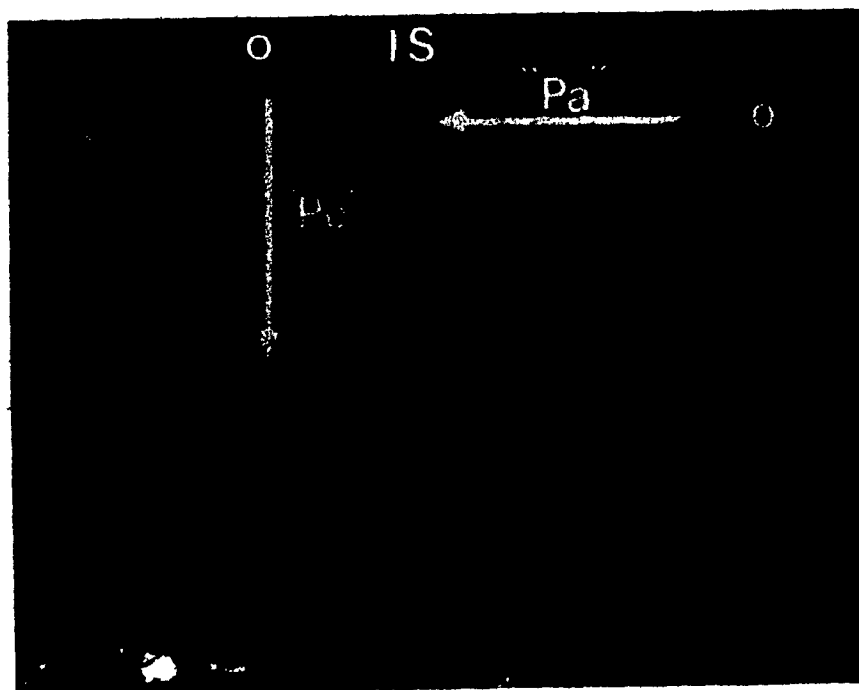
Figure 92   Magnification: 13x

General view of the inboard sidewall (IS) member. The
origins and the directions of propagation are indicated.

The second fatigue field ("Pe") had initiated from
multiple origins located on the inboard side, adjacent to the
central ridge. The direction of propagation was
perpendicular to the inboard side, Figure 93. Scanning
electron microscope examination carried out across both
fractures revealed that vane loading conditions prevailed:
the microscopic fracture imprint was similar to the one
described in section 4.3.1.2., Figure 74 (i.e. no significant
crack advance due to sequences "a", "b" and "c" of the block
loading spectrum). Therefore the stresses which initiated
and propagated the fatigue cracking originated from the vane
loading.

Qualitative fractographic examination revealed in the case of the fracture originated at saw cut #40, a fatigue morphology typical of relatively high stress concentration level (secondary cracking, and tearing). In the case of the inboard member crack, the fatigue morphology was typical of low growth rate regime (cleavage like morphology) which is indicative of a lower stress level.

Quantitative fractographic examinations were carried out across both fractures and the results are tabulated in Tables 23-25. These results indicate that, in the case of the fracture originated at the saw cut #40, a minimum of 17500 flights were necessary to propagate the crack from the bottom of the saw cut, to a point located approximately 3.7 mm from the origin. In the case of the fracture of the inboard member, both fields "Pa" and "Pe" respectively required a much higher number of flights to propagate the crack from the surface of the member: 83800 flights to a point located at approximately 3.05 mm from the corner (field "Pa") and 76600 flights to a point located at approximately 1.7 mm from the inboard side (field "Pe"). It is considered that field "Pa" initiated and propagated before field "Pe". The initiation and propagation of field "Pe" could be associated with a shifting of loads, possibly as a result of the complete fracture of the outboard member.

CL-600, INBOARD FLAP, CRADLE ASSY, OUTBOARD UPPER SIDEWALL MEMBER SAW CUT #40

cs.	Dist from Origin -mm	Block Count No.	Block Count In Length of -mm	Mag.	Block Density Block/mm	Block Spacing x10⁻⁴ mm/Block	Estimated Number of Blocks	Cumm.	Avg. da/dn x10⁻⁵ mm/cycle
1	0.8356	1	0.0127	-	-	127	66	66	6.33
2	0.9474	1	0.0127	-	-	127	9	75	6.32
3	1.2675	1	0.0177	-	-	177	18	93	6.81
4	2.1641	1	0.0228	-	-	228	39	132	8.20
5	2.3622	1	0.0254	-	-	254	8	140	8.44
6	2.3902	1	0.0279	-	-	279	1	141	8.48
7	2.6772	1	0.0330	-	-	330	9	150	8.92
8	3.1978	1	0.0381	-	-	381	14	164	9.75
9	3.4417	1	0.0432	-	-	432	6	170	10.12
10	3.7084	1	0.0508	-	-	508	5	175	10.60

Total number of cycles   35000

Total number of flights 17500

Saw Cut Depth = 0.060"

CL-600, INBOARD FLAP, CRADLE ASSY, INBOARD UPPER SIDEWALL MEMBER, FIELD "PE"

cs.	Dist from Origin -mm	Block Count No.	Block Count In Length of -mm	Mag.	Block Density Block/mm	Block Spacing x10⁻⁴ mm/Block	Estimated Number of Blocks	Cumm.	Avg. da/dn x10⁻⁵ mm/cycle
1	0.2616	8	39	8200	1682	5.9	440	440	0.30
2	0.3124	3	8	4000	1500	6.7	76	516	0.30
3	0.3505	2	10	4000	800	12.5	31	547	0.32
4	0.4140	7	33	4000	848	11.8	54	601	0.34
5	0.4978	4	22	4000	727	13.8	61	662	0.88
6	0.6629	6	40	2000	300	33.3	50	712	0.47
7	1.1125	1	0.0203	-	-	203.0	22	734	0.76
8	1.2014	1	0.0177	-	-	177.0	5	739	0.81
9	1.6713	-	-	-	-	177.0*	27	766	1.09

*Assumed

Total number of cycles 153200

Total number of flights 76600

166

Table 25

CL-600, INBOARD FLAP, CRADLE ASSY, INBOARD UPPER SIDEWALL MEMBER, FIELD "PA"

Pos.	Dist from Origin -mm	Block Count No.	In Length of -mm	Mag.	Block Density Block/mm	Block Spacing $\times 10^{-4}$ mm/Block	Estimated Number of Blocks	Cumm.	Avg. da/dn $\times 10^{-5}$ mm/cycle
1	0.1244	9	21	4000	1714	5.83	213	213	0.29
2	0.3937	13	61	1875	399.5	25.00	108	321	0.61
3	0.4674	5	38	3800	500.0	20.00	37	358	0.65
4	0.6909	5	20	1950	487.5	20.51	109	467	0.74
5	1.3462	7	36	1950	379.2	26.37	249	716	0.94
6	1.3970	7	45	3900	606.6	16.48	31	747	0.94
7	2.1336	1	0.0127	-	-	127.00	58	805	1.33
8	2.3368	1	0.0254	-	-	254.00	8	813	1.44
9	2.5146	1	0.0203	-	-	203.00	9	822	1.53
10	2.7406	1	0.0279	-	-	279.00	8	830	1.65
11	3.0429	1	0.0381	-	-	381.00	8	838	1.82

Total number of cycles   167600
Total number of flights   83800
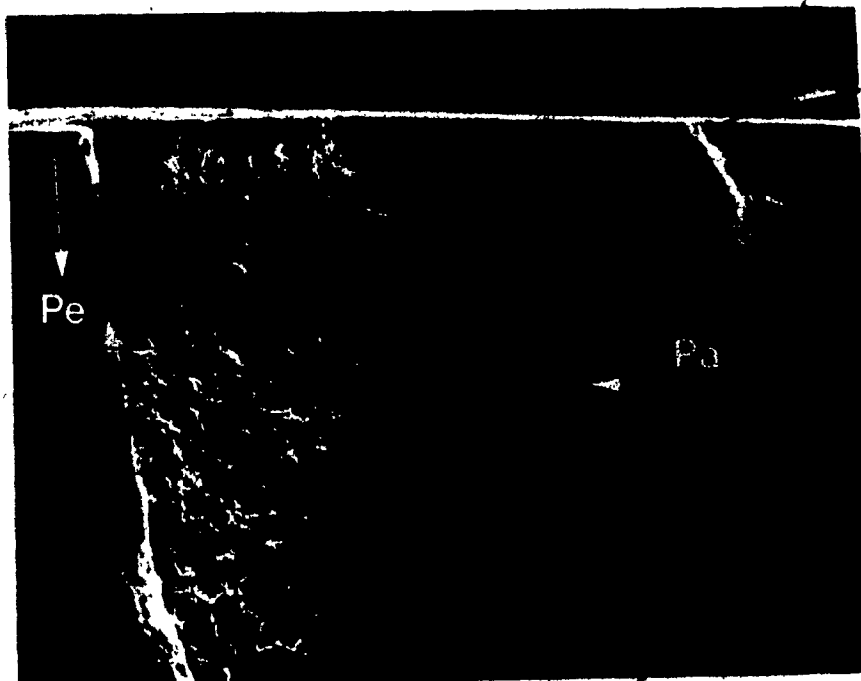
Figure 93 Magnification: 15x

Enlarged view of the area adjacent to the central ridge, showing the perpendicular propagations of fields "Pa" and "Pe".

167

4.3.1.5.1. Determination of fatigue cracking initiation and N.D.T. inspection intervals /

The F.C.P. curves are shown in Figure 94. The moment of fatigue cracking initiation can be determined from the formula:

$$N_{INIT} = N_{FF} - N_{PROP}$$

$$N_{FF} = 119000 \text{ flights}$$

$$N_{PROP} \quad \text{for field Pa} = 83800$$

$$N_{INIT} = 119000 - 83800 = 35200 \text{ flights}$$

Based on a minimum inspectable crack size of 0.10" (2.5 mm) the first N.D.T. inspection interval was established at 99900 flights. The failure to detect it will allow another 19100 flights before the final failure of the component.

4.3.1.5.2. Discussion regarding the fatigue crack closure effect

This particular test was considered to be representative of the crack closure effect on the F.C.P. If one extrapolates the F.C.P. curve generated from the saw cut, it is clear that the F.C.P. rate of this crack is higher than the F.C.P. rate for the crack initiated without the saw cut. This is a confirmation of Elber's crack closure model (see section 2.3.1.2). As shown in this section, it was determined that in the case of real fatigue cracks the plastic zones left in the wake of the crack tip have a tendency to decrease the crack opening displacement and

therefore to decrease the F.C.P. rate. Hence when comparing
a fatigue crack intiated from a saw cut, with a fatigue crack
initiated without the saw cut, one must expect to see
(according to this theory) higher F.C.P. rates in the fatigue
cracking initiated from a saw cut. Our findings, in this
particular component confirm this hypothesis.
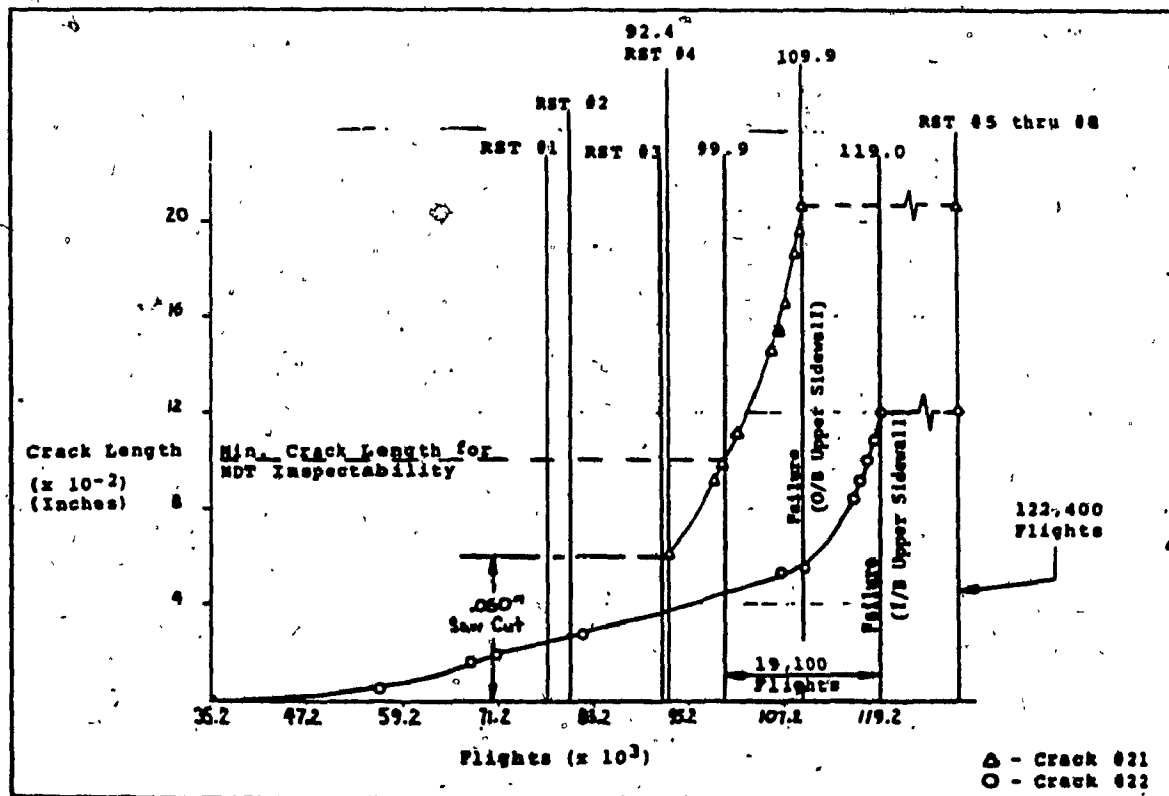
Figure 94

F.C.P. curves of the vane actuator cradle assembly initiated
at saw cut #40 (crack #21) and without saw cut (crack #22).

4.3.1.6 Inboard flap, hinge box, W.S. 76.50

Failed at 67800 flights

A general view of the damaged assembly as received in the Laboratory is shown in Figure 95. Visual examination of the fractures revealed the origins and the directions of propagation, Figure 96 and Figure 97. The fatigue cracking had initiated on both components at the rivet holes located on the lower side, and propagated first diagonally in respect to the lower side and subsequently along the outboard and the inboard sides, respectively toward the upper side.

Scanning electron microscope examinations were carried out across all four fractures. The identification of the loading spectrum with the microscopic fracture imprint, Figure 98, revealed that the flap loading conditions predominated over the vane loading conditions. The examination of the microscopic fracture imprint revealed that 5 out of 6 sequences of the block contributed to the crack advance. However, the sequence "a", seems to be retarded by the higher loads of previously applied sequence "f".

The qualitative fractographic examination suggested that the fatigue cracking was first initiated probably on the outboard hinge from the lower side rivet hole and propagated diagonally along the lower side in both directions "in-out" and "out-in". No evidence of crack front tunnelling was found. The fatigue cracking of the inboard hinge was
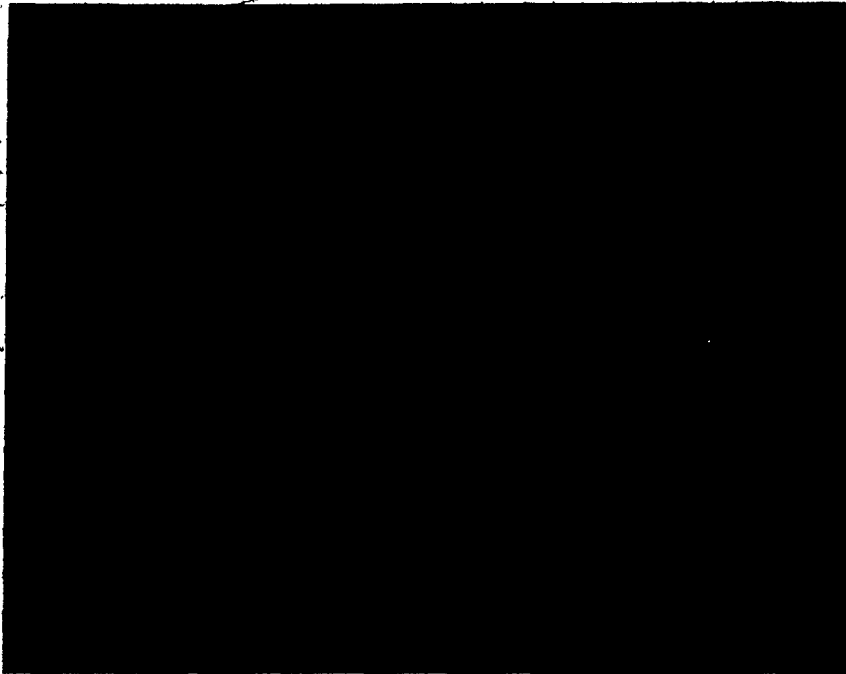
Figure 95 Magnification: .9x

General view of the damaged assembly as received.
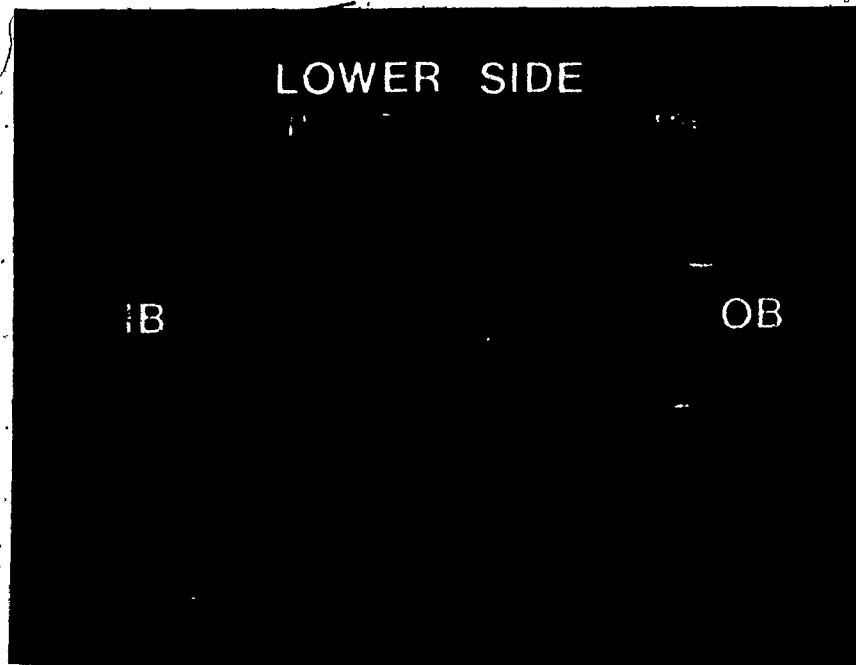
Figure 96 Magnification: 1.44x

General view of the fractures. (see Figure 97 for details)
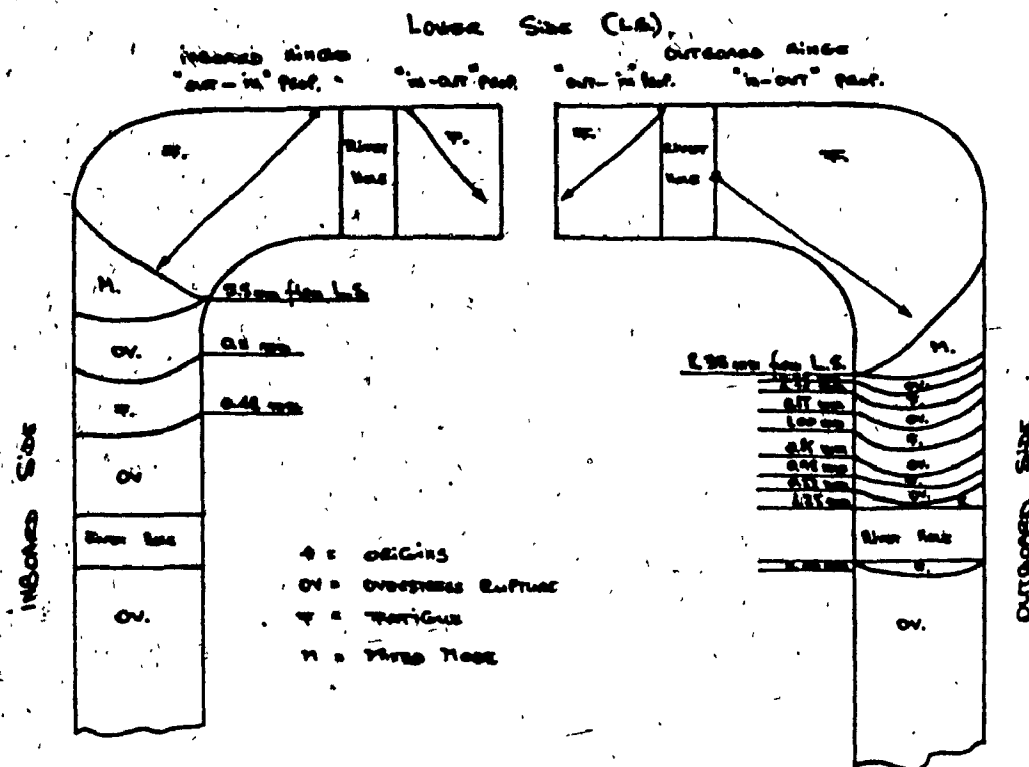
Figure 97

Sketch showing the general morphology, origins and the
fatigue cracking directions.
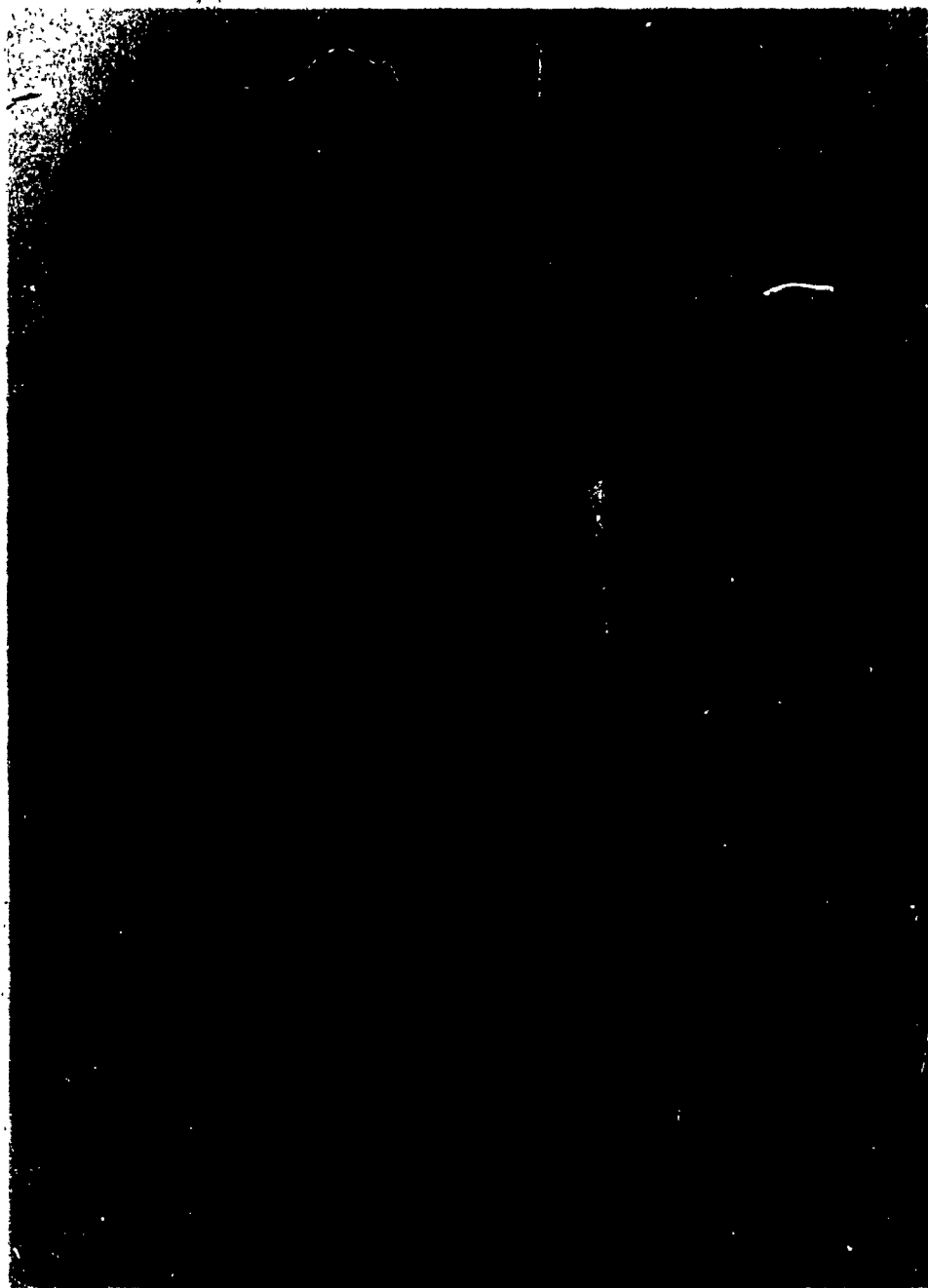
Figure 98

Showing a typical flap predominant loading spectrum
microscopic fracture imprint.

initiated somewhat at a later stage, and propagated in a
similar manner. Adjacent to the corner of the lower side and
the outboard side (in the outboard hinge) and the inboard
side (in the inboard hinge), respectively, the fatigue
morphology changed into a mixed mode of coarse fatigue
striations and Overstress rupture. The fatigue cracking
front changed its orientation as well, from "diagonal" to the
lower side to "perpendicular" to lower side, with evident
signs of front tunnelling. The fracture morphology along the
lateral sides of the assembly consisted of alternate zones
containing patches of coarse fatigue striations, followed by
fields with a typical overstress fracture morphology.

Quantitative fractographic examinations were carried out
along the fractures of the lower side, from the origins to
positions located approximately at 6 - 7 mm from these
origins (see Tables 26-29). No quantitative fractographic
examinations were carried out along the fractures of the
outboard and inboard sides because the evidence of the crack
front tunnelling; moreover the alternative patches of fatigue
striations and overstress rupture, indicate an instability of
the crack front which make the computation of the crack
growth rate irrelevant. The extent of these alternative
zones of fatigue and overstress rupture was measured and the
approximative results are indicated in Figure 97.

174

IN-OUT PROPAGATION

BLOCK COUNT   Table 26

CL-600, INBOARD FLAP, HINGE BOX, OUTBOARD HINGE, LOWER SIDE.

Pos.	Dist. from Origin -mm	Block Count No.	Block Count In Length of -mm	Mag.	Block Density Block/mm	Block Spacing x10⁻⁴ mm/block	Estimated Number of Blocks	Cum.	Avg. da/dn x10⁻⁵ mm/cycle
1	0.1143	4	19	2100	442	22.62	51	51	1.12
2	0.2057	7	17	850	360	25.57	32	83	1.24
3	0.2540	4	45	2100	187	53.57	9	92	1.38
4	0.4572	4	17	850	200	50.00	41	133	1.72
5	0.5461	1	0.0381	-	-	381.00	2	135	2.02
6	0.7924	1	0.0558	-	-	558.00	4	139	2.85
7	0.9017	1	0.0508	-	-	508.00	2	141	3.20
8	1.2141	1	0.0685	-	-	685.00	5	146	4.16
9	1.6256	1	0.0635	-	-	635.00	7	153	5.31
10	1.9053	1	0.0813	-	-	813.00	3	160	5.95
11	2.6162	1	0.0711	-	-	711.00	10	170	7.69
12	3.1292	1	0.0838	-	-	838.00	6	176	8.99
13	3.7084	1	0.0762	-	-	762.00	8	184	10.08
14	4.7371	1	0.1270	-	-	1270.00	8	192	12.34
15	7.7597	-	-	-	-	1270.00*	24	216	17.96

*Assumed

Total number of cycles   43200
Total number of flights   21600

OUT-IN PROPAGATION

BLOCK COUNT   Table 27

CL-600, INBOARD FLAP, HINGE BOX, OUTBOARD HINGE, LOWER SIDE.

Pos.	Dist. from Origin -mm	Block Count No.	Block Count In Length of -mm	Mag.	Block Density Block/mm	Block Spacing x10⁻⁴ mm/block	Estimated Number of Blocks	Cum.	Avg. da/dn x10⁻⁵ mm/cycle
1	0.1270	3	18	880	146.6	68.2	19	19	3.34
2	0.3810	6	52	450	52.0	192.5	13	32	5.95
3	0.8001	2	54	880	31.4	318.1	13	45	8.09
4	1.4859	3	57	440	23.1	431.8	16	61	12.18
5	2.1336	1	0.0279	-	-	279.4	23	84	12.70
6	2.2123	1	0.0406	-	-	406.4	2	86	12.86
7	2.8425	1	0.0762	-	-	762.0	4	90	14.13
8	2.9032	1	0.0818	-	-	818.0	5	95	15.28
9	3.1877	1	0.0898	-	-	898.0	3	98	16.86
10	3.6093	1	0.1563	-	-	1563.0	3	101	17.87
11	4.7396	1	0.1228	-	-	1228.0	9	110	21.54
12	5.5626	1	0.1270	-	-	1270.0	7	117	23.77
13	6.3296	1	0.0787	-	-	787.0	10	127	24.92
14	7.6758	1	-	-	-	787.0*	17	144	26.66

*Assumed

Total number of cycles   28800
Total number of flights   14400

175

OUT-IN PROPAGATION

BLOCK COUNT   Table 28

CL-600, INBOARD FLAP, HINGE BOX, INBOARD HINGE, LOWER SIDE

Pos.	Dist. from Origin -mm	Block Count No.	Block Count In Length of -mm	Mag.	Block Density Block/mm	Block Spacing x10^{-4} mm/block	Estimated Number of Blocks	Cum.	Avg. da/dq x10^{-5} mm/cycle
1	0.1702	2	60	2000	66.67	150.0	11	11	7.74
2	0.2972	5	66	800	61.53	162.5	8	19	7.82
3	0.4697	5	66	800	60.60	165.0	10	29	7.92
4	0.7364	5	61	400	38.78	305.0	9	38	9.69
5	0.9753	1	0.0228	-	-	228.0	11	49	9.95
6	1.1506	1	0.0254	-	-	254.0	7	56	10.27
7	1.3462	1	0.0127	-	-	127.0	16	72	9.35
8	1.4960	1	0.0279	-	-	279.0	5	77	9.71
9	1.6078	1	0.0410	-	-	410.0	3	80	10.05
10	2.4257	1	0.0304	-	-	304.0	27	107	11.34
11	2.6670	1	0.0381	-	-	381.0	6	113	11.80
12	3.2386	1	0.0255	-	-	255.0	23	136	11.91
13	3.7414	1	0.0254	-	-	254.0	20	156	11.99
14	4.9784	1	0.0685	-	-	685.8	18	174	14.31
15	6.3119	-	-	-	-	685.8*	19	193	16.35

*Assumed

Total number of cycles 38600
Total number of flights 19300

IN-OUT PROPAGATION

BLOCK COUNT   Table 29

CL-600, INBOARD FLAP, HINGE BOX, INBOARD HINGE, LOWER SIDE

Pos.	Dist. from Origin -mm	Block Count No.	Block Count In Length of -mm	Mag.	Block Density Block/mm	Block Spacing x10^{-4} mm/block	Estimated Number of Blocks	Cum.	Avg. da/dq x10^{-5} mm/cycle
1	0.5080	7	57	820	100.70	99.30	61	61	4.98
2	0.7162	4	59	850	57.62	173.52	12	63	5.68
3	1.0237	1	30	850	28.33	352.94	31	94	9.70
4	2.1158	1	0.05096	-	-	609.60	5	99	10.69
5	2.2967	1	0.05080	-	-	508.00	4	103	11.15
6	2.5019	1	0.05588	-	-	558.80	3	106	11.80
7	3.1674	1	0.1041	-	-	1041.4	6	112	14.14
8	3.5779	1	0.1219	-	-	1219.2	4	116	15.05
9	4.2062	1	0.1041	-	-	1041.4	5	121	17.38
10	4.8609	1	0.1524	-	-	1524.0	3	124	18.79
11	5.1181	1	0.1905	-	-	1905.0	3	127	20.15
12	7.0129	-	-	-	-	1905.0*	10	137	25.59

*Assumed

Total number of cycles 27400
Total number of flights 13700

176

4.3.1.6.1. Determination_of_fatigue_cracking_initiation_and N.D.T._inspection_intervals

The F.C.P. curves as determined by fractographic examination are shown in Figures 99-100. The fatigue cracking initiation could be determined by using the simple formula given in previous sections:

$$N_{INIT.} = N_{FF} - N_{PROP}$$

- for inboard hinge the earliest initiation was estimated to occur on outboard-inboard propagation and therefore

$$N_{FF} = 67200 \text{ flights}$$

$$N_{PROP} = 19300 \text{ flights}$$

$$N_{INIT} = 67200 - 19300 = 47900 \text{ flights}$$

- for outboard hinge the earliest initiation was estimated to occur on inboard-outboard propagation and therefore

$$N_{FF} = 67800 \text{ flights}$$

$$N_{PROP} = 21600 \text{ flights}$$

$$N_{INIT} = 67800 - 21600 = 46200 \text{ flights}$$

Considering a minimum detectable crack size of 0.08 inches (≈ 2 mm) the first N.D.T. inspection must be carried-out at 59000 flights for the outboard hinge and 56900 flights for the inboard hinge. Failure to detect these cracks will still allow 4300 flights until the outboard hinge will reach the minimum residual strength and 5700 flights,

177

respectively until the inboard hinge will reach the minimum
residual strength.

4.3.1.6.2. Discussion_regarding_the_mixed_mode_-_fatigue_-

tensile_jumping

The mode of failure of this component exemplifies very
well the phenomena of crack tunnelling and the phenomena of
tensile crack jumping as has been described by Forsyth [40 ,
41] (see section 2.3.2). The fractographic examination
revealed that the fracture on both outboard and inboard hinge
along the lower side, propagated on a flat plane, which was
indicative that the plane strain conditions predominated.
Along these fractures no signs of crack front tunnelling were
observed. Taking into account the small thickness of the
component as the crack penetrated deeper, the plane stress
conditions are expected to become predominant. As the
transition from plane strain to plane stress occurs, the
plane stress plastic zones located at the specimen side walls
(see Figure 10) become larger and therefore the amount of
energy used to create these plastic zones increases as well.
The crack needs less energy to propagate in the middle of the
specimen than near the edges and hence the crack propagates
faster in the specimen center. Fractographic examination
confirmed indeed the existance of tunnelling as the crack
propagates along the outboard and the inboard side. The crack

front assumes a curvature which becomes increasingly sharper
as the crack grows deeper. As Forsyth predicted when the
curvature reaches a critical size, the ratio $\sqrt{a/1}$ (a = crack
depth and 1= total length of the crack front) becomes smaller
than the equilibrium ratio and therefore tensile jumping is
expected to occur. Fractographic examination confirmed
indeed the existance of overstress rupture morphology which
is indicative of tensile jumping (see Figure 97) along the
inboard and the outboard sides of the component.
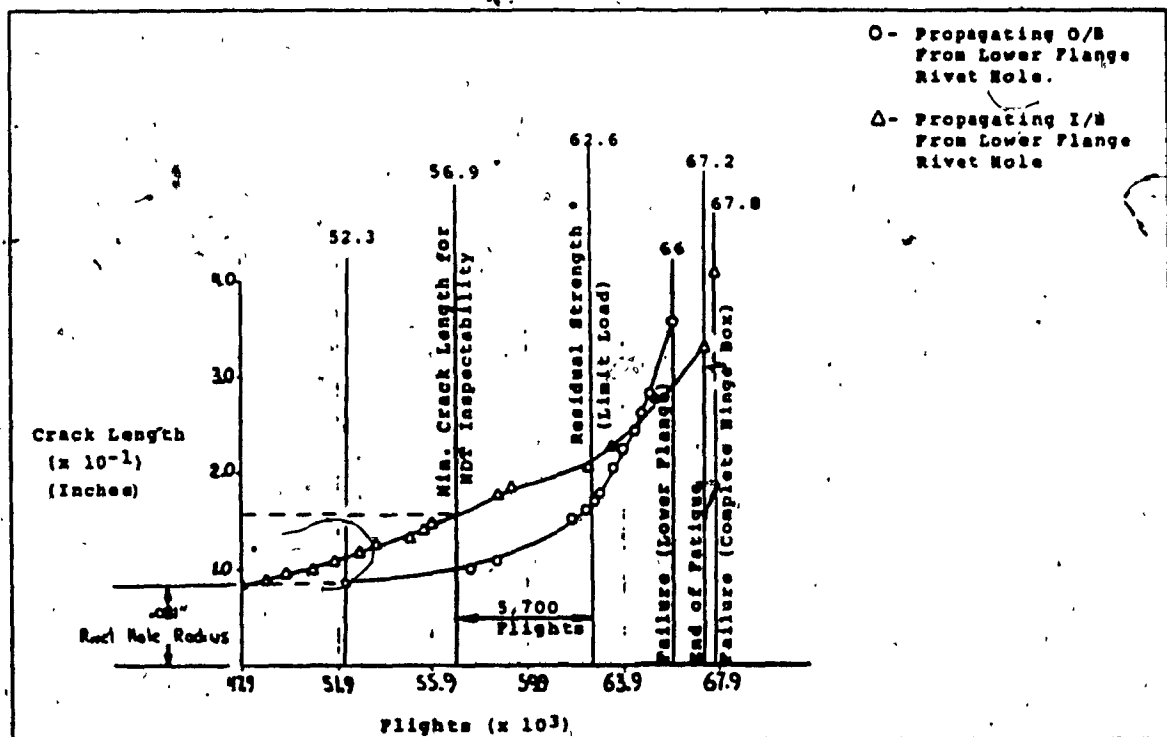
Figure 99

F.C.P. curves of the inboard hinge, hinge box, w.'s. 76.50:
"out-in" propagation (O/B) and "in-out" propagation (I/B).
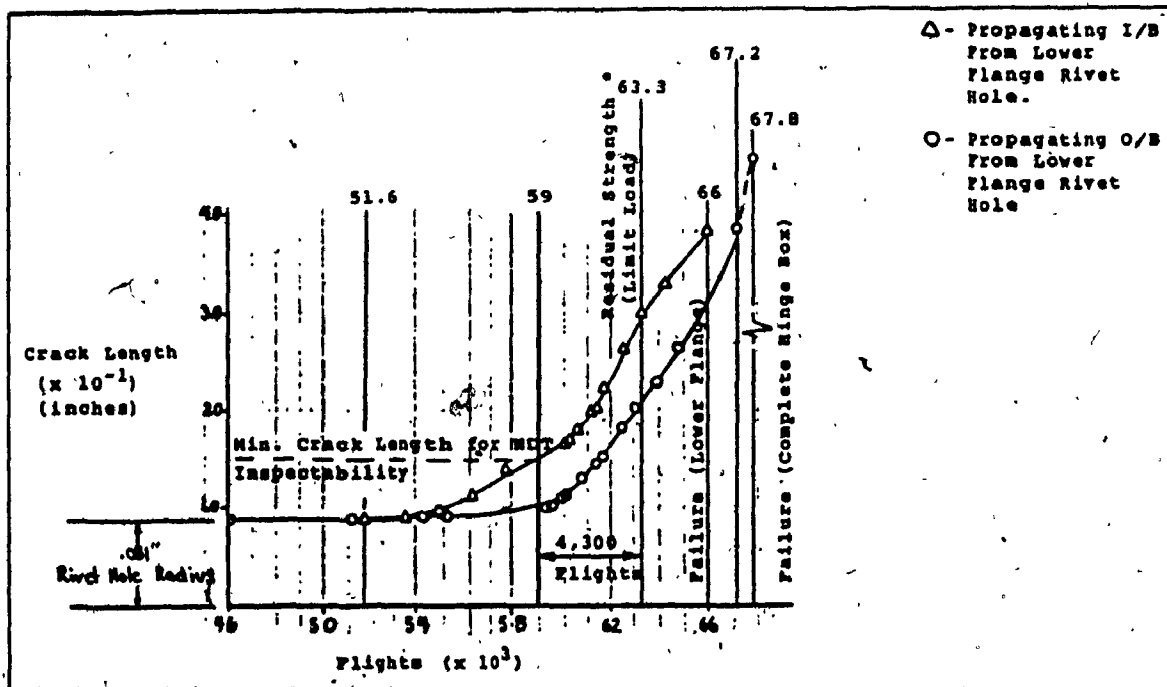
Figure 100

F.C.P. curves of the outboard hinge, hinge box, w.s. 76.50;
"out-in" propagation (O/B) and "in-out" (I/B).

5. CONCLUSIONS

The experimental work was carried out at Canadair Ltd,
Materials and Process Engineering Laboratory between
1981-1983. Two programs are presented in this thesis:

Program #1 was designed to demonstrate the applicability
of quantitative fractographic examination as a reliable
method to determine the extent of the propagation stage of
specimens subjected to fatigue loading. This program was
conducted on ASTM - standard specimens using a constant
amplitude loading spectrum.

This experimental program proved the following:

a) Quantitative fractographic examination is a practical
method of determining the crack growth rate.

b Quantitative fractographic examination provides more
accurate data than the macroscopic monitoring of the crack
during testing. A good example of this accuracy is
illustrated in the case of 7475 Aluminum Alloy where the
pronounced tendency of this alloy for crack tunnelling
produces a much slower crack growth on the inspectable sides
of the specimen than in the center of the specimen, and
therefore the macroscopic crack growth rate is lower than the
real crack advance.

c) Determination of the stress intensity factor ΔK using
quantitative fractography and the Bates and Clark equation
provides data which are in the same range as the stress

181

intensity factor calculated from linear elastic stress analysis equations. Moreover, for the regions close to the origin, quantitative fractography provides more accurate data than macroscopic observations.

Program #2 Basically this program consisted of the findings of the failure analysis investigations carried out during the Challenger CL600/601, fatigue and damage tolerance tests. For the purpose of this thesis four components from the flap/vane assembly were chosen. The parts were real production parts and the loading spectrum was of a block-type designed to accurately represent typical missions of a business jet airplance.

This experimental program proved the following:
a) Quantitative fractography is an alternative method to construct fatigue crack growth curves; particularly in situations where macroscopic crack growth monitoring during the test is impossible or cannot provide the necessary data. Based on the results of the quantitative fractographic examination of these aircraft components the fatigue cracking initiation moment was estimated, as well as the first N.D.T. inspection interval.
b) In cases where a complicated loading system is involved, quantitative fractography is the only method that can identify the source of loading for a specific component.
c) Quantitative fractography was instrumental in determining the effects of retardation and acceleration of the crack

182

growth.

d) A comparison between fatigue cracking initiation from a saw cut member and from an uncut member confirmed the effect of fatigue crack closure phenomena.

e) The effects of crack front tunnelling and tensile jumping were studied and appeared to confirm the theoretical hypothesis.

f) The numerical results of this experimental program, together with the F.C.P. curves and additional information such as: fatigue cracking initiation moment and the first N.D.T. inspection interval formed a part of the official submission for certification of the CL-600/601 Challenger large body business airplane to flight safety authorities in Canada (MOT) and United States (FAA).

```
C      PROGRAM CRAKPRO(INPUT,OUTPUT)
C
C      PROGRAM FOR COMPUTING THE CRACK GROWTH RATE AND THE STRESS
C      INTENSITY FACTOR FOR MATERIALS SUBJECTED TO A CONSTANT
C      AMPLITUDE FATIGUE TEST.
C      THIS PROGRAM COMPUTES THE CRACK GROWTH RATE DA/DN FROM A
C      CONSTANT-AMPLITUDE FATIGUE TEST USING A COMPACT TYPE (CT)
C      SPECIMEN.
C      THE PROGRAM IS DESIGNED TO USE THE INCREMENTAL POLYNOMIAL
C      METHOD WHICH INVOLVES FITTING A SECOND-ORDER POLYNOMIAL &
C      (PARABOLA) TO SETS OF (2*M+1) SUCCESIVE DATA POINTS,
C      WHERE M IS USUALLY 1,2,3 OR 4. IN THE PRESENT PROGRAM
C      M WAS CHOSEN 3.
C      THE FORM OF EQUATION FOR THE LOCAL FIT IS:
C
C      A(I)=B0+B1*[N(I)-C1]/C2+B2*[N(I)-C1]/C2
C
C      WHERE -1<=[N(I)-C1]/C2=>1
C      AND B0,B1,B2 ARE REGRESSION PARAMETERS DETERMINED BY THE
C      LEAST SQUARES METHOD.
C      THE PARAMETERS  C1=0.5*[N(I-N)+N(I+N)]
C             AND      C2=0.5*[N(I+N)-N(I-N)]
C
C      ARE USED TO SCALE THE INPUT.
C
C      THE CRACK GROWTH RATE AT A NUMBER OF CYCLES N(I) IS
C      OBTAINED FROM THE DERIVATIVE OF THE ABOVE PARABOLA
C      GIVEN BY THE FOLLOWING EXPRESSION:
C
C      DA/DN(I)=B1/C2+2*B2*[N(I)-C1]/C2
C
C      THE VALUE OF THE STRESS INTENSITY FACTOR DELTA K
C      ASSOCIATED WITH THIS CRACK GROWTH RATE IS CALCULATED USING A
C      FORMULA DERIVED FROM THE LINEAR ELASTIC STRESS ANALYSIS:
C
C      DELTAK=[(PMAX-PMIN)/B*SQRTW]*[(2+T)/(1-T)**1.5]*
C      *(0.886+4.64*T-13.32*T**2+14.72*T**3-5.62*T**4)
C      WHERE
C             T=A/W
C             B=SPECIMEN THICKNESS
C             W=SPECIMEN WIDTH
C             A=CRACK EXTENSION AFTER N CYCLES
C             PMAX=MAXIMUM LOAD
```

```
C          PMIN=MINIMUM LOAD
C          NPTS=NUMBER OF PAIRED (A,N) DATA POINTS
C          AM=MACHINED NOTCH
C          YS=YIELD STRENGTH
C      THE PROGRAM CAN GIVE ALSO A GRAPHIC REPRESENTATION OF
C      THE RELATIONSHIP DA/DN VERSUS DELTA K.
C      THE GODNESS OF THE FIT OF THE EQUATION IS GIVEN BY THE
C      MULTIPLE CORELATION COEFFICIENT(M.C.C.)CFOR THE PERFECT
C
C      FIT M.C.C.=1]
C      IN ORDER FOR THE RESULTS TO BE VALID,IT IS REQUIRED THAT
C      THE SPECIMEN BE PREDOMINANTLY ELASTIC AT ALL VALUES OF
C      APPLIED LOAD.WHEN THE CRACK EXTENSION BECOMES TOO DEEP
C      THE PROGRAM WILL PRINT A MESSAGE INDICATING THAT THE
C      SPECIMEN VIOLATES THE MINIMUM IN-PLANE REQUIREMENTS.
C
      DIMENSION A(200),N(200),BB(3),DADN(200),DELK(200)
      DIMENSION AA(10),NN(10)
      REAL N,NN,AA,BB,R2,T,AM,AR,B,C1,C2,AX,PI,PMAX,PMIN,PP,R,S,W
      REAL TEM,YS
      INTEGER GQ,NPTS,I,J,K,ID
   10 FORMAT(//,5X,'CT SPECIMEN',5X,'B=',F6.3,'IN.',5X,'W=',F6.3,
     *'IN.',5X,'AN=',F6.3,'IN.')
   15 FORMAT(1H1,15X,'SEVEN POINT INCREMENTAL POLYNOMIAL METHOD
     *FOR DETERMINING DADN')
   17 FORMAT(/)
   18 FORMAT(1H1)
   20 FORMAT(/,3X,'PMIN=',F6.3,'KIPS',5X,'PMAX=',F6.3,'KIPS',5X,
     *'R=',F6.3,5X)
   22 FORMAT(/,3X,'TEMP.=',F4.0,'F',5X)
   35 FORMAT(///,3X,'SPEC.NO.  ',I6,10X,'NO.POINTS=',I3)
   55 FORMAT(/,3X,'OBS.NO.',5X,'CYCLES',11X,'A(MEAS.)',8X,'A(REG.)',',
     *'9X,'M.C.C.',14X,'DELK',14X,'DA/DN')
   92 FORMAT(3X,I4,9X,F8.0,7X,F8.3,8X,F8.3,8X,F8.6,11X,F8.2,12X,E8.3)
   95 FORMAT(3X,I4,9X,F8.0,7X,F8.3)
   98 FORMAT(3X,I4,9X,F8.0,7X,F8.3,8X,F8.3,8X,F8.6,11X,F8.2,12X,E8.3,
     *2H *)
C
  200 FORMAT(//)
  300 FORMAT(/,3X,'*DATA VIOLATE SPECIMEN SIZE/REQUIREMENTS')
C
      READ *,ID
      READ (*,*,END=1000) NPTS
      READ *,PMIN,PMAX,B,W,AM,TEM,YS
      DO 12 I=1,NPTS
      READ *,A(I)
   12 CONTINUE
      DO 13 I=1,NPTS
```

185

```fortran
      READ *,N(I)
   13 CONTINUE
C
      PRINT 15
      PRINT 35, ID,NPTS
      PRINT 10, B,W,AM
      R=PMIN/PMAX
      PRINT 20,PMIN,PMAX,R
      PRINT 22,TEM
      PRINT 55
      PRINT 200
C
      CALL CRLEN(A,AM,NPTS)
C
C
      K=0
      PI=3.1416
      PP=PMAX-PMIN
C
      DO 110 I=1,3
      PRINT 95,I,N(I),A(I)
  110 CONTINUE
C
      NPTS=NPTS-6
      DO 100 I=1,NPTS
C
      CALL PARAM(C1,C2,N,A,K,AA,NN)
      CALL LSQM(DADN,AR,AA,BB,C1,C2,I,NN,R2)
C
      GQ=I+3
      CALL SIF(DELK,AR,B,I,PP,W,T)
      S=YS*SQRT(PI*W*(1-T))/2
      AX=DELK(I)/(1-R)
C
      IF(AX.LE.S) THEN
      PRINT 92,GQ,N(GQ),A(GQ),AR,R2,DELK(I),DADN(I)
      ELSE
      PRINT 98,GQ,N(GQ),A(GQ),AR,R2,DELK(I),DADN(I)
      ENDIF
  100 CONTINUE
C
      J=NPTS+4
      K=NPTS+6
      DO 120 I=J,K
      PRINT 95,I,N(I),A(I)
  120 CONTINUE
C
      PRINT 17
      PRINT 17
```

```
C        PRINT 300
C        PRINT 18
C        CALL MAXMIN(YMAX,YMIN,DADN,NPTS)
         CALL MAXMIN(XMAX,XMIN,DELK,NPTS)
         CALL DRAW(NPTS,DELK,DADN,XMIN,XMAX,YMAX,YMIN)
1000     STOP
         END
C
C        SUBROUTINE CRLEN(A,AM,NPTS)
C        THIS SUBROUTINE COMPUTES THE CRACK LENGTH.
C        REAL A(200),AM

         DO 31 I=1,NPTS
         A(I)=A(I)+AM
31       CONTINUE
         RETURN
         END
C
C        SUBROUTINE PARAM(C1,C2,N,A,K,AA,NN)
C        THIS SUBROUTINE COMPUTES THE PARAMETERS C1 AND C2
C
         INTEGER K
         REAL C1,C2,AA(10),NN(10),N(200),A(200)
         L=0
         K=K+1
         K1=K+6
         DO 60 J=K,K1
         L=L+1
         AA(L)=A(J)
         NN(L)=N(J)
60       CONTINUE
         C1=0.5*(NN(1)+NN(7))
         C2=0.5*(NN(7)-NN(1))
C
         RETURN
         END
C
C        SUBROUTINE LSQM(DADN,AR,AA,BB,C1,C2,I,NN,R2)
C        THIS SUBROUTINE COMPUTES DA/DN USING THE LEAST SQUARE METHOD.
C
         INTEGER J
         REAL C1,C2,AA(10),BB(3),DADN(200)
```

187

```fortran
      REAL X,YY,NN(10)
      SX=0
      SX2=0
      SX3=0
      SX4=0
      SY=0
      SYX=0
      SYX2=0
C
      DO 70 J=1,7
      X=(NN(J)-C1)/C2
      YY=AA(J)
      SX=SX+X
      SX2=SX2+X**2
      SX3=SX3+X**3
      SX4=SX4+X**4
      SY=SY+YY
      SYX=SYX+X*YY
      SYX2=SYX2+YY*X**2
   70 CONTINUE
C
CCC
      DEN=7.0*(SX2*SX4-SX3**2)-SX*(SX*SX4-SX2*SX3)+SX2*(SX*SX3-SX2**2)
      T2=SY*(SX2*SX4-SX3**2)-SYX*(SX*SX4-SX2*SX3)+SYX2*(SX*SX3-SX2**2)
C
      BB(1)=T2/DEN
C
      T3=7.0*(SYX*SX4-SYX2*SX3)-SX*(SY*SX4-SYX2*SX2)+SX2*(SY*SX3-
     *SYX*SX2)
C
      BB(2)=T3/DEN
C
      T4=7.0*(SX2*SYX2-SX3*SYX)-SX*(SX*SYX2-SX3*SY)+SX2*(SX*SYX-
     *SX2*SY)
C
      BB(3)=T4/DEN
C
      YB=SY/7.0
      RSS=0
      TSS=0
C
      DO 75 J=1,7
      X=(NN(J)-C1)/C2
      YHAT=BB(1)+BB(2)*X+BB(3)*X**2
      RSS=RSS+(AA(J)-YHAT)**2
      TSS=TSS+(AA(J)-YB)**2
   75 CONTINUE
```

188

```
C       R2=1.0-RSS/TSS
C
        DADN(I)=BB(2)/C2+2.0*BB(3)*(NN(4)-C1)/C2**2
        X=(NN(4)-C1)/C2
        AR=BB(1)+BB(2)*X+BB(3)*X**2
        RETURN
        END

        SUBROUTINE SIF(DELK,AR,B,I,PP,W,T)
C       THIS SUBROUTINE COMPUTES THE STRESS INTENSITY FACTOR DELTA K.
C
        INTEGER I
        REAL AR,W,T,DELK(200)
        T=AR/W
C
        FT=((2+T)*(0.886+4.64*T-13.32*T**2+14.72*T**3-5.6*T**4))/(1-T)
     *  **1.5
C       DELK(I)=(FT*PP)/(B*SQRT(W))
C
        RETURN
        END

        SUBROUTINE MAXMIN (YMAX,YMIN,D,NPTS)
C       THIS SUBROUTINE SORTS THE MAXIMUM AND THE MINIMUM VALUES
C       OF DADN AND DELTA K.
C
        REAL D(200)
C
        YMAX=D(1)
        DO 10 I=1,NPTS
        IF(D(I).GT.YMAX) THEN
        YMAX=D(I)
        ENDIF
10      CONTINUE
        YMIN=D(1)
        DO 20 I=1,NPTS
        IF(D(I).LT.YMIN) THEN
        YMIN=D(I)
        ENDIF
20      CONTINUE
```

189

```fortran
      RETURN
      END

C     SUBROUTINE DRAW(NPTS,DELK,DADN,XMAX,XMIN,YMAX,YMIN)
C     THIS SUBROUTINE PLOTS THE DADN VERSUS DELTA K CURVE.
C
      INTEGER NPTS
      REAL DELK(200),DADN(200)
      CHARACTER*1,POINTS(66,132),BL,PT,VT,HR
      DATA BL,PT,VT,HR/' ','*','!','-'/
      CT=32
      DO 2 I=1,NPTS
      DADN(I)=DADN(I)*10.0E+6
      YMIN=YMIN*10.0E+5
      YMAX=YMAX*10.0E+5
      DO 10 I=1,66
      DO 10 J=1,132
      POINTS(I,J)=BL
   10 CONTINUE
      DO 12 I=1,NPTS
      RII=(XMAX-XMIN)/CT*DELK(I)
      RJJ=ABS(YMIN-YMAX)/58*DADN(I)
      II=RII
      JJ=RJJ
      POINTS(II,JJ)=PT
      PRINT 70
   70 FORMAT(3X,'CRACK PROPAGATION RATE DADN,X10.0E-5')
      DO 14 I=2,58
      POINTS(I,1)=VT
   14 CONTINUE
      DO 16 J=1,130
      POINTS(60,J)=HR
   16 CONTINUE
      DO 20 I=1,60
      PRINT 25,(POINTS(I,J),J=1,132)
   25 FORMAT(1X,132A1)
   20 CONTINUE
      PRINT 77
   77 FORMAT(30X,'STRESS INTENSITY FACTOR,DELTA K')
      RETURN
      END
```

List of References

[1] Metals Handbook, Vol. 1, 8th Edition, American Society for Metals.

[2] Goranson, U.G., Hall, J., Maclin, J.R., Watanabe, R.T., Long-Life Damage Tolerant Structures, ASTM-STP 761, pp. 47 - 87.

[3] Collins, J.A. Failure of Materials in Mechanical Design--Analysis, Prediction, Prevention, John Willey & Sons, 1981.

[4] Turner, D.R., Manders, C. The Damage Tolerance Approach to the Canadair C1600, Canadian Aeronautics and Space Journal, Vol. 29, No. 3, September 1983, pp. 228 - 242.

[5] Dainty, R.V. The Use of "Marker Blocks" as an Aid in Quantitative Fractography in Full-Scale Aircraft Fatigue Testing--A Case Study, NAE-NRC, LTR-ST-1374, May 1982.

[6] McMillan, J.C., Hertzberg, R.W. Application of Electron Fractography to Fatigue Studies, ASTM-STP 436, pp. 89-123.

[7] Meyers, M.A., Chawla, K.K. Mechanical Metallurgy, Principles and Applications, Prentice-Hall, 1984.

[8] Laird, C. The Influence of Metallurgical Structure on the Mechanisms of Fatigue Crack Propagation, ASTM-STP 415, p. 131-168.

[9] Holm, D.K., Blom, A.F. Short Cracks and Crack Closure in Al 2024-T3, Proceedings of International Council of Aeronautical Sciences, 1984, pp. 783 - 790.

[10] Rich, D.L., Impellizzeri, L.F. Fatigue Analysis of Cold-Worked and Interference Fit Fastner Holes. ASTM-STP 637, pp. 153 - 175.

[11] Engel, L., Klingele, H. An Atlas of Metal Damage, Prentice-Hall.

[12] Eylon, D., Kerr, W.R. Fractographic and Metallographic Morphology of Fatigue Initiation Sites, ASTM-STP 645, pp. 235-249.

[13] Hertzberg, R.W., Deformation and Fracture Mechanics of Engineering Materials, J. Wiley and Sons, 1976.

[14] McLean, D. Mechanical Properties of Metals, 1962.

[15] Wadsworth, N.J. Conference on Dislocations and Mechanical Properties of Crystals, John Willey and Sons, 1956.

[16] Jaquet, P.A. International Conference on Fatigue of Metals, INST. MECH. ENGRS. London, 1956.

[17] Hemper, M., Schrader, A., ARCH. Eisenhutten W., 1957, 28, 547.

[18] Lukas, P., Klesnil, M., Phys. Status. Solidi. 37, 1970, 833.

[19] Kramer, I.R., Met. Trans., 5, 1974, 1785.

[20] Laird, C., The General Cyclic Stress-Strain Response of Aluminum Alloys, ASTM STP 637, pp. 3-35.

[21] Kanninen, M.F., Atkinson, C., Feddersen, C.E., A Fatigue Crack Growth Analysis Method Based on a Simple Representation of Crack-Tip Plasticity. ASTM-STP 637, pp. 122 - 140.

[22] Broek, D. Course on Damage Tolerance of Structures. Fracture Research Technical Report TR-8206.

[23] Lankford, L., Davidson, D.L., Cook, T.S. Fatigue Crack Tip Plasticity, ASTM-STP 637, pp. 36- 55.

[24] Elber, W. The Significance of Fatigue Crack Closure, ASTM STP 486, p. 230 -242.

[25] Fleck, N.A., Smith, R.A. Crack Closure--is it Just a Surface Phenomena? Int. J. Fatigue, July 1982, pp. 157 - 160.

[26] Bailon, J.P., Elboujdaini, M., Dickson, J.I., Environmental Effects on delta K Thr in 70-30 alpha-Brass and 2024-T351 Aluminum Alloy, Proceedings of International Symposium on Fatigue Crack Growth Threshold Concepts, Philadelphia, October 1983.

[27] de Koning, A.U. A Simple Crack Closure Model for Prediction of Fatigue Crack Growth Rates Under Variable - Amplitude Loading, ASTM-STP 743, 1981, pp. 63 - 85.

[28] Stewart, A.T. The Influence of Environment and Stress Ratio on Fatigue Crack-Growth at Near-Threshold Stress Intensities in Low-Alloy Steels. Eng. Fract. Mech., 1980, Vol. 13, pp. 463 - 478.

[29] Hertzberg, R.W., Von Euw E.F.G, Roberts, R., Delay Effects in Fatigue Crack Propagation, ASTM-STP 513, pp. 230 - 259.

[30] Eastabrook, J.H. Retardation of Fatigue Crack Growth by a Single Overload, R.A.E. Technical Report 83075, October 1983.

[31] Albertin, L., Hudak, S.J. Jr. Effect of Compressive Loading on Fatigue Crack Growth Rate and Striation Spacing in Type 2219-T851 Aluminum Alloy ASTM-STP 733, pp. 187-201.

[32] Brown, D.K., Cowling, M.J. Numerical Simulation of Fatigue Crack Growth, Int. J. Fatigue, October 1983, pp. 199 - 206.

[33] Ritchie, R.O. Influence of Microstructure on Near-Threshold Fatigue Crack Propagation in Ultra-High Strength Steel. Met.Sci.11, August 1977, p. 368.

[34] Irwing, P.E.,McCortney, L.N. Prediction of Fatigue Crack Growth Rates: Theory, Mechanisms and Experimental Results. Met.Sci. 11, 1977, p. 351.

[35] Johnston, W.S. Multi-Parameter Yield Zone Model for Predicting Spectrum Crack Growth ASTM-STP 748, pp. 85 - 102.

[36] Bilby, B.A., Swinden, K.H. Proceedings, Royal Society, Vol. 22, 1965, p. 4285.

[37] Atkinson, C., Kay, T.R. Acta Metallurgica, Vol. 19, 1971, p. 679.

[38] Saff, C.R. Crack Growth Retardation and Acceleration Models, ASTM STP 842, pp. 36 - 49.

[39] Metals Handbook, Vol. 10, 8th Edition, American Society for Metals.

[40] Forsyth, P.J.E., The Causes of Mixed Fatigue/Tensile Crack Growth and The Significance of Microscopic Crack Behaviour, R.A.E. Tech. Report 75143, 1975.

[41] Forsyth, P.J.E., A Unified Description of Micro and Macroscopic Fatigue Crack Behaviour, Int. J. Fatigue, January 1983, pp. 3 - 14.

[42] Overbury, K.C. Unpublished Fractographic Report, Canadair Ltd., 1981.

[43] Hertzberg, R.W. Fatigue Fracture Surface Appearance, ASTM-STP 415, p. 205-222.

[44] Abramovici, E., Overbury, K.C. Laboratory Report GM 14910, Canadair, 1983.

[45] Campbell, J.E., Gerberich, W.W.; Underwood, J.H.
Applications_of_Fracture_Mechanics_for_Selection_of_Metallic
Structural_Materials, American Society for Metals, 1982.

[46] Hertzberg, R.W., Mills, W.J. Character of Fatigue Fracture
Surface Micromorphology in the Ultra Low Growth Rate Regime,
ASTM-STP_600, pp. 220 - 234.

[47] Gell, M., Leverant, G.R. Acta_Metallurgica Vol. 16, 1968,
p. 553.

[48] Forsyth, P.J.E., Bowen, A.W. The Relationship Between
Fatigue Crack Behaviour and Microstructure in 7178 Aluminum
Alloy Int._J._Fatigue, January 1981, pp. 17 - 25.

[49] Madeyski, A., Albertin, L. Fractographic Method of
Evaluation of the Cyclic Stress Amplitude in Fatigue Failure
Analysis, ASTM-STP_645, pp. 73 - 83.

[50] Hahn, G.T. Battelle Memorial Institutue, Report
AF-33615-70-C-1630.

51. Hertzberg, R.W. Metallurgical_Transactions, Vol. 4, 1973, p.
887.

[52] Christensen, R.H., Harmon, M.B. Limitation of Fatigue Crack
Research in the Design of Flight Vehicle Structures,
ASTM-STP_415, pp. 5 - 24.

[53] Hartman, E. Int._J._of_Fract._Mechanics, 1(3), 1965, p.
167.

[54] Vogelsang, L.B. Fatigue Crack Growth in Aluminum Alloys,
Fifth_International_Conference_on_Fracture, 1981.

[55] Stubbington, C.A., Forsyth, P.J.E. Some Corrosion Fatigue
Observations on a High-Purity Aluminum-Zinc-Magnesium Alloy
and Commercial D.T.D. 683 Alloy, Journal_of_The_Institute_of
Metals, Vol. 90, 1961-62, p. 347.

[56] Metals_Handbook, Vol. 9, 8th Edition, American Society for
Metals.

[57] McEvily, A.J. Jr., Boettner, R.C. "On F.C.P. in F.C.C.
Metals" Acta_Metallurgica, Vol. 11, No. 7.

[58] Kaufmann, J.G. Design of Aluminum Alloys for High Toughness
and High Fatigue Strength. AGARD_Conference_Proceedings_No.
185, Brussels, Belgum, 1975, p. 2-1.

[59] Wanhill, R.J.H., Kolkman, H.J., Schla, L., Fatigue Crack
Propagation and Fracture in 7050 and 7091 Aluminum Alloys
Forgings, AGARD_Conference_Proceedings_No._328.

[60] Bhandarkar, M.D., Lisagor, W.B. Metallurgical
Characterization of the Fracture of Aluminum Alloys,
ASTM_STP_645, pp. 176 - 209.

[61] Embury, J.D. Basic Microstructural Aspects of Aluminum
Alloys and Their Influence on Fracture Behaviour, AGARD_-_CP
-_185 1975, p. 1.1.

[62] Forsyth, P.J.E. The Metallurgical Aspects of Fatigue and
Fracture Toughness. AGARD_Conference_Proceedings_No._610,
1973, pp. 1 - 22.

[63] Calabrese, C., Laird, C. Materials_Science_and_Engineering,
Vol. 13, 1974, pp. 141-157.

[64] Calabrese, C., Laird, C. Materials_Science_and_Engineering,
Vol. 13, 1974, pp. 159 - 174.

[65] Yan, M., Wang, Z. Some Microscopic Features and Mechanisms
of Fatigue Behaviour in Metals, First_China-USA_Bilateral
Metallurgical_Conference, Beijing, China, 1981.

[66] Klingele, H. Essential Features in Fatigue Fractures and
Remarkable Phenomena in Fatigue Crack Growth, AGARD
Conference_Proceedings_No._376 Sienna, Italy, 1984, p. 1-1.

[67] Thompson, J. Trends in Structural Qualifications of Civil
Transport Aircraft, Metal_Progress, April 1984, p. 41.

[68] Wiebe, W., Dainty, R.V. Notes on the value of Fractography
in Failure Analysis, N.R.C._N.A.E._Report_LTR-ST.591 1973.

[69] Wiebe, W., Dainty, R.V. Fractographic Determination of
Fatigue Crack Growth Rates in Aircraft Components, Canadian
Aeronautics_and_Space_Journal, Vol. 27, No. 2, 1981, p. 107.

[70] Dainty, R.V. Application of Optical and Electron
Microscopic Techniques in the Fractographic Determination of
Fatigue Crack Growth Rates, NRC._NAE_Report_LTR-ST-1493
1984.

[71] Potter, J.M., Yee, B.G.W. Use of Small Crack Data to Bring
About and Quantify Improvements to Aircraft Structural
Integrity, AGARD_328 p. 41.

[72] Anderson, D.M., McGee, W.M. Development and Application of Marker Loads for a Fatigue Crack Growth Study on a Full Scale Test Article, ICAS 1984, pp. 126 - 132.

[73] Wang, D.Y. An Investigation of Initial Fatigue Quality, ASTM-STP 761, pp. 191-211.

[74] Abramovici, E., Burak, M., Overbury, K.C., Turner, D.R., Quantitative Fractographic Examination of Aircraft Components Tested Under a Fatigue Spectrum Loading. Proceedings of the 7th International Conference on the Strength of Metals and Alloys, Montreal, August 1985.

[75] Madeyski, A. A Systematic Approach to Failure Analysis, Metal Progress May, June, July, 1984.

[76] Wulpi, D.J. How Components Fail?, ASM, 1966.

[77] Gray, A.G. Source Book in Failure Analysis ASM, 1974.

[78] Microstructure and Fractography, ASTM STP 600.

[79] Nica, A. Mechanics of Aerospace Materials, Materials Science Monographs, 9, Elsevier, 1981.

[80] Abramovici, E. CL-600, Inboard Flap, Flap/Vane Fatigue and Damage Tolerance Test, Fractographic Examination, Canadair Ltd. Laboratory Report GM 15754.

[81] Forsyth, P.J.E. Fatigue Fracture Topography, AGARD 37G Sienna, Italy, 1984, pp. 3 - 2.

[82] Abelkis, P.R. Use of Microfractography in the Study of Fatigue Crack Propagation Under Spectrum Loading, ASTM-STP 645, pp. 213 - 234.

[83] Featherby, M. Fractography of Advanced Composites and High Strength Aluminum CASD ERR-73-049, Convair Aerospace Division, General Dynamics.

[84] Au, J.J., Ke, J.S. Correlation Between Fatigue Crack Growth Rate and Fatigue Striation Spacing in AISI 9310 (AMS 6265) Steel ASTM-STP-733, pp. 202 - 221.

[85] Canadair Ltd., Fatigue and Damage Tolerance Tests on The Inboard Flap and Vane Assemblies, CL600 Type Approval Submission, Report RAT-6000-207.

[86] Canadair Ltd. Fatigue and Damage Tolerance Tests on The Outboard Flap and Vane Assemblies, Cl-600 Type Approval Submission, Report RAT-6000-206.

[87]   Canadair Ltd.   CL-600 Test Plan Flap and Vane Assembly
       Fatigue and Damage Tolerance Tests, Memorandum MAS-600-217.

[88]   Abramovici, E. Cl-600, Outboard Flap, Flap/Vane Fatigue and
       Damage Tolerance Test, Fractographic Examination, Canadair
       Ltd. Laboratory Report GM 15682.

[89]   Abramovici, E. CL-600, Inboard Flap, Flap/Vane Fatigue and
       Damage Tolerance Test, Fractographic Examination, Canadair
       Ltd. Laboratory Report GM 15684.